(BL1A)

Ni 3p and 3s resonant photoionization at the Ni 2p excitation of Ni

Yasutaka Takata, Takaki Hatsui and Nobuhiro Kosugi

The Graduate University for Advanced Studies, Institute for Molecular Science, Myodaiji, Okazaki 444-8585

Recently core excitation and deexcitation processes have been investigated in detail for various systems. For the planar nickel complexes, a number of satellite series in the Ni 3p and 3s regions are strongly enhanced by the Ni 2p resonant excitations and lowers its kinetic energy for the higher resonance energy, showing one-to-one correspondence with the excited state [1–3]. Furthermore, it was revealed that the kinetic energy shift relative to the photon energy is strongly influenced by the intermolecular interaction [3].

In the present study, we have measured resonant photoelectron spectra in the Ni 3p and 3s ionization regions at the Ni 2p edge of Ni. It is interesting to know the resonant behaviors in Ni which has metallic bond with a much shorter Ni–Ni distance than those of the molecular solids.

Experiments were performed at BL1A soft x-ray beamline. A sample of Ni was evaporated on Ni plate in a vacuum of 2×10^{-10} Torr. A pair of beryl ($10\bar{1}0$) crystal was used as a monochromator. The Ni 2p photoabsorption spectra were measured by monitoring the total electron yield. A SCIENTA SES200 electron energy analyzer was used to measure the photoelectron spectra. The total energy resolution in the photoelectron spectra was about 0.7 eV.

Figure 1 shows the Ni 2p photoabsorption spectrum of Ni. Figure 2 shows the resonant photoelectron spectra in the Ni 3p and 3s ionization regions measured at the excitation energies (0–6) marked in Fig. 1. The normal Auger spectrum (N) measured at the photon energy of 900 eV is also shown. Similarly to the case of Ni planar complexes, Ni 3p and 3s primary ionization peaks labeled with an asterisk (*) are not enhanced by the resonant excitation. On the other hand, the weak satellite bands (a–e) in the non-resonant spectrum (0) are strongly enhanced at the lowest Ni $2p_{3/2}$ resonance (1). The kinetic energies of these bands are linearly dispersive as a function of the photon energy below the resonance maximum (1). Above the maximum, photon energy dependence changes drastically; i.e., the kinetic energies are independent of the photon energy and are the same as those in the normal Auger spectrum (N). These photon energy dependences of the kinetic energy shift have been reported by Weinelt at al. for the 6 eV satellite in the valence band of Ni [4]. However, the observed photon energy dependence in Ni is different from that in the planar nickel complexes and indicates that the photoexcited electron in the intermediate and/or the Auger final states does not strongly localized. In the Ni $2p_{1/2}$ excitation region, the new satellite bands (a'–e') are enhanced and show similar photon energy dependence as in the Ni $2p_{1/2}$ excitation region.

References

[1] Y. Takata, M. Nakamura and N. Kosugi, UVSOR Active. Rep. (1995) 50.

Y. Takata, M. Nakamura and N. Kosugi, Chem. Phys. Lett., in press.

[2] Y. Takata, M. Nakamura, Y. Yamamoto, T. Yokoyama, T. Ohta and N. Kosugi, UVSOR Active. Rep. (1996) 48.

Y. Takata, M. Nakamura and N. Kosugi, J. Electron Spectrosc. in press.

[3] Y. Takata, T. Hatsui and N. Kosugi, ibid.

[4] M. Weinelt, A. Nilsson, M. Magunson, T. Wiell, N. Wassdahl, O. Karis, A. Föhlisch, N. Mårtensson, J. Stöhl and M. Samant, Phys, Rev. Lett., 78 (1997) 967.

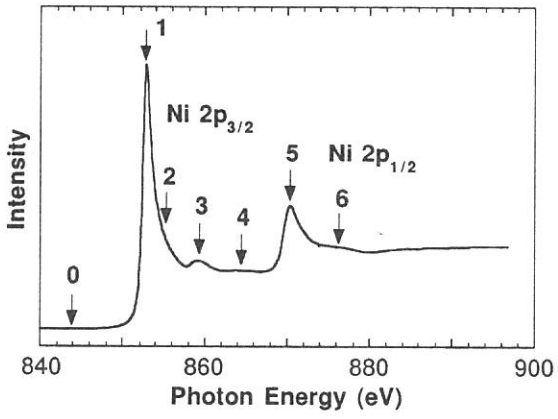

Fig. 1. Ni 2p photoabsorption spectrum of Ni.

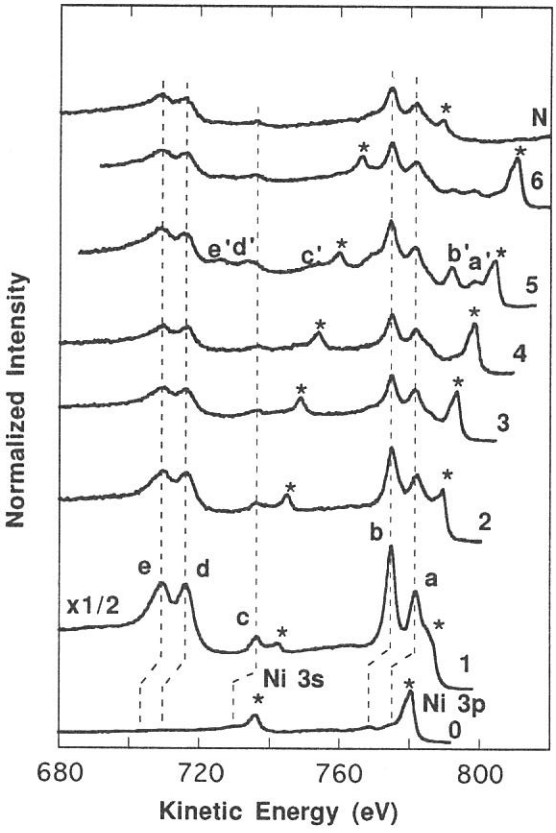

Fig. 3. Resonant photoelectron spectra in the Ni 3p and 3s regions of Ni at the photon energies marked in Fig. 2.

(BL1A)

Polarized Ni 2p photoabsorption spectra of $Ni^{II}(mnt)_2^{2-}$ and $Ni^{III}(mnt)_2^{1-}$.

Takaki HATSUI, Yasutaka TAKATA, Nobuhiro KOSUGI

The Graduate University for Advanced Studies, Myodaiji, Okazaki 444-0864
Institute for Molecular Science, Myodaiji, Okazaki 444-0864

The metal *2p* photoabsorption spectra of *3d* transition metal compounds have been extensively studied. For ionic compounds such as oxides and halides, the spectra are successfully explained by model hamiltonians taking into account the crystal field, intra-atomic multiplet coupling and, if necessary, ligand-to-metal charge transfer (LMCT) effect, or covalency hybridization between ligand and unoccupied metal *3d** orbitals. On the other hand, for compounds with π-backbonding such as organometallic compounds, the metal *2p* excitation is not well understood. One of the reasons is the insufficient knowledge of the metal-to-ligand charge transfer (MLCT) transitions, namely transitions to unoccupied low-lying ligand π* orbitals hybridized with occupied metal *3d* orbitals. In the previous studies, we measured linearly polarized Ni *2p* photoabsorption spectra of $K_2Ni(CN)_4 \cdot H_2O$ and nickel dimethylglyoxime, and revealed that strong bands above the most intense *2p-3d** atomic lines are associated with MLCT transitions [1]. In this study, we measured linearly polarized Ni *2p* photoabsorption spectra of two nickel complexes $[(C_4H_9)_4N]_2[Ni^{II}(mnt)_2]$ and $[(C_2H_5)_4N][Ni^{III}(mnt)_2$ (mnt = 1,2-dicyano-ethylene-1,2-dithiolato (maleonitrile-dithiolate)). The observed polarization dependence was interpreted in terms of the symmetry and the character of unoccupied molecular orbitals (MO).

Single crystal samples were prepared as described in ref. [2]. The molecular axes *x*, *y* and *z* are determined by X-ray diffraction analyses (the axes are chosen as shown in Fig. 1). Both the $Ni^{II}(mnt)_2^{2-}$ and $Ni^{III}(mnt)_2^{1-}$ anions have D_{2h} symmetry in a good approximation [2]. The Ni *2p* photoabsorption spectra were measured at the BL1A soft X-ray beamline with a pair of beryl (1010) crystals by monitoring total electron yields.

Fig. 2 shows the polarized Ni *2p* photoabsorption spectra of single crystalline $[(C_4H_9)_4N]_2[Ni^{III}(mnt)_2]$. Distinct anisotropy is observed for three isolated peaks B, C, D and E. Because $Ni^{II}(mnt)_2^{2-}$ in the ground state has low-spin Ni $3d^8$ configuration, the only unoccupied metal *3d* orbital is $3d_{xy}\sigma^*$ with b_{1g} symmetry. Thus, it is reasonable to assign peak B to the intra-atomic transition to b_{1g}^* ($3d_{xy}\sigma^*$) orbital. Employing the dipole selection rule, the transition to $3d_{xy}\sigma^*$ is allowed in E//*x* and E//*y* directions and forbidden in E//*z*, which is consistent with the observed polarization dependence of peak B. Peaks C and D are plausibly described in terms of intra-atomic multiplet, LMCT, or MLCT effects. The intra-atomic multiplet effect, however, cannot explain the polarization dependence of peak C because it is expected to cause the second lowest peak stronger in E//*z* than the other directions [3]. Peaks C and D cannot be interpreted as LMCT satellites, or transitions to $\underline{2p}3d^0\underline{L}$ ($\underline{2p}$ and $\underline{L}$ denotes 2p and ligand hole, respectively) which should show the same polarization dependence as peak B. On the other hand, the mnt^{2-} ligand has unoccupied ligand π* orbitals. Two mnt ligands produce two low-lying unoccupied b_{3g}^* (d_{yz} in central symmetry) and a_g^* (d_{x2-y2}, d_{z2}, *s*) orbitals, which may cause MLCT transitions. Based on the observed polarization dependencies, the peaks C and D can be assigned to the MLCT transitions to the b_{3g}^* and a_g^* orbitals, respectively.

Fig. 3 shows the polarized Ni *2p* photoabsorption spectra of $[(C_2H_5)_4N][Ni(^{III}mnt)_2]$. A strong peak A is observed on the lower energy side of the peak B. Peak A is strong in E//*z*, weak in E//*x*, and very weak in E//*y*. Because $Ni(mnt)_2^{1-}$ anions are not completely parallel to one another [2], peak A should be forbidden in E//*y*. Thus, peak A can be assigned to the transition to an orbital with b_{2g} (d_{xz}) symmetry. This is consistent with the electronic structure of $Ni(mnt)_2^{1-}$ with an singly occupied $3b_{2g}$ orbital. Peaks C and D can be assigned to the transition to b_{3g}^* and a_g^* orbitals, respectively on the basis of the polarization dependence,

In conclusion, the peak C and D (Fig. 2 and Fig. 3) are undoubtedly assigned to the transitions

to MLCT transitions. These results indicate that the MLCT effect is indispensable in interpreting the metal *2p* photoabsorption spectra of compounds with π-backbonding. Furthermore, the symmetry of the singly occupied $3b_{2g}$ orbital in $Ni(mnt)_2^{1-}$ is successfully determined by polarized Ni *2p* photoabsorption.

References

[1] T. Hatsui, et al., J. Electron Spectrosc. Relat. Phenom., in press.

[2] A. Kobayashi and Y. Sasaki, Bull. Chem. Soc. Jpn., 50, 2650 (1977)

[3] G. van der Laan, et al., Phys. Rev. B37, 6587 (1988)

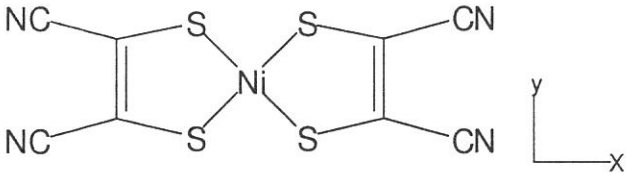

Fig. 1 The structural formula of $Ni(mnt)_2^{n-}$ (n=1,2) with D_{2h} symmetry.

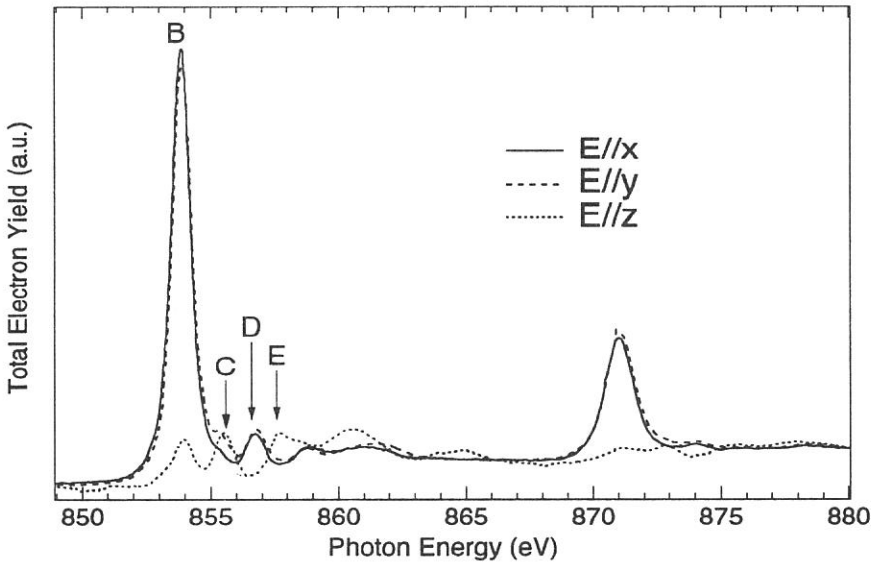

Fig. 2 Polarized Ni *2p* photoabsorption spectra of $[(C_4H_9)_4N]_2[Ni^{II}(mnt)_2]$.

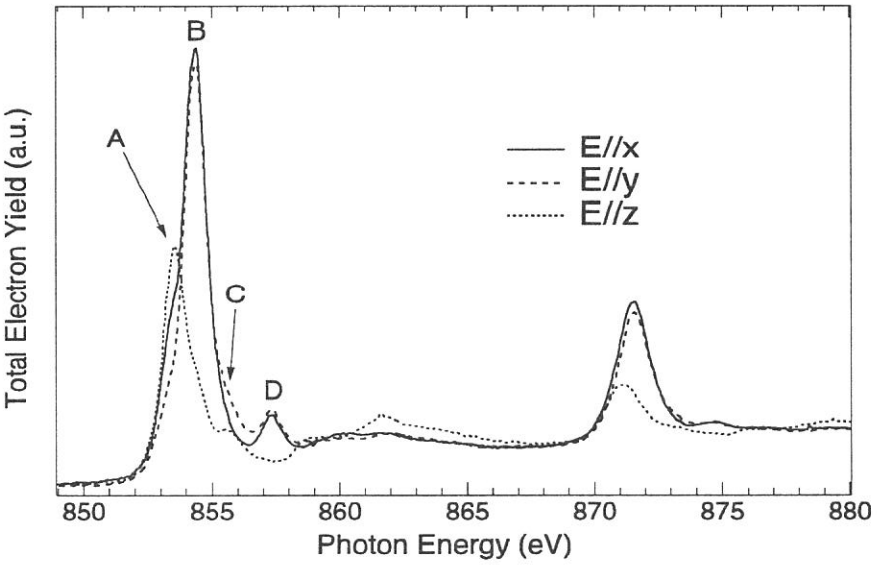

Fig. 3 Polarized Ni *2p* photoabsorption spectra of $[(C_2H_5)_4N][Ni^{III}(mnt)_2]$.

(BL1A)

Resonant behavior of satellite photoelectrons in the Ni 3p and 3s regions at the Ni 2p excitation of $Ni(Hgly)_2$

Yasutaka Takata, Takaki Hatsui and Nobuhiro Kosugi

The Graduate University for Advanced Studies, Institute for Molecular Science, Myodaiji, Okazaki 444-8585

We have investigated resonant behavior of photoelectrons at the Ni 2p excitation for nickel compounds. For the planar nickel complexes, $K_2Ni(CN)_4$[1] and Ni(Hdmg)2 [bis-(2,3butanedione dioximato)nickel(II)] [2], a number of satellite series in the Ni 3p and 3s regions, which are mostly forbidden in the non-resonant spectrum, become strongly observable via the resonant excitations. For both samples, each satellite lowers its kinetic energy for the higher resonance energy, showing one-to-one correspondence with the excited state. This behavior is characteristic of molecular system in solid. It was also revealed that kinetic energy shift relative to the increment of the excitation energy differs considerably between these samples. One possible reason for the difference supposed to be the different degree of the intermolecular interaction.

In the present study, the resonant behavior of satellite electrons in the Ni 3p and 3s regions at the Ni 2p excitation of $Ni(Hgly)_2$ [bis-(dioximato)nickel(II)] was investigated to clarify the effect of intermolecular interaction upon the kinetic energy shift. $Ni(Hgly)_2$ is a good sample for this purpose because the local bonding character around the Ni atom is nearly the same as in $Ni(Hdmg)_2$ as shown in Fig.1 but the intermolecular (Ni-Ni) distance (4.20Å) is much longer than $Ni(Hdmg)_2$ (3.25Å).

Experiments were performed at BL1A soft x-ray beamline. A sample of $Ni(Hgly)_2$ was evaporated on a gold plate in a vacuum of $1x10^{-9}$ Torr. A pair of beryl $(10\bar{1}0)$ crystal was used as a monochromator. The Ni 2p photoabsorption spectra were measured by monitoring the total electron yield. A SCIENTA SES200 electron energy analyzer was used to measure the photoelectron spectra. The total energy resolution in the photoelectron spectra was about 0.7 eV.

Figure 2 shows the Ni 2p photoabsorption spectrum of $Ni(Hgly)_2$. The shape is nearly the same as that of the $Ni(Hdmg)_2$[3]. This is reasonable because both the complexes have almost the same local bonding character around the Ni atom. Figure 3 shows the resonant photoelectron spectra in the Ni 3p and 3s ionization regions measured for three resonant excitations (1-3) in Fig. 2, together with an non-resonant photoelectron spectrum (0). Two weak peaks labeled as sharp (#) are the Au $4f_{5/2}$ and $4f_{7/2}$ photoelectron lines originating from the substrate. Similarly to the case of Ni(Hdmg)2, Ni 3p and 3s primary ionization peaks labeled with an asterisk (*) are not enhanced by the resonant excitation but satellite bands (a–e) weakly observed or absent in the non-resonant spectrum (0) are enhanced. Peaks (a, b), (c) and (d, e) are attributable to the resonant photoionization $\underline{2p_{3/2}}\varphi i - \underline{3p3d}\psi i$, $\underline{2p_{3/2}}\varphi i - \underline{3s3d}\psi i$ and $\underline{2p_{3/2}}\varphi i - \underline{3p3p}\psi i$, respectively. Here, each under bar denotes a single hole. φi is an excitonic electron bound by the $\underline{2p_{3/2}}$ singly charged state, and ψi is an excitonic electron bound by the doubly charged state such as $\underline{3p3d}$.

The kinetic energies of the distinct peak (a) were measured then the slopes ($\Delta K.E./\Delta h\nu$) were obtained, where $\Delta K.E.$ and $\Delta h\nu$ denote the increments of the kinetic energy and the photon energy, respectively. The slopes have a nearly constant value of -0.42 ± 0.05 between the resonance (1) and (3), and are considerably different from the results in $Ni(Hdmg)_2$ [2]. In $Ni(Hdmg)_2$, the slope between the resonance (1) and (2) is about -0.7 but is only about -0.1 between the resonance (2) and

(3) [2]. The molecular orbitals to which the Ni 2p electron is excited are the in-plane Ni 3d* and the out-of-plane ligand orbitals for the resonance (1) and the resonances (2, 3), respectively[3]. Therefore, the effect of the intermolecular interaction upon the kinetic energy shift is stronger in the case that the molecules are more closely stacked with one another. The intermolecular (Ni-Ni) distance is much longer in $Ni(Hgly)_2$ so that the effect is much weaker than those in $Ni(Hdmg)_2$. As a result the kinetic energy shift is not so influenced by the intermolecular interaction in $Ni(Hgly)_2$ and shows strong photon energy dependence as in the ionic complex $K_2Ni(CN)_4$[1].

References

[1] Y. Takata, M. Nakamura and N. Kosugi, UVSOR Active. Rep. (1995) 50.
Y. Takata, M. Nakamura and N. Kosugi, Chem. Phys. Lett., in press.

[2] Y. Takata, M. Nakamura, Y. Yamamoto, T. Yokoyama, T. Ohta and N. Kosugi, UVSOR Active. Rep. (1996) 48.
Y. Takata, M. Nakamura and N. Kosugi, J. Electron Spectrosc. in press.

[3] T. Hatsui, Y. Takata, N. Kosugi, K. Yamamoto, T. Yokoyama and T. Ohta, UVSOR Active. Rep., (1996) 46.
T. Hatsui, Y. Takata, N. Kosugi, K. Yamamoto, T. Yokoyama and T. Ohta, J. Electron Spectrosc., in press.

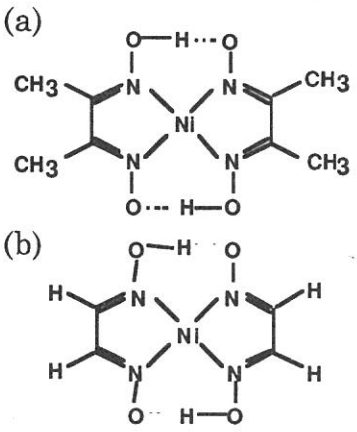

Fig. 1. Molecular structure of (a) $Ni(Hdmg)_2$ and (b) $Ni(Hgly)_2$.

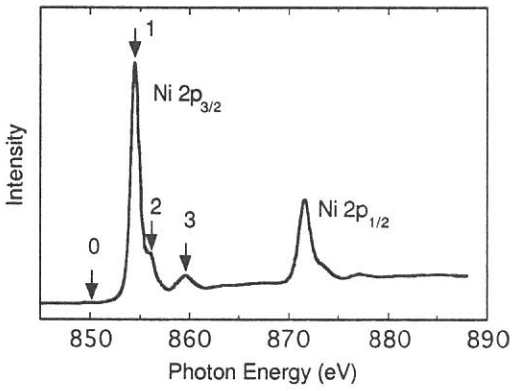

Fig. 2. Ni 2p photoabsorption spectrum of $Ni(Hgly)_2$.

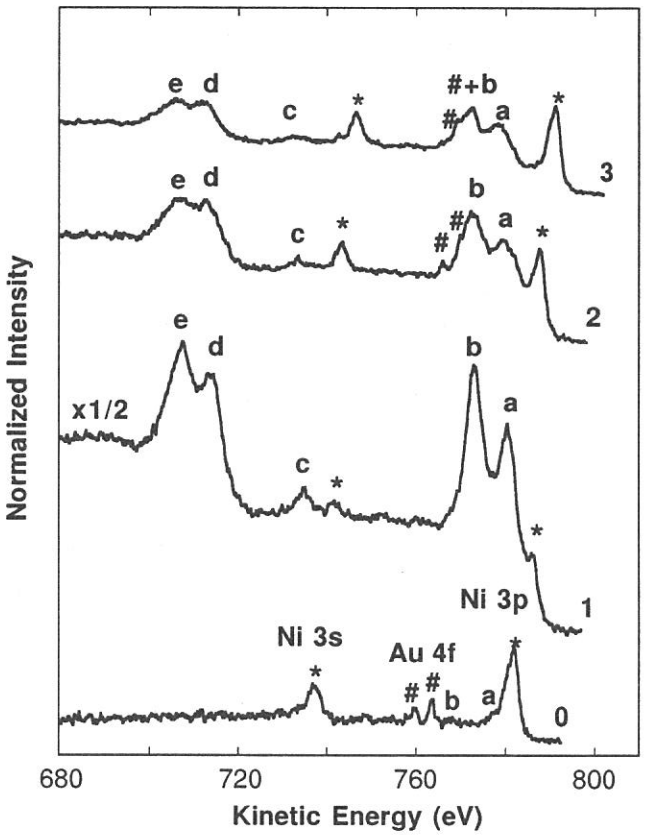

Fig. 3. Resonant photoelectron spectra in the Ni 3p and 3s regions of Ni $(Hgly)_2$ at the photon energies marked in Fig. 2.

(BL1A)

Resonant Photoemission Study of Temperature-Induced Valence Transition Material $EuNi_2(Si_{1-x}Ge_x)_2$

Heralu Pathirannehelage Nihal Jayalath GUNASEKARA*, Yasutaka TAKATA, Shin-ichi KIMURA, Toyohiko KINOSHITA, Nobuhiro KOSUGI, Krishna Gopal NATH[1], Hirofumi WADA[2], Akihiro MITSUDA[2] and Masayuki SHIGA[2]

Institute for Molecular Science, Myodaiji, Okazaki 444-8585, Japan

[1]Department of Structural Molecular Science, Graduate University for Advanced Studies, Okazaki 444-8585, Japan

[2]Department of Materials Science and Engineering, Kyoto University, Kyoto 606-01, Japan

Study of the electronic structures of rare earth compounds has been attracted much attention because of their interesting physical properties which are derived from the localized nature of $4f$ electrons. Among the intermediate valent systems, Eu compounds are known to exhibit strong temperature dependence of the mean valence. Very recently, it was found that the $EuNi_2(Si_{1-x}Ge_x)_2$ compounds with $0.70 \leq x \leq 0.82$ show a temperature induced valence transition below room temperature[1)] and magnetic field induced transition. In the previous report[2)], it has been concluded that the $3d$-$4f$ resonant photoemission of such kind of mixed valent $4f$ compounds is a useful technique to clarify the different $4f$ electronic states owing to different valence. In this study, we have applied the $3d$-$4f$ resonant photoemission method to investigate the valence transition of the $EuNi_2(Si_{1-x}Ge_x)_2$ compound. We have also measured the photoemission spectra around the Ni $2p$-$3d$ resonant excitation region in order to investigate the Ni $3d$ states of the same sample. The sample of x=0.75 which shows the mean valence transition from ~2.3 (high temperature) to ~2.8 (low temperature) at T=110K was used.

The samples were prepared by melting stoichiometric amount of constituent elements in argon furnace. The ingots were annealed in an evacuated quartz tube at 800°C for one week. The resonant photoemission experiments were performed at the double crystal monochromator beamline BL1A, where the high performance photoemission spectroscopy system SCIENTA SES-200 is equipped. A pair of beryl $(10\bar{1}0)$ crystals was used to obtain the monochromatized light around both the Eu $3d$-$4f$ and Ni $2p$-$3d$ excitation regions. The total energy resolution of the photoelectron spectra was estimated to be about 0.7 eV. Photoelectron total yield (TY) spectra around these excitation condition were also measured by recording sample drain current as a function of photon energy. The clean surface of the sample was obtained by filing in ultra high vacuum condition.

Figure 1 shows the TY spectra around the Eu $3d$-$4f$ excitation region ($M_{IV, V}$ edge) at about 300K and 80K. Several peaks are appeared due to the final state multiplet and mixed valent nature of the sample. It is noticed from Fig. 1 that the peaks 2, and 3 are enhanced at the low temperature phase. From the comparison with the previous report of L_{III} edge spectra[1)], it is concluded that these peaks are enhanced due to increasing the trivalent Eu ion component at low temperature. The resonant photoemission spectra around these excitation conditions are shown in Fig. 2. It is found that the trivalent components of Eu $4f$ states are enhanced at the excitation conditions of 2 and 3. On the other hand, the divalent 4f states are dominant at 1, 4 and 5. From these results, the features around 0-4eV binding energy are estimated to be mostly divalent $4f$ states and those around 6-12eV are trivalent ones in these on-resonant spectra. The features of the off-resonant spectrum at "0" might be mainly hybridized states of divalent Eu $4f$ and Ni $3d$.

The Ni $2p$-$3d$ resonant photoemission spectra have also been measured (not shown here). It was considered that the spectra reflect the contribution of the Ni $3d$ bands. The resonant behavior of the Ni $3d$ band is almost same as that reported for the Ni metal[3)]. It is noted that the $3d$ bands seem to be situated higher binding energy (about 0.8-0.9eV) than those of Ni metal.

It is concluded that the $3d$-$4f$ resonant photoemission spectra and the Eu $M_{IV, V}$ edges absorption spectra behave as similar manner as the Eu L_{III} edge spectra[1)] in their temperature dependence, which reflects

valence transition from Eu^{2+} at room temperature to Eu^{3+} at low temperature. To clarify each valence state, the 3*d*-4*f* resonant photoemission is very useful as reported for Tm compounds[2]. The estimation procedure of the mean valence for each temperature is now in progress as will be described elsewhere[4].

Acknowledgements

Authors would like to thank to the staff members of the UVSOR facility for the support.

References

* Permanent Address; Ceylon Institute for Scientific and Industrial Research, P.O.Box 787, 363, Bauddhaloka Mawatha, Colombo 7, Sri Lanka.

1) H. Wada, A. Nakamura, A. Mitsuda, M. Shiga, T. Tanaka, H. Mitamura and T. Goto, *J. Phys., Condens. Matter.* 9 (1997) 7913.

2) T. Kinoshita, Y. Ufkutepe, K. G. Nath, S. Kimura, H. Kumigashira, T. Takahashi, T. Matsumura, T. Suzuki, H. Ogasawara and A. Kotani, *J. Electron Spectrosc. Relat. Phenomn.* (1998), in press: Y. Ufkutepe, S. Kimura, K. G. Nath, T. Kinoshita, H. Kumigashira, T. Takahashi, T. Matsumura, T. Suzuki and H. Ogasawara, *UVSOR Activity Report* (1996) p.200.

3) For example, M. Weinelt, A. Nilsson, M. Magnuson, T. Wiel, N. Wassdahl, O. Karis, A. Föhlisch and N. Mårtennsson, *Phys. Rev. Lett.* 78 (1997) 967.

4) H. P. N. J. Gunasekara, Y. Takata, S. Kimura, T. Kinoshita, N. Kosugi, K. G. Nath, H. Wada, A. Mitsuda and M. Shiga, in preparation.

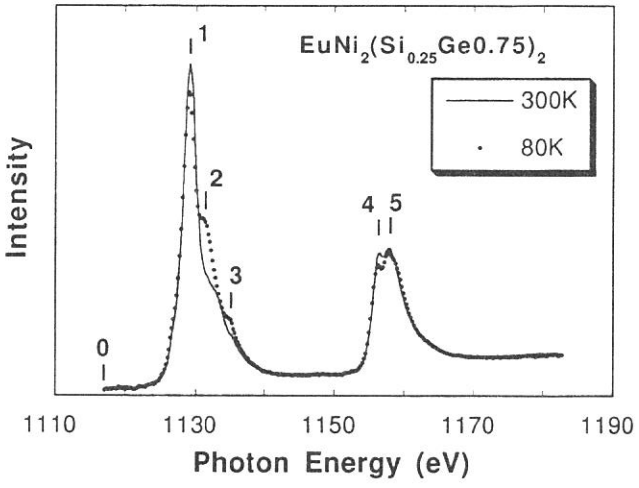

↑

Figure 1. TY spectra for $EuNi_2(Si_{1-x}Ge_x)_2$ (x=0.75) around Eu $M_{IV, V}$ edges at 300K and 80K.

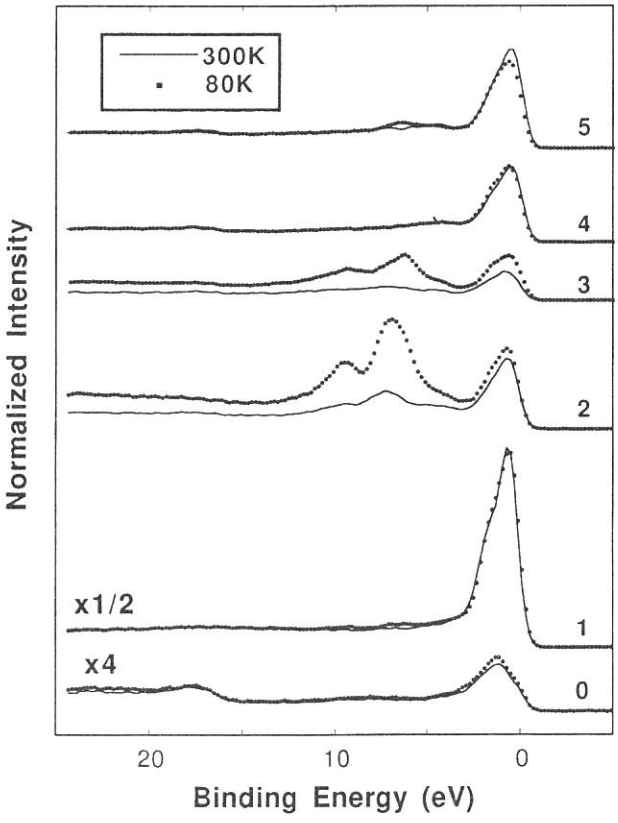

→

Figure 2. Resonant photoemission spectra of $EuNi_2(Si_{1-x}Ge_x)_2$ (x=0.75) around Eu $M_{IV, V}$ edges at 300K and 80K. The photon energy position of each spectrum corresponds to the peak position of the TY spectrum in Fig. 1.

(BL2B1) X-ray absorption study of $Ce_{1-x}Sr_xTiO_3$

T. Yokoya, T. Sato, A. Chainani[A], and T. Takahashi

Department of Physics, Tohoku University, Sendai 980-8578, Japan
[A] *Institute for Plasma Research, Gandhinagar 382428, India*

Titanium oxide with a perovskite structure is classified as a Mott-Hubbard (M-H) type by the phase diagram based on the work of Zaanen, Allen, and Sawatzky, where early transition metal compounds (TMC's) are a M-H type and late TMC's are a charge transfer type [1]. However, in our previous study on $CeTiO_{3+\delta}$, we have observed spectral changes across the δ-controlled metal-insulator (M-I) transition due to doped hole states in the O 1s x-ray absorption spectra and showed that M-H system can have a charge-transfer (C-T) character due to a strong hybridization [2]. In this study, to further investigate the electronic structure of Titanium oxide, we have performed x-ray absorption spectroscopy (XAS) on $Ce_{1-x}Sr_xTiO_3$, which exhibits M-I transition by a substitution of trivalent Ce with divalent Sr.

XAS was carried out at BL2B1 in the total electron yield mode at a resolution of 1 eV. Samples were scraped *in-situ* with a diamond file to obtain clean surfaces. Fig. 1 shows O 1s XAS of $Ce_{1-x}Sr_xTiO_3$ [x=0 (semiconducting), 0.05 and 0.2(metallic)]. We find two structures in the spectrum of $CeTiO_3$. One is a prominent peak centered at 535 eV and the other is a weak shoulder around 532eV. The overall spectral shape is similar to that of $LaTiO_3$ [3], where a feature at 532 eV is ascribed to O 2p states hybridized with the upper Hubbard band and a feature at 535 eV corresponds to Ce 5d states with O 2p admixture. In the spectrum of x=0.05 compound, we can clearly see that the weak feature at 532 eV observed in x=0.0 compound is strongly enhanced, forming a peak structure. The intensity of the peak structure is stronger in x=0.2 compound than in x=0.05 compound. This indicates that the new hole-doped state evolves as a function of x, and may cause the M-I transition. The spectral changes across the x-controlled M-I transition are similar to that across the δ-controlled one [2]. These results provide a direct confirmation of the C-T nature of early TMC's due to a strong hybridization.

We thank Prof. M. Onoda for providing us $Ce_{1-x}Sr_xTiO_3$ samples.

[1] J. Zaanen, G.A. Sawatzky, and J.W. Allen, Phys. Rev. Lett. 55, 418 (1985).
[2] O. Akaki et al., Phys. Rev. B 56, 12050 (1997).
[3] A. Fujumori et al, Phys. Rev. B 46, 9841 (1996).

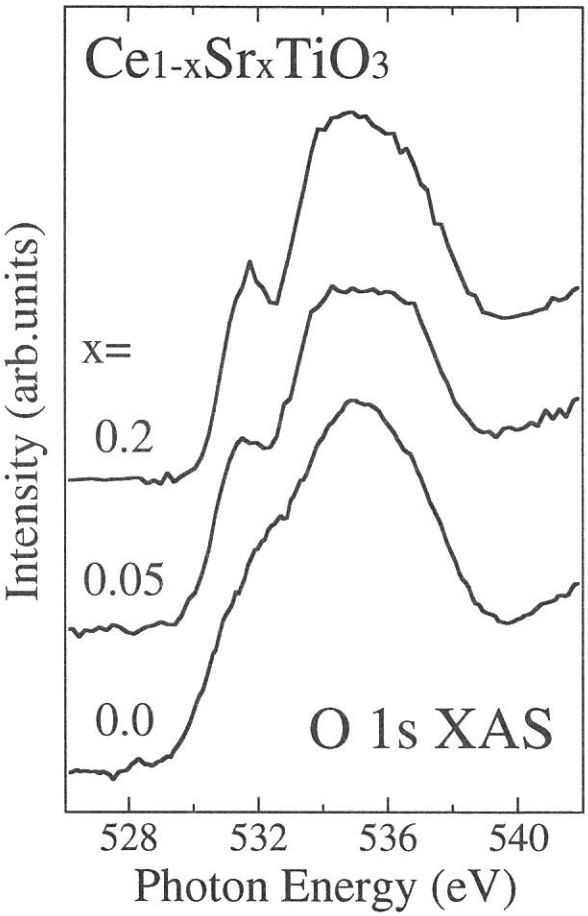

Fig. 1. O 1s-p XAS of $Ce_{1-x}Sr_xTiO_3$ (x=0.0, 0.05 and 0.2).

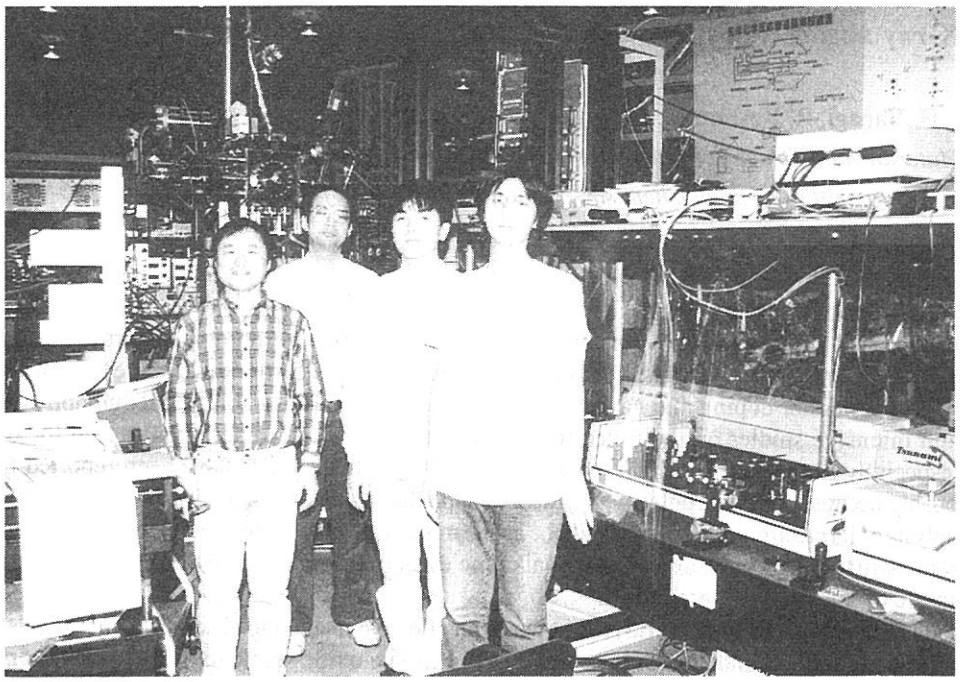

Mitsuke Group at BL3A2

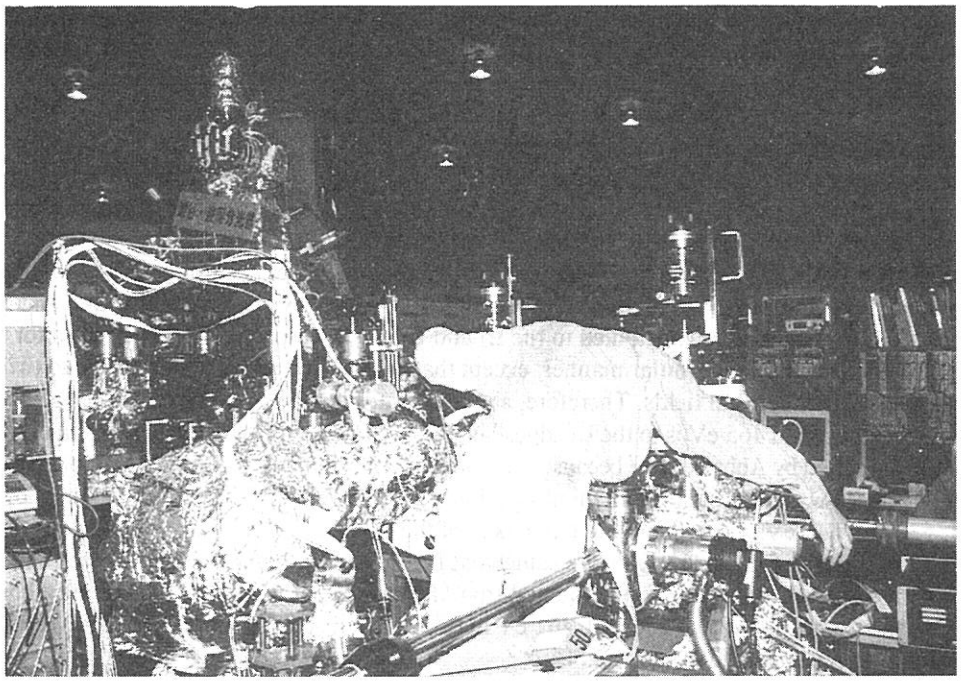

Investigation at BL1A

(BL2B1)

X-ray absorption spectra for Ca $L_{2,3}$, Ti $L_{2,3}$, and O K edges in $CaTiO_3$

K. Ueda, H. Yanagi, R. Noshiro, H. Hosono, H. Kawazoe, M. Takemoto[A], N. Miyagawa[A], and H. Ikawa[A]

Materials and Structures Laboratory, Tokyo Institute of Technology, Yokohama 226-8503

[A] Department of Applied Chemistry, Kanagawa Institute of Technology, Atsugi 243-0292

$CaTiO_3$ is one of alkaline earth titanates with perovskite structure. However, the crystal structure of $CaTiO_3$ is not an ideal cubic perovskite type but a $GdFeO_3$ type with orthorhombic distortion, because the ionic radius of Ca ions is smaller than that of Sr or Ba ions.[1] These alkaline earth titanates are known to show n-type conduction by proper donor doping and have several fascinating properties in electrical and optical applications. Extensive and intensive studies on their electronic structures have been undertaken to find the origins of the properties, especially in the cases of $SrTiO_3$ and $BaTiO_3$. Only a few studies have been reported in the case of $CaTiO_3$, probably because of less popularity in practical applications and the complication in the crystal structure. However, analysis of its electronic structure would be as meaningful as that of other titanates', because understanding of the electronic structures through a series of the alkaline earth titanates may provide us with an essential clue to reveal the nature of the attractive properties.

Photoemission spectroscopy (PES) is known as an effective method to observe valence bands of materials. However, since conduction bands play important roles in n-type oxide semiconductors, the observation of the conduction bands is significant to understand the electroconductive properties of the n-type oxide semiconductors. Therefore, inverse photoemission spectroscopy (IPES), X-ray absorption spectroscopy (XAS), and electron energy loss spectroscopy (EELS) are more useful for the n-type oxide semiconductors than PES. In the present report, the XAS spectra of $CaTiO_3$ were measured and compared with the EELS spectra obtained on a transmission electron microscope and the results of an energy band calculation, mainly the partial density of states (PDOS).

Single crystals of $CaTiO_3$ were prepared by the floating zone method using an infrared furnace. H_2-reduced crystals doped with Y 0.01at% were used in the XAS measurements to avoid charging effects. On the other hand, nominally non-doped crystals were used in the EELS measurements. XAS measurements for Ca $L_{2,3}$ edges, Ti $L_{2,3}$ edges and O K edge were carried out on BL2B1 of UVSOR in Institute for Molecular Science. The surface of a sample was scraped by a diamond file at a pressure of $\sim 10^{-9}$ Torr before the measurements and the spectra were obtained under a vacuum of $\sim 10^{-10}$ Torr. EELS spectra for Ca $L_{2,3}$ edges, Ti $L_{2,3}$ edges and O K edge were measured on the transmission electron microscope (Hitachi : H9000NAR) equipped with a LaB_6 electron source and an electron energy loss spectrometer (Gatan : 676). An empirical energy band calculation by the tight-binding method was carried out to interpret the spectra.

Figure 1 shows the XAS and EELS spectra for (a) Ca $L_{2,3}$, (b) Ti $L_{2,3}$, and (c) O K edges in $CaTiO_3$. The XAS spectra are adjusted to the EELS spectra in energy scale so that the energy of peak tops will meet each other between these spectra. Intensities of these spectra are arbitrarily arranged to enable a comparison of the spectra. The XAS spectra and EELS spectra provide analogous structure in the three absorption edges although the former gives sharper bands because of the higher energy resolution. Two bands were observed at 348 and 351 eV in the Ca $L_{2,3}$ edges (fig.1a), and they are attributed to the L_2 and L_3 edges, respectively. The spectra for Ti $L_{2,3}$ edges (fig.1b) are also interpreted in the similar manner, except that each unoccupied band is split into two bands under the influence of octahedral crystal fields. Therefore, a pair of bands at 458 and 460 eV is ascribed to the L_2 edge, and the other one at 463 and 465 eV is to the L_3 edge. The XAS spectrum for the Ti $L_{2,3}$ edges in $CaTiO_3$ is similar to that in $SrTiO_3$ reported by Abbate et.al.[2] because of analogous environments for Ti ions. Although the observation of Ca and Ti L_1 edges was tried, no prominent absorption was detected. The O K edge (fig.1c) shows four bands at 531, 534, 536 and 544 eV. Since the relative intensity of the O K edge was lower than those of the Ca $L_{2,3}$ and Ti $L_{2,3}$ edges, the spectra of the O K edge were somewhat noisy, especially for the EELS spectrum. The energies of the absorption edges are approximately estimated from the lower-energy edge of the observed bands to be 346 and 349 eV for the Ca L_2, L_3 edges, 456 and 461 eV for the Ti L_2, L_3 edges, 530 eV for the O K edge, which are close to the energies reported by Bearden and Burr.[3]

XAS and EELS spectra generally provide PDOSs of conduction bands. Therefore, the spectra correspond mainly to intra-atomic excitations and they are unique to each element in materials. Recalling the selection rule for the electric dipole transition, transitions to s or d orbitals are allowed for $L_{2,3}$ edges and transitions to p orbitals are permitted for a K edge. Therefore, it is expected that the Ca $L_{2,3}$ edges show the transition to a Ca 4s band, the Ti $L_{2,3}$ edges do the transition to Ti 3d and 4s bands, and the O K edge does the transition to an O 2p band in the anti-bonding states. If we assume that the band width of the initial states, that is the core levels, in each transition is negligibly small, the structure of the spectra is substantially derived from the structure of the final states, that is, the PDOSs of the conduction bands for each element. Therefore, the XAS spectra were

compared with the results of an energy band calculation. In the cases of the Ca and Ti spectra, the L_3 edges were eliminated in the way that the high energy sides of the L_2 edges were smoothly extrapolated to zero. Although this operation erases the information about PDOSs at higher energy such as the PDOS of a Ti 4s band, the processing of the spectra is clear and reproducible because of its simplicity.

Figure 2 shows the comparison of the XAS spectra with the PDOSs obtained by the tight-binding energy band calculation. Although there is no relation in intensity between the XAS spectra and PDOSs, the XAS spectra of Ca, Ti, and O edges or the PDOSs of these elements are relatively arranged in intensity among themselves. The bottom of the conduction band is set to zero in energy scale for the PDOSs. The energy scale for the XAS spectra was taken so that they will fit to the respective PDOSs. Although the comparison may be somewhat artificial, it is based on the selection rule and provides reasonable results; The degree of the energy splitting by crystal fields for Ti ions is almost the same between its XAS spectrum and PDOS, and the energies of three bands in the O K edge agree well with the energies of the cations' bands in the XAS spectra indicating the anti-bonding states of O 2p bands. Although some deviation can be seen between the XAS spectra and PDOSs in intensity because of the neglect of the transition probability, they agree with each other qualitatively.

In conclusion, the XAS and EELS spectra of $CaTiO_3$ were measured to understand the electronic structure of the conduction band. The XAS and EELS spectra gave almost the same features between them, and the energy resolution of the XAS spectra was higher than that of the EELS spectra in the present experiments. It was understood from the comparison of the XAS spectra with the calculated PDOSs that the conduction band mainly consists of Ca 4s and Ti 3d bands with a small contribution of the O 2p anti-bonding bands.

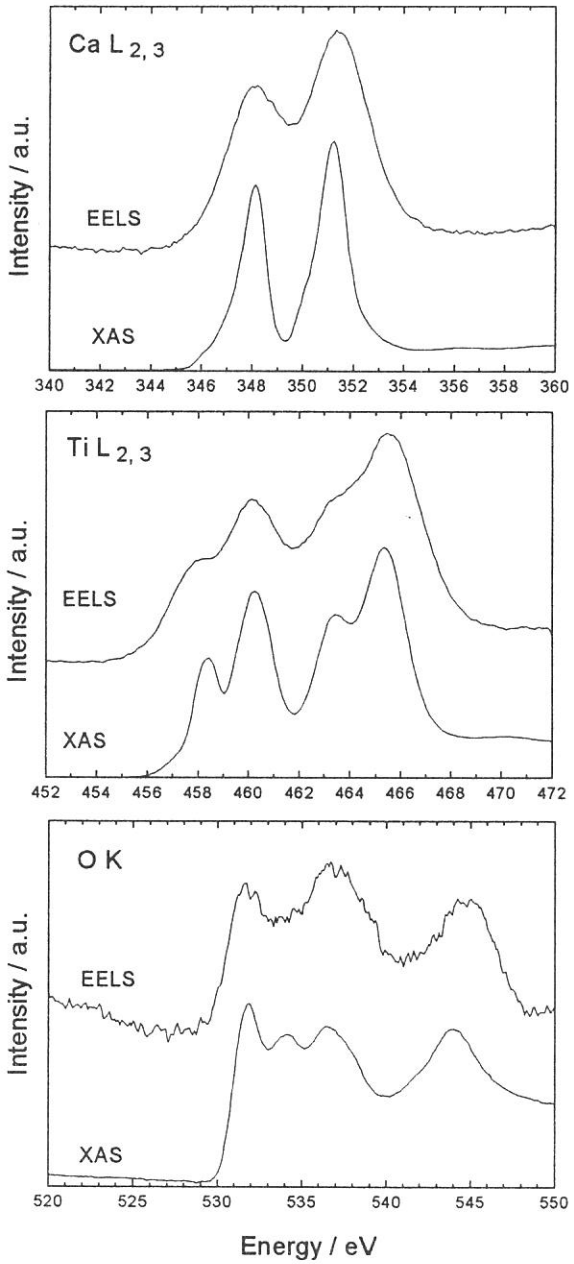

Figure 1 The XAS and EELS spectra for Ca $L_{2,3}$ (a), Ti $L_{2,3}$ (b), O K (c) edges in $CaTiO_3$.

References

[1] S. Sasaki, C.T. Prewitt, J.D. Bass, and W.A. Schulze, Acta Cryst. C43, 1668 (1987)

[2] M. Abbate, F.M.F. de Groot, J.C. Fuggle, A. Fujimori, Y. Tokura, Y. Fujishima, O. Strebel, M. Domke, G. Kaindl, M. Sacchi and N. Tsuda, Phys. Rev. B 44, 5419 (1991)

[3] J.A. Bearden, and A.F. Burr, Rev. Mod. Phys. 39, 125 (1967)

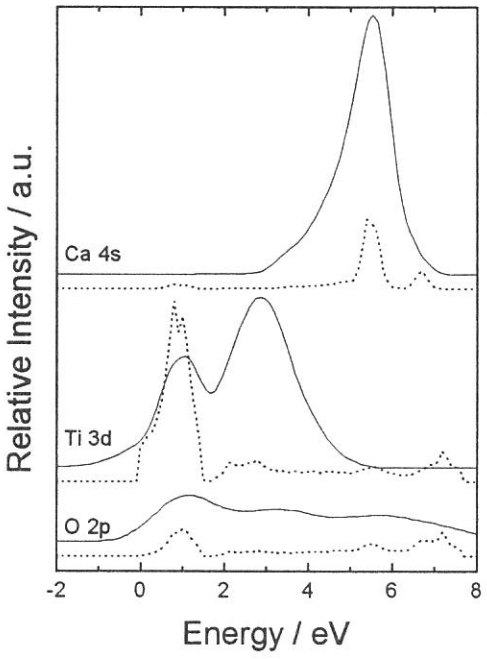

Figure 2 The comparison of the XAS spectra (solid lines) for Ca L_2 (top), Ti L_2 (middle), and O K (bottom) edges with the PDOSs (dotted lines) of Ca 4s, Ti 3d, and O 2p orbitals.

(BL2B1)

Tm5*p* resonant photoemission study of TmX (X=S, Se and Te) around 4*d*-excitation region

Krishna G. NATH, Yüksel UFUKTEPE[A*], Shin-ichi KIMURA[A], Toyohiko KINOSHITA[A], Takeshi MATSUMURA[B], Takashi SUZUKI[B], Haruhiko OGASAWARA[C] and Akio KOTANI[C]

Department of Structural Molecular Science, Graduate University for Advanced Studies, Okazaki 444 -8585
A) UVSOR facility, Institute for Molecular Science, Okazaki 444-8585
B) Department of Physics, Tohoku University, Sendai 980-77
C) Institute for Solid State Physics, University of Tokyo, Tokyo 106

In the 4*d*-4*f* resonant process of rare earth compounds, study of resonance behavior of core levels (5*p* or 5*s*) is important to understand overall decay processes related to different electronic states. In fact, the core level photoemission spectra in rare earth systems show complex multiplet structures due to existence of unfilled and localized 4*f*-shell[1]. Sometimes it is rather difficult to separate the spin-orbit peaks and the valence components if the system is mixed-valence. In this point of view, the resonance study of core levels is also significant to get clear picture of complex muliplet structures. Recently we have measured the resonant photoemission of 4*f*-states at the 4*d*-4*f* excitation condition of thulium compounds (TmS, TmSe, and TmTe) for divalent and trivalent Tm-ions[2]. It was found in that experiment that a large resonant enhancement occurs in Tm 4*f* emission around Tm4*d* absorption edges. As a consequence of that experiment, we measured the resonant photoemission of 5*p* levels around 4*d* threshold. In this report, we present the Tm-5*p* photoemission results at the 4*d*-4*f* absorption edges (hν = 150-200eV) of Tm-compounds.

The experiments were performed at the beam line, BL2B1, with Grasshopper monochromator. Photoelectrons from the sample were collected and analyzed by a double-pass cylindrical mirror analyzer. The base pressure of the chamber was 2×10^{-10} torr. The overall energy resolution was less than 0.5eV. The clean surfaces of the single crystal were obtained by scraping with diamond filler.

Figure 1(a) shows the on- and off- resonant 5*p* resonant photoemission results of mostly divalent compounds TmTe. The excitation energies are selected from the total yield (TY) spectra in Fig.1 (b). The peak position (~173eV) in Fig. 1(b) corresponds to 4*d*-4*f* resonance of Tm^{2+}. The shoulder at photon energy of ~178eV indicates the presence of small amount of Tm^{3+} in this mostly divalent compound. All dotted curves represent the calculation. The on-resonance spectra for 5*p* (Tm^{2+}) are shown in the upper panel in Fig.1 (a). The off-resonance spectra taken at hν=169eV are in the lower panel. It can be easily seen that Tm5*p* states show resonance enhancement at on-resonance condition. It is noticed that the resonance effect is larger for higher binding energy states, i.e. around 30eV than lower ones around 24eV.

In Figure 2(a), it is shown the resonance behavior of trivalent Tm5*p* of TmSe, a typical mixed-valent compound. Though the mostly trivalent TmS is the best to show the trivalent characteristics, the 5*p*-photoemission peaks taken at several on-resonance conditions are overlapped by LMM Auger transition from sulfur (S). So the true resonance effect can not be separated easily for TmS. Figure 2(b) represents the 4*d*-4*f* absorption spectrum for the both Tm^{3+} and Tm^{2+} components. This absorption spectrum is considered as a superposition of two spectra for two Tm-valences as shown by the calculated curves. The off –resonance photoemission spectrum taken at hν=169eV is shown in the lower panel of Fig. 2(a). At this photon energy position in the TY spectra, the both valence components are present with different ratio. As a result, the photoemission also shows the both Tm^{3+} and Tm^{2+} components as seen by comparing the calculated curves for two valences. In the upper panel, the on-resonance spectrum taken at the photon energy of ~178eV reflects the trivalent characteristics. It is found that the spectrum shows the enhancement in trivalent parts due to the resonant effect.

The decay channel 4*d*5*p*4*f* explains the resonance behavior of Tm5p at 4*d*-4*f* resonance. Though the intrinsic photoionization cross-section of 5*p* level is not so strong as compared with the 4*f* level at the 4*d*-4*f* absorption ranges, the 5*p*-photoemission still shows resonance at this 4*d*5*p*4*f*-decay channel. 5*p*-photoemission cross section (total) for photon energy $h\nu_{4d}$ near 4*d* edge can be written as:

$$\sigma(h\nu_{4d}) = \sigma^{0}(h\nu_{4d}), \text{ normal part } + \sigma^{res}(h\nu_{4d}), \text{ resonance part.}$$

The resonance contrast can be written as:

$$\xi_{nl}(h\nu_{4d}) = \sigma(h\nu_{4d})/\sigma^{0}(h\nu_{4d}).$$

For 5*p*(Tm^{3+} in TmSe), the value of resonance contrast is about 3. On the other hand this value is 4.25 for 4*f*(Tm^{3+} in TmSe). So at 4*d*-4*f* resonance,

$$[\xi_{5p}/\xi_{4f}] \times 100\% = 70\%$$

This indicates that 4*d*5*p*4*f*-decay channel is also active but not so strong as 4*d*4*f*4*f* decay channel.

Another interesting observation of this 5*p* resonant photoemission is that the apparent values of spin-orbit splitting between $5p_{3/2}$ and $5p_{1/2}$ states are not easily defined because of multiplet structure. Oh and co-workers[3] have reported the values of 5*p* spin-orbit splitting of Tm^{3+} and Tm^{2+} for TmSe. They did not mention the multiplet structure in 5*p* photoemission. Recently, resonant effect of 5*p* for Tm-metal has been studied by Nicklin *et al*[4]. Though they mentioned multiplet peaks by the help of calculation, they also defined $5p_{3/2}$ and $5p_{1/2}$ states for several peaks. In fact, there is no meaning to estimate the values 5*p* spin-orbit-splitting peaks or to define directly the $5p_{3/2}$ and $5p_{1/2}$ peaks in the presence

of multiplet structures. Our experiments show broadened feature of $5p$ photoemission peaks due to complex structure in both figures, 1(a) and 2(a). At the same time the calculated line and convoluted spectra indicate the same feature like experiment.

In conclusion, the $5p$ photoemission shows resonance behavior at $4d$-$4f$ excitation range for Tm-compounds. The strength of $5p$-decay channel is comparable with $4f$-decay channel in 4d-$4f$ excitation process. The photoemission spectra for two Tm-valences are defined by complex multiplet structures, not by single $5p_{3/2}$ or $5p_{1/2}$ peak.

We would like to thank the staff members of UVSOR facility staff for their technical support.

*Visiting Scientist on leave from Physics Department, University of Cukurova, 01330 Adana, Turkey

1. A.Kotani, Inner shell photoelectron process in solids, (Hand book on synchrotron Radiation, vol.2, edited by G.V.Marr (North-Holland Physics publishing, Amsterdam, 1987).
2. Y.Ufuktepe et al. submitted to J. Phys. Soc. Jpn.: UVSOR activity report (1996), p102.
3. S. -J. Oh *et al.*, Phys. Rev. B **30,** 1937 (1984).
4. C. L. Nicklin *et al.*, Phys. Rev. B **52,** 4815 (1995).

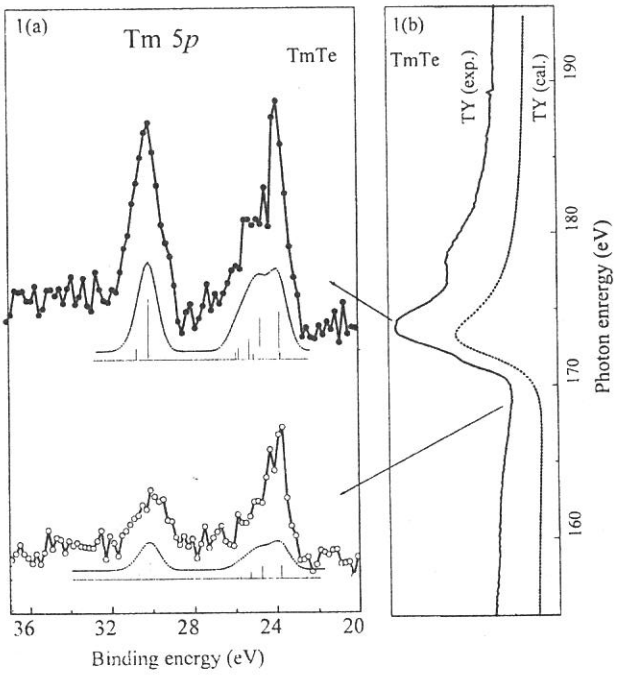

Figure 1. (a):Tm $5p$ resonant photoemission spectra for TmTe. (Upper): the on resonant. (Lower): the off resonant. The dotted curves represent the calculation. The excitation energies are taken from the total yield (TY) spectrum given in Fig. 1(b). In this absorption spectrum, the peak at ~173eV is the on-resonance condition of divalent Tm-ion.

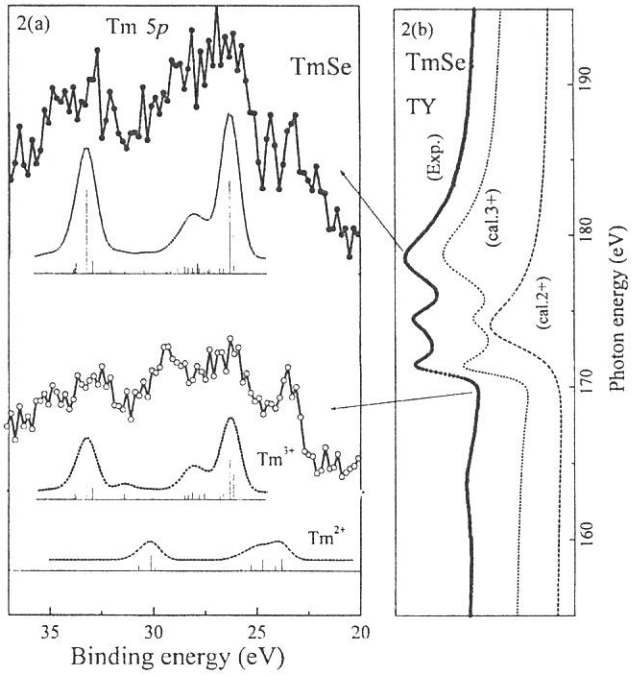

Figure 2. (a):Tm $5p$ resonant photoemission spectra for TmSe. (Upper): the on-resonance spectrum to show the trivalent characteristics. (Lower): the off resonant one. The dotted curves represent the calculation. The excitation energies are taken from the total yield (TY) spectrum given in Fig. 2(b). The TY shows the mixed valent characteristics as shown by calculation. Because of long tail of the divalent part, the off-resonance $5p$-photoemission show mixed behavior. This is also shown by calculation.

(BL5B)

Photoelectron Spectromicroscopy Study of $(DI\text{-}DCNQI)_2M$ (M=Ag, Cu)

Yuichi Haruyama[A], Krishna G. Nath[B], Yüksel Ufuktepe[C], Ko-ichi Hiraki[D,A], Kazushi Kanoda[D,A], Shin-ichi Kimura[A], and Toyohiko Kinoshita[A]

[A] *Institute for Molecular Science, Myodaiji, Okazaki 444-8585, Japan*

[B] *Department of Structural Molecular Science, Graduate University for Advanced Studies, Okazaki 444-8585, Japan*

[C] *Physics Department, University of Cukurova, 01330 Adana, Turkey*

[D] *Department of Applied Physics, University of Tokyo, Bunkyo-ku, Tokyo 113-0033, Japan*

The crystal structures of $(DI\text{-}DCNQI)_2M$ (M=Ag, Cu), where DI-DCNQI is 2,5-diiodo-*N*,*N'*-dicyanoquinonediimine, are isostructural with a space group $I4_1/a$, whereas the physical properties are quite different from each other. In the electrical resistance [1], $(DI\text{-}DCNQI)_2Cu$ (abbreviated DI-Cu) shows metallic conductivity down to low temperature, on the other hand, $(DI\text{-}DCNQI)_2Ag$ (DI-Ag) shows semiconducting nature with a gap of 490K. The difference in the physical properties is considered to arise from the *d* band position of M ion. Although the photoemission is a direct method to investigate these electronic structures, the photoemission study for the single crystals DI-Ag and DI-Cu has not been performed so far. The reason is that the size of these single crystals is not large enough to carry out the photoemission experiments. However, photoelectron spectromicroscopy apparatus can do the experiment. Therefore, we have measured the photoemission spectra for DI-Ag and DI-Cu using the photoelectron spectromicroscopy [2].

Needlelike shaped single crystals of DI-Ag and DI-Cu were synthesized by electrochemical reduction as reported elsewhere [1]. The typical sample size used here was smaller than $\phi 100\times1000\mu m^2$. These samples were characterized by x-ray diffraction, electrical resistance, magnetic susceptibility and NMR measurements [1]. The clean sample surfaces were obtained by 0.5 keV Ar ion sputtering for 10 min. The cleanliness was confirmed by x-ray photoemission spectroscopy for the absence of extra features arising from the contaminations. Photoemission experiments were carried out by using a conventional UHV system (FISONS, ESCALAB-220i-XL) at a base pressure of 2×10^{-8} Pa [2]. Total instrumental energy resolution was 0.3 ~ 0.6 eV full width at half maximum (FWHM), depending on the photon energy ($h\nu$) in the energy range of 30 ~ 200 eV. All experiments were performed at room temperature.

Figures 1(a) and 1(b) show the photoemission spectra of DI-Ag and DI-Cu, respectively. The detection area of the photoemission spectra was 50μm, which is smaller than the sample size. The light polarization (**E**) was parallel to the c-axis of DI-Ag and DI-Cu. The photoemission spectra were normalized to the maximum intensity of the valence band. For DI-Ag, four features in this valence band are observed at ~1.0, 3.5, 5.0 and 8.0 eV labeled A, B, C and D, respectively. Although the prominent feature C has the maximum intensity for every photon energy, the relative intensity of these features is varied as the photon energy changes. From the photon energy dependence of the photoionization cross section [3], the features A, B and D are predominantly derived from N and C 2*p*, and the feature C is from Ag 4*d* bands. Another feature is observed at ~10 eV with $h\nu$ = 40 eV. This feature is assigned to the Auger signal. For DI-Cu, three features are observed at ~3.5, 6.5 and 10.0 eV labeled E, F and G, respectively. The relative intensity of the features F and G to the feature E is gradually decreased with increasing $h\nu$. This photon energy dependence shows that the features F and G are predominantly derived from N and C 2*p*, and the feature E is from Cu 3*d* bands. Here, we compare the *d* bands of the M ion in both DI-Ag and DI-Cu. As assigned above, the Ag 4*d* bands for DI-Ag are located around 5 eV and localized within 2.5 eV width. For DI-Cu, the Cu 3*d* bands are situated around 3.5 eV and show broader

band width. This is a direct evidence of the localized nature of Ag 4*d* electrons and the itinerant nature of Cu 3*d* electrons. As Ag has much deeper *d* levels than Cu, DI-Ag has smaller $p\pi$-*d* hybridization with the DCNQI molecule than DI-Cu. These results are consistent with the band calculation [4].

In figures 2(a) and 2(b), the polarization dependence of the photoemission spectra is shown for DI-Ag and DI-Cu, respectively. The photoemission spectra were normalized to the background intensity at ~12 eV. Although the polarization dependence of both DI-Ag and DI-Cu is observed reflecting the anisotropy of the crystal structure, the stronger dependence is seen for DI-Ag as compared with that for DI-Cu. This results indicate that the anisotropy of the electronic states is stronger for DI-Ag than DI-Cu.

References

[1] K. Hiraki and K. Kanoda, Phys. Rev. **B 54**(1996)17276.

[2] T. Kinoshita, K. G. Nath, Y. Haruyama, M. Watanabe, S. Yagi, S. Kimura, and A. Fanelsa, submitted to J. Electron Spectrosc. Relat. Phenom.; T. Kinoshita, K. G. Nath, M. Watanabe, S. Yagi, S. Kimura, and A. Fanelsa, UVSOR Activity Report 1996, p.154.

[3] J. J. Yeh and I. Lindau, Atomic Data and Nuclear Data Tables **32**(1985)1.

[4] T. Miyazaki and K. Terakura, Phys. Rev. **B 54**(1996)10452.

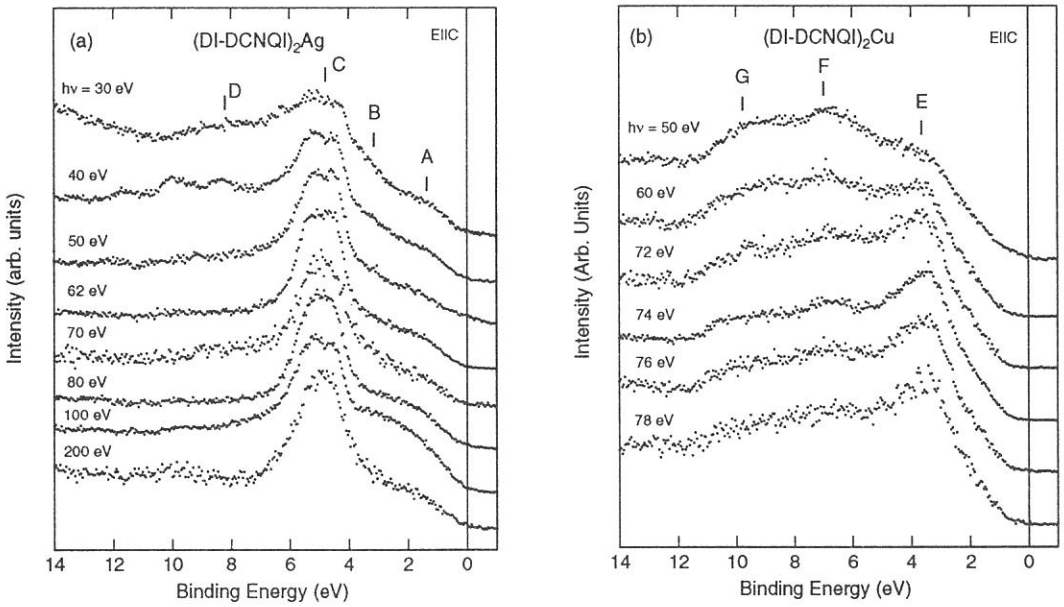

Figure 1. The photon energy dependence of the photoemission spectra (a) of $(DI\text{-}DCNQI)_2Ag$, (b) of $(DI\text{-}DCNQI)_2Cu$. The detection area was 50μm.

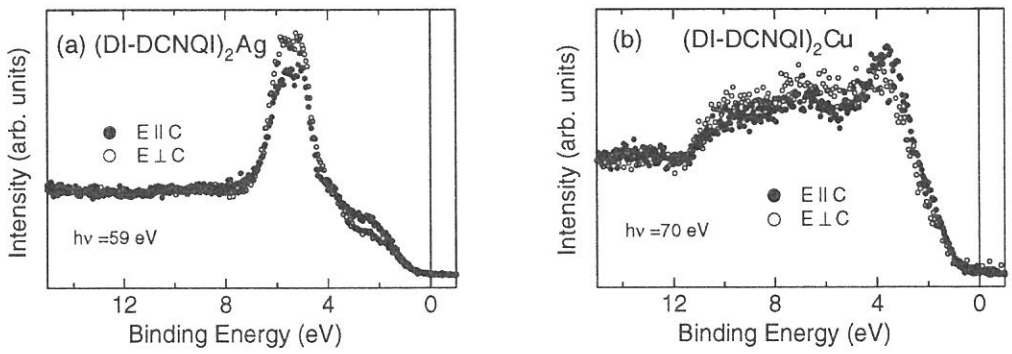

Figure 2. The polarization dependence of the photoemission spectra (a) of $(DI\text{-}DCNQI)_2Ag$, (b) of $(DI\text{-}DCNQI)_2Cu$. The detection area was 50μm.

(BL5B)

Study of magnetism in Ni-thin film by magnetic linear dichroism (MLD) of Ni-3*d* states around the Ni-3*p* threshold

Krishna G. NATH, Yuichi HARUYAMA[A], Shin-ichi KIMURA[A]

Yüksel UFUKTEPE[A*] and Toyohiko KINOSHITA[A]

Department of Structural Molecular Science, Graduate University for Advanced Studies, Okazaki 444-8585
A) UVSOR facility, Institute for Molecular Science, Okazaki 444-8585

It is now well known and firm established that the ultrathin film in nanometer range of 3*d*-materials often shows very interesting and striking magnetic properties different from its bulk. Because of rich variety of unusual magnetic properties in these nearly two-dimensional systems, the thin film magnetism is getting much more interest from both experimentalists and theoreticians[1]. By varying the preparation conditions, i.e., different substrates (non-magnetic, magnetic or semiconductor), substrate temperatures or deposition rate, film thickness, one can modify the structural properties as well as the magnetic properties of the film.

Magnetic Dichroism (MD) effect in both the photoemission and photoabsorption is considered to be one of the most powerful methods to study the magnetism. It provides information of both the surface and interface magnetism. The absolute value of MD intensity can be used to identify the degree of magnetic ordering, since it is proportional to the net system magnetization[2]. The study of element specific magnetism can be done easily by the MD effect selecting different electronic levels of multilayer component. MD experiment in the photoelectron spectroscopy can be performed by using circularly, linearly, or unpolarized light. By using linearly polarized light in the UVSOR facility, it is possible to perform successfully the dichroism experiment for studying the magnetism in thin film system. Here we report the results of magnetic linear dichroism (MLD) of Ni-3*d* states around the Ni-3*p* threshold of ultrathin Ni film grown on fct Co (100).

In order to perform these experiments, the VG ESCALAB 220i-XL[4] system with base pressure of 2×10^{-10} mbar was connected to the beam line. The total energy resolution of the photoelectron spectra at photon energy of 67.2eV was 300meV, which is estimated from the width of the Fermi edge in the spectra of Ni. The photoemission experiments and film evaporation were carried out in room temperature. The Cu (100) substrate was prepared by several cycles of Ar ion sputtering and subsequent careful annealing until sharp LEED pattern was seen. The magnetic substrate Co (100) was grown on Cu (100) to thickness of approximately 10 ML (~18Å). The Co film in this range of thickness exhibits a tetragonally distorted fcc structure having layer spacing of ~1.73Å along Cu [001] direction[3]. The Ni film evaporated on the fct Co (100) also shows same growth structure like Co on Cu (100) that was confirmed by LEED. All films were evaporated from a water-cooled evaporator. High purity (4N) Ni and Co rods were used for the evaporation. The deposition rate, ~0.8ML/min, was calibrated by a quartz thickness monitor placing the same position of sample before and after the deposition.

The geometry of the MLD experiment is described in Figure 1. The sample surface is parallel to the XY plane. Cu [100] direction is along Y-axis. The electric vector (E) of s-polarized light impinges on the sample surface at an angle $\alpha=15°$ out of XY-plane. Electrons are collected at an angle $\theta=8°$ out of the sample Z-axis (see inset). Thin film is magnetized along the both X and Y-directions in the XY-plane (in-plane magnetization). The dichroism signal is obtained by calculating the asymmetry; i.e. the difference between those two spectra divided by sum of them. In the linear dichroism measurements, the asymmetry between two spectra depends on the experimental geometry of light electric vector, electron emission and magnetization direction in the presence of spin-orbit (SO) splitting and exchange interaction[5].

In Figure 2, we show the Ni-3*d* MLD result for Ni(8ML)/Co(10ML)/Cu(100) taken at the photon energy of 67.2eV, i.e. the Ni-3*p* excitation energy.

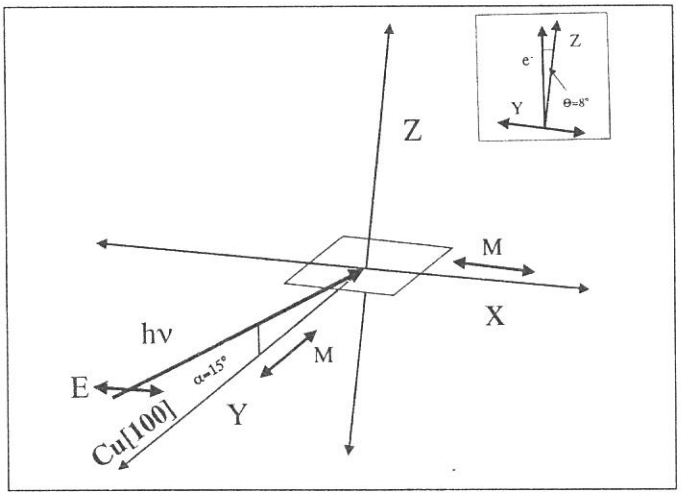

Figure 1. Schematic geometry of MLD experiment (see text).

The photoemission spectra (upper panel) show the two dominant peaks. One is near the Fermi level stated as main peak with $3d^9$ configuration. Other peak stays at 6eV below of the main peak. This is the so-called 6eV satellite peak assigning as $3d^8$ final state configuration. This satellite peak shows a strong resonant enhancement at the $3p$-excitation energy that was explained via super-Coster-Kronig (sCK) process[6]. The lower panel in Fig. 2 shows the intensity asymmetry between the two spectra taken for two magnetization directions parallel to X and Y-axes as in Fig. 1. This MLD signal is the direct evidence of the long-range ferromagnetic orderings on the Ni-film.

In the lower panel in Fig.2, both the main peak ($3d^9$) and the satellite peak ($3d^8$) show asymmetry but in opposite direction from each other. The $3p$-resonance effect on dichroism of different $3d$ states has been reported by S. Ueda *et al.* for Ni(110) sample[7]. In this previous result, the MLDAD (magnetic linear dichroism in angular distribution) does not show any asymmetry for 6eV-satellite region. But the MCDAD (magnetic circular dichroism in angular distribution) in their results shows asymmetry for 6eV-satellite region with an opposite direction of main peak. Our results are similar to this MCDAD result. Moreover we did not find any asymmetry for satellite peak at other off-resonance conditions. It can be interpreted that the resonance effect on MLD for satellite region is mainly guided by sCK process. A detailed theoretical interpretation is needed for clear understanding of dichroism behavior in this satellite region.

We can use these dichroism results to explorer the magnetic property in Ni-thin film. It has been reported that Ni-film on Cu (100) shows a transition from in-plane magnetization to perpendicular magnetization in the average region of ~7ML up to ~12 ML[8-9]. It was also reported by XMCD measurement[9] that Ni-film of above 9 ML on Cu (100) does not show any in-plane magnetization. But the situation is different for Ni/Co/Cu (100) system. In our MLD experiment, we found the in-plane magnetization for 11 ML Ni-film growth on magnetic Co substrate. But Ni of 12 ML on Cu (100) does not show any in-plane magnetization in our measurement, which is consistent with previous results.

Our dichroism measurement concludes that the resonance effect is present on MLD of 6eV satellite in the valence band photoemission whereas the main valence band peak shows same MLD signal for the both on and off resonance conditions. Magnetic orderings on different Ni-films are also verified by this experiment. The calculation of Ni-MLD is in progress.

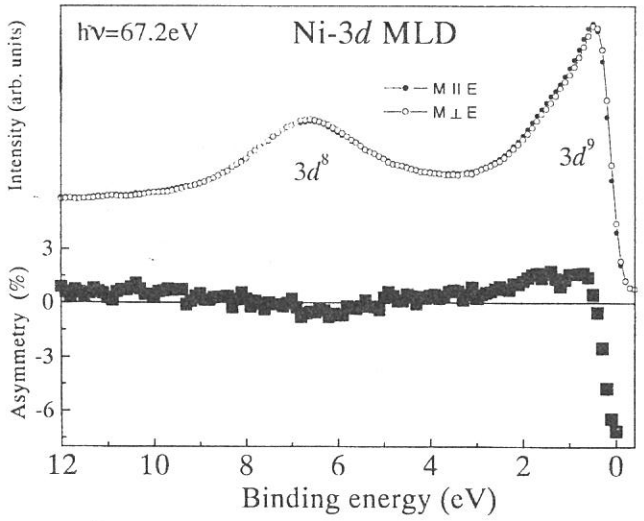

Figure 2. (Upper): Ni-3*d* photoemission spectra taken at 67.2eV- photon energy with s-polarized light (E||X). Dark circles: M ||E and open circles: M ⊥ E. Lower: Asymmetry of those two EDC's showing MLD in photoemission.

We would like to thank the staff members of UVSOR facility for their technical support.

* Visiting Scientist on leave from Physics Department, University of Cukurova, 01330 Adana, Turkey

1. M. T. Johnson *et al.,* Magnetic anisotropy in metallic multilayers: Rep. Prog. Phys. **59** (1996) 1409.
2. W. L. O'Brien *et al.*, Surf. Sci. **334** (1995) 10.
3. J. R. Cerdá *et al.*, J. Phys. Cond. Matt. **5** (1993) 2055.
4. T.Kinoshita *et al.*,UVSOR Activity Report, 96 (1997) 154: J. Electron Spectrosc. Relat. Phenom., in press.
5. R. Feder *et al.*, Magnetic Dichroism and Spin Polarization in Valence Band Photoemission, in Spin-Orbit-Influenced Spectroscopies of Magnetic Solids, edited by H. Ebert and G. Schütz, Springer (Berlin, 1995), p.85.
6. C. Guillot et *al.*, Phys. Rev. Lett. **39** (1977) 1632.
7. S. Ueda *et al.* J. Electron Spectrosc. Relat. Phenom., in print (private communication).
8. B. Schulz *et al.*, Vacuum **46** (1995) 1189.
9. W. L. O'Brien *et al.*, Phys. Rev. B **49** (1994) 15370.

(BL6A2)

SIMULTANEOUS MEASUREMENTS OF PHOTOELECTRON AND LUMINESCENCE OF BARIUM HALIDES

Masao Kamada, Shigeki Fujiwara,[a] Osamu Arimoto,[a] Yasuo Fujii,[b] and Shin-ichiro Tanaka

UVSOR Facility, Institute for Molecular Science, Myodaiji, Okazaki 444-8585, JAPAN
[a]Dept. of Physics, Okayama University, Okayama 700-8530, JAPAN
[b]Dept. of Appl. Physics, Osaka City University, Osaka 558, JAPAN

Barium halides have attracted much interest in recent years, because they show a variety of luminescence and resonant photoemission processes. The so-called Auger-free luminescence (AFL) due to a radiative transition between the valence band and a core level is observed in BaF_2 (1,2). A strong recombination luminescence is observed in BaFCl and BaFBr, which include impurities of rare-earth elements (3). Photoelectron spectra of barium halides show clear solid-state effects on the resonant photoelectron spectra (4). The luminescence has been applied to fast scintillation or registration of x-rays, but the detailed mechanism of the luminescence is sill not clear. Detailed comparison of the photoelectron and luminescence spectra is strongly desired. However, photoelectron and luminescence of barium halides have been measured independently so far. In this work, the irradiation effect on BaF_2 films is investigated using both photoelectron and luminescence spectroscopies. Time-correlation between photoelectrons and AFL photons is also studied for the first time, bringing additional information on the relaxation process of the core-level excited states.

Experiments were carried out at plane-grating monochromator beam line BL6A2. Photoelectron spectra were observed by using a hemispherical energy analyzer installed on a two-axes goniometer in an analyzer chamber, the base pressure of which was about $2x10^{-8}$ Pa. The angle of incidence of the exciting photon was 60°. The emission angle of the photoelectrons and the angular resolution were about 15° and 1.1°, respectively. Luminescence was collected with a quartz lens mounted in the analyzer chamber, and was focused in a conventional monochromator (Jobin-Yvon HR-320). The luminescence was observed by a photomultiplier (HAMAMATSU R943-02) or a CCD system (Princeton Inc.). The present spectra were not corrected for the spectral sensitivity of the detection system. To avoid charging up effects, BaF_2 thin films of 10-20 nm in thickness were prepared on the gold substrate by in-situ evaporation in a preparation chamber, the base pressure of which was $5x10^{-8}$ Pa, and then transferred to the analyzer chamber. The Baf_2 films were irradiated with zero-th order light from the plane-grating monochromator through an aluminum filter in order to investigate the irradiation effects. The energy range and flux of the incident photons were 17-150 eV and about 10^{14} phs/s/mm^2, respectively. The time-correlation between the photoelectrons and the AFL photons was observed by using a time-to-amplitude converter (TAC) system with a micro-channel plate photomultiplier (MCP-PM).

Figure 1 shows the luminescence spectra observed at every five-minute's irradiation intervals. The spectra consist of two luminescence bands at about 4.1 and 5.5 eV. The 4.1-eV band may be attributed to the self-trapped exciton (STE), although the energy position of the STE luminescence in BaF_2 films is slightly different from that in single crystals. The 5.5-eV band is AFL, which is due to an electron transition from a valence band to a Ba 5p core-level. Obviously, intensities of the STE luminescence and AFL decrease as the irradiation dose is increased. This figure shows that the decrease in AFL is larger than that in STE luminescence. It should be noted that the spectral shapes of the STE luminescence and AFL changed with irradiation. Especially, a shoulder becomes clear at 5.2 eV as the irradiation dose is increased. This result cannot be interpreted with the simple idea based on the density of states in the valence band. The present result indicates that AFL may be strongly affected by the crystal field around a core hole. This is consistent with the lattice-relaxation model proposed by Kayamuma et al (5).

Figure 2 shows the photoelectron spectra observed at every-five minute's irradiation intervals. The excitation photon energy is 90 eV, and the binding energy is presented relative to the maximum of the valence band. The valence band, Ba 5p3/2, and Ba 5p1/2 photoelectrons are observed at 2.5, 8.5, and 10.5 eV binding energy, respectively. The intensity of these photoelectrons decreases as the irradiation dose is increased, while new bands acquire appreciable intensity at +1.8 and +3.7 eV. According to Karlsson et al. (6), the F 2p states of CaF_2 on Si(111) are redistributed in energy by irradiation, and a new state with an initial-state energy of +5.5 eV is created. A half-filled band due to metallic surface and the suface Ca in a 1+ oxidation state are also observed near fermi level in their spectra. The present photoelectron spectra of BaF_2 show no clear structures due to Ba+1 states and metallic states near fermi level, but new structures are observed around +1.8 and +3.7 eV.

These irradiation-induced structures may be due to the F 2p states, which is different from unirradiated BaF_2. The decrease in intensity of the valence band and Ba-5p photoelectrons may also be attributed to irradiation effects of BaF_2 thin films.

Before irradiation, the condition Evc<Eg is satisfied, resulting in AFL, where Evc and Eg are the energy difference between a valence band and a Ba-5p core level and the band gap energy between a maximum of the valence band and a minimum of the conduction band, respectively. The irradiation-induced structures are produced at Ex (Ex=1.8-3.7 eV) above valence band, and then the condition changes to Evc>Eg-Ex. This causes the decrease in intensity of AFL as the irradiation dose is increased. The decrease in the intensity of the STE luminescence may be due to the defect-induced nonradiative decay process.

The time-correlation between Ba-4d photoelectrons and AFL photons was also observed. The result indicates that photoemission and luminescence processes correlate with each other.

REFERENCES

1) S. Kubota, M. Itoh, J. Ruan(Gen), S. Sakuragi, and S. Hashimoto, Phys. Rev. Lett. 60 (1988) 2319.
2) M. Itoh, S. Kubota, J. Ruan(Gen) and S. Hashimoto, Solid State Sci. 4(1990) 467.
3) A. Onishi, K. Kan'no, Y. Iwabuchi, and N. Mori, Nucl. Instrum. Methods B91 (1994) 210.
4) M. Kamada, K. Ichikawa, and O. Aita, Phys. Rev. B47 (1993) 3511.
5) Y. Kayanuma and A. Kotani, J. Electron Spectrosc. Relat. Phenom. 79 (1996) 219.
6)U. O. Karlsson, F. J. Himpsel, J. F. Morar, F. R. McFeely, D. Rieger, and J. A. Yarmoff, Phys. Rev. Lett. 57 (1986) 1247.

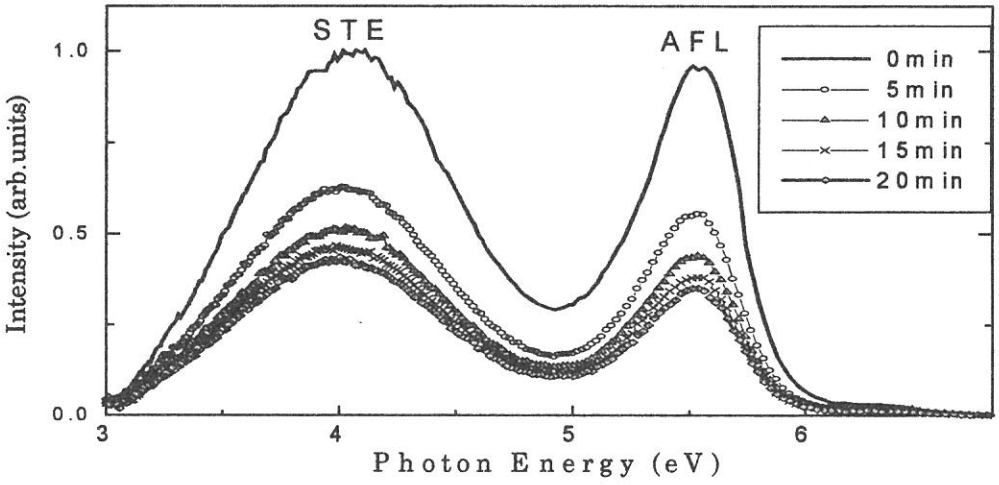

Fig. 1. Luminescence spectra of BaF2.

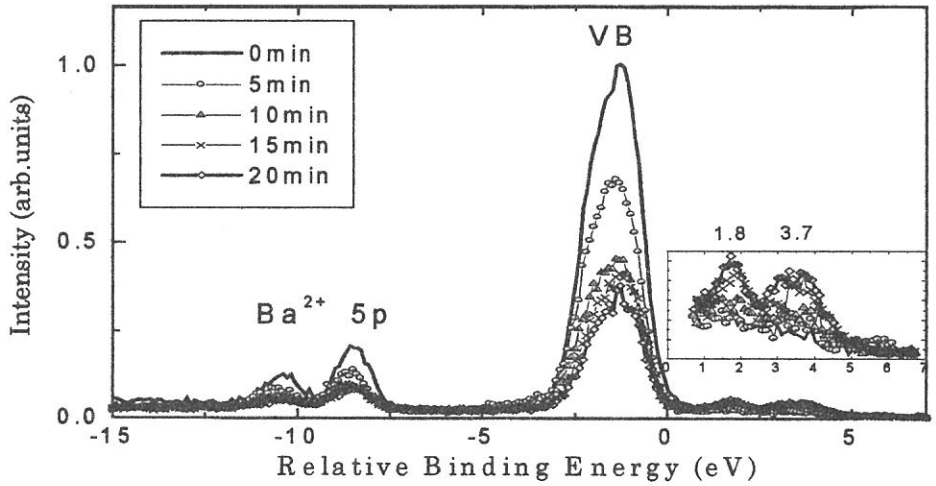

Fig. 2. Photoelectron spectra of BaF2.

(BL6A2)

Valence-Band Photoemission from PbF_2 and $PbCl_2$

M. Itoh, T. Shiokawa, K. Sawada and M. Kamada*

Faculty of Engineering, Shinshu University, Nagano 380-8553
**UVSOR Facility, Institute for Molecular Science, Okazaki 444-8585*

Lead-halide crystals exhibit a variety of interesting physical properties, with possible applications to high-energy particle detectors. Although there have been some earlier photoemission studies of Pb-halides, the nature of their valence bands (VB's) has not yet been understood satisfactorily. In the present experiment, we have performed ultraviolet photoemission spectroscopy (UPS) of PbF_2 and $PbCl_2$ with use of synchrotron radiation as a light source.

Photoelectron spectra were measured with an angle-resolved hemi-spherical analyzer, its resolution being kept at 0.2 eV. Thin film samples were fabricated *in-situ* by evaporation on gold substrates in a preparation chamber, and were then transferred into an analyzing chamber. Reagent-grade powders of PbF_2 and $PbCl_2$ from Merck were used as the starting materials. Thickness of the specimens was maintained at about 100 Å to avoid any charging effect.

For PbF_2, it was found that the spectral shape in the valence region changes seriously with irradiation time. A typical example observed under the excitation with 100-eV photons is shown in Fig. 1. Here, the measurements progressed repeatedly from (a) to (e), with a scanning time of 8 min for each spectrum. The curve (a) is the spectrum taken for a previously unexposed sample. The sample was exposed to 100-eV photons for 25 min before the next measurement. The binding energy is given relative to the top of the VB. Judging from the spectrum (a), the VB in PbF_2 is composed of, at least, three unresolved bands. As obviously seen, the central part of the VB spectra is reduced remarkably with irradiation time. On the other hand, the intensity of the Pb^{2+} 5*d* doublet around 20 eV increases slightly during the measurements, and its peaks shift toward the lower binding-energy side.

In contrast to PbF_2, the VB spectra of $PbCl_2$ did not change seriously even when a sample was exposed to photons for more than 1 hr. Figure 2 shows UPS spectra of $PbCl_2$ excited at different photon energies. It is clear that spectral shape of the VB in $PbCl_2$ is not sensitive to the change in excitation energies in the range 60 to 120 eV.

It seems very likely that the VB spectra of PbF_2 are deformed as a result of photon-stimulated desorption of fluorine atoms from the sample surface. In alkali and alkaline-earth halides, it has been believed that the decay of excited electronic states results in the formation of F-H defect pairs, which leads to ejection of the halogen atom from the sample surface [1]. We suppose that the similar dynamical process of defect formation, occurring within a few atomic layers of the surface, is also responsible for the fluorine desorption in PbF_2 which has fluorite

structure. On the other hand, $PbCl_2$ crystallizes in orthorhombic structure, where the interstitial space is not so open as PbF_2. Accordingly, the defect formation process leading to the chlorine desorption may not be easy to occur in $PbCl_2$.

Based on the present results, we suggest strongly that the central part of the VB in PbF_2 is dominated by fluorine $2p$ state, and the remaining upper and lower parts have lead $6s$ character with small contribution of fluorine $2p$ state. This is consistent with the theoretical calculation of the electronic structures of the VB in PbF_2 [2,3]. Furthermore, because of the similarity in the VB shape between PbF_2 and $PbCl_2$, it is also supposed that the electronic structure of the VB in PbC_2 is essentially the same as that in PbF_2.

Finally, it is noted in Fig. 1 that, when a PbF_2 sample is continuously exposed to photons, the Pb^{2+} $5d$ doublet shifts toward the low-binding-energy side, accompanied by a slight increase in intensity. This is likely due to environmental changes around Pb^{2+} ions induced by the fluorine desorption, with the result that the upper surface layer becomes increasingly lead enriched.

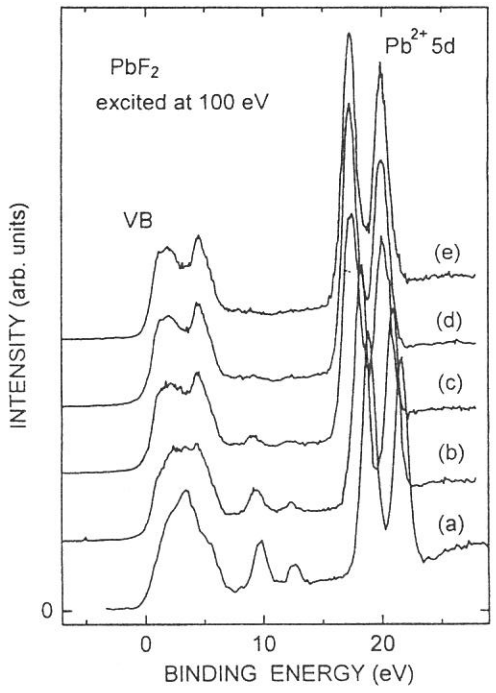

Fig. 1. UPS spectra of PbF_2 excited at 100 eV.

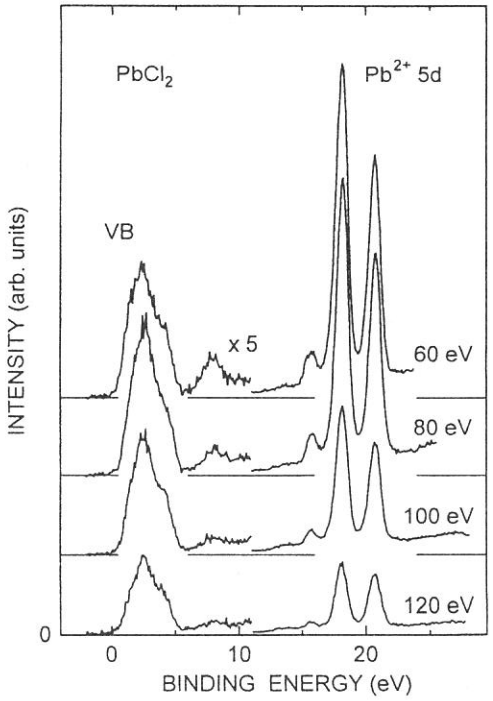

Fig. 2. UPS spectra of $PbCl_2$ excited at 60, 80, 100 and 120 eV.

[1] R.T. Williams: Rad. Effects and Defects in Solids 109 (1989) 175.

[2] M. Nizam, Y. Bouteiller, B. Silvi, C. Pisani, M. Causa and R. Dovesi: J. Phys. C: Solid State Phys. 21 (1988) 5351.

[3] R.A. Evarestov, I.V. Murin and A. V. Petrov: Sov. Phys. Solid State 26 (1984) 1563.

(6A2) **Photoemission studying of Ca-Mg-Ga amorphous alloys**

Nobuhiko Takeichi, Kazuo Soda and Uichiro Mizutani

Department of Crystalline Material Science, Nagoya University, Chikusa-Ku, Nagoya, 464-8603

Introduction

The electron transport properties of many nonmagnetic amorphous alloys have been reported. Especially a number of Ca-based amorphous alloys have been studied because of the fascinating electron transport properties. The resistivity is only 40μΩcm for Ca-Mg binary amorphous alloys, whereas more than 400μΩcm for Ca-Al and Ca-Ga binary ones. Mizutani et al.[1][2] revealed that the replacement of Al and Mg by Ga further increases the resistivity in the Ca-Al-Ga and Ca-Mg-Ga ternary amorphous alloys.

In the present work, We have measured UPS spectra for a series of $Ca_{10}Mg_{90-x}Ga_x$ amorphous alloys (x=0, 10, 20, 30, and 40) and the valence band structure has been discussed in comparison with the XPS spectra measured with the use of the laboratory XPS spectrometers. We show that the narrow Mg-Ga bonding states are formed immediately below the Fermi level as a result of the hybridization of Mg-3p and Ga-4p states and that the formation of this narrow p-states are responsible for the rapid increase in resistivity upon addition of Ga.

Experimental technique

UPS spectra were measured at the BL 6A2 in UVSOR of Institute for Molecular Science, Okazaki, Japan. The excitation energies in the range 12-20 eV was used to study the fine structure of the valence band structure near the Fermi level. Here the Fermi level was determined with reference to that of pure Au. The working pressure of the main chamber during measurement was kept less than 3.0×10^{-10} torr. A clean surface was achieved by using Argon sputtering technique.

Result and Discussion

We have measured the XPS valence band spectra for a series of the amorphous alloys in our laboratory (Surface Science). As is clearly seen in Fig 1, the XPS spectrum for the amorphous $Ca_{10}Mg_{90}$ alloy is well extended only with a shallow depression at the binding energy of 4 eV. However, we can see a substantial growth in the density of states immediately below the Fermi level when Ga is added to the amorphous $Ca_{10}Mg_{90}$ binary alloy. From the XPS valence band profile of the Mg_2Ga compound we conclude that the peak at 1.5 eV can be attributed to the formation of the bonding states between the Ma and Ga atom.

Further detailed information about valence band structure near the Fermi level can be extracted by studying the excitation energy dependence of the photoemission valence band spectra.This is accomplished by using the synchrotron radiation in the energy range 10-20eV. Fig 2 shows the photoemission spectra with different excitation energies for the two amorphous alloys with x=0and 30.

As is clearly from observed spectra, the intensities just below the Fermi level are high when the excitation energy is below 14 eV and are much stronger in the x=30 than in the x=0 amorphous alloy. Intensities just below the Fermi level gradually

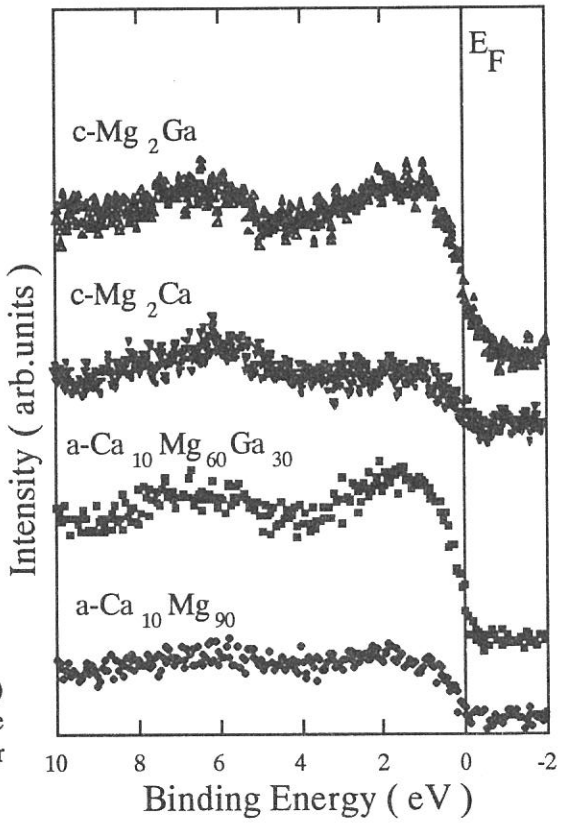

Figure 1.
XPS spectra for two amorphous $Ca_{10}Mg_{90-x}Ga_x$ (x=0,30) alloys. The data for $MgZn_2$-type Mg_2Ca and $LiSb_2$-type Mg_2Ga intermetallic compounds are also shown for comparison.

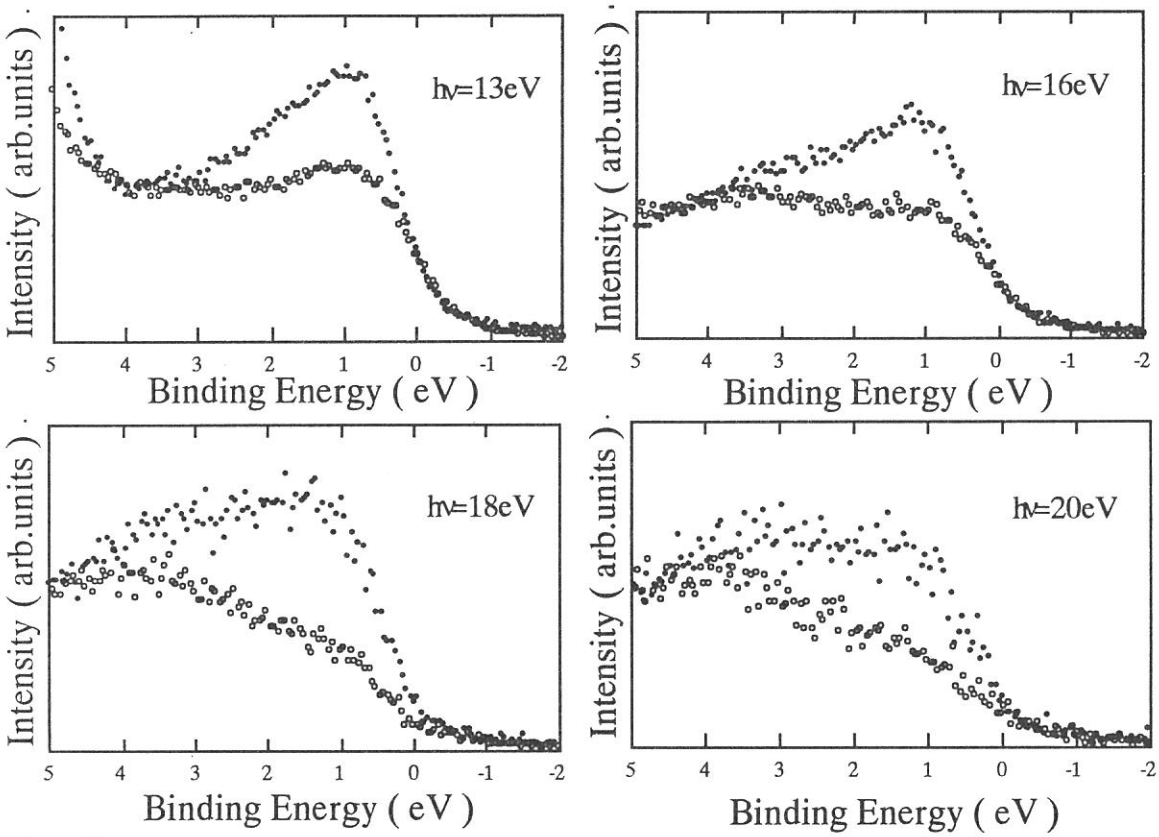

Figure. 2.
UPS spectra for two amorphous $Ca_{10}Mg_{90}$ (○) and $Ca_{10}Mg_{60}Ga_{30}$ (●) alloys.The spectra were taken with the excitation energies of hn = 13, 16, 18 and 20 eV.

decrease with increasing excitation energies in both amorphous alloys. In contrast, the intensities at the binding energy around 4eV increase with increasing excitation energy in both amorphous alloys. According to the calculations of the atomic subshell photoionization cross section[3], the cross section due to p electrons is larger than that of the s electrons in the excitation energy range below 14 eV. But this situation reverses when the excitation energy is increased above 14 eV. The valence band in the $Ca_{10}Mg_{90}$ amorphous alloy is dominated by the Mg-3p,3s states. From the excitation energy dependence of the cross section, We conclude that the Mg-3p states dominate near the Fermi level and the Mg-3s states at binding energy around 4eV.

In contrast to the x=0 amorphous alloy, the intensities immediately below the Fermi level are greatly increased in the x=30 amorphous alloy. This enhancement can be now attributed to the growth of the Ga-4p states hybridized with the Mg-3p states. This hybridization produces the narrow density of states immediately below the Fermi level for the x=30 amorphous alloys and leads to a substantial increase in resistivity in this system.

[1]U. Mizutani, M. Sasaura, Y. Yamada and T. Matsuda; J. Phys. F: Metal Phys. **17** (1987) 667
[2]Z. Diao, Y. Yamada, T. Fukunaga, T. Matsuda and U. Mizutani; Mat. Sci. Eng. **A181/A182** (1994) 1047
[3]J. J. Yeh and I. Lindau; At. Data Nucl. Data Tables **32** (1985) 1

(BL7A)

Mo L_3-edge XANES Study of Hydrogen Molybdenum Bronze

Kentaro NAKAMURA, Kazuo EDA, Noriyuki SOTANI

Department of Chemistry, Faculty of Science,
Kobe University, Nada, Kobe, 657, Japan

Introduction

Hydrogen molybdenum bronze, H_xMoO_3 ($0<x\leqq 2$), is obtained from MoO_3 by reduction of hydrogen in an acidic media or by hydrogen spillover. Four distinct phases have been confirmed in the region $0<x\leqq 2$ by Birtill and Dickens.[1] Eda[2] has studied the thermal decomposition of Type-I ($0.21\leqq x\leqq 0.4$) in a nitrogen atmosphere and discussed the decomposition mechanism. He suggested that the decomposition process took two ways depending on the density of defect in the sample. One is the way to MoO_2 through high defect density and the other, to MoO_3 through the MoO_3 like structure. In both cases, the removal of lattice oxygen in nitrogen or *in vacuo* produces a defect structure. The defect structure can be expected to be effective for catalytic reaction, so that it is interesting to know the detailed structure. We investigated Type-I by heat treatment *in vacuo* by XANES.

Experimental

Hydrogen molybdenum bronze, H_xMoO_3, (x=0.25:Type-I) was obtained by the method described previously.[3]

XANES (X-ray Absorption Near Edge Structure) spectrum was measured at BL-7A of UVSOR at Institute of National Laboratory for Molecular Science, Okazaki, Japan, using a Ge (111) two-crystal monochrometer. After the sample was evacuated to $< 1.0\times10^{-7}$ torr in the sample chamber, the spectrum was measured in total electron yield mode at room temperature.

Result and Discussion

We measured the XANES spectra by the total electron yield mode method and the penetration range of the spectra was possibly several tens angstroms into the bulk. The observed XANES spectra can reflect the surface and/or near the surface structure of the sample. Figure 1 shows the Mo L_3-edge XANES spectra of standard materials of Type-I, MoO_3, and MoO_2. Type-I and MoO_3 has a octahedral symmetry and the spectra show two distinct peaks. The peak at a lower energy side is higher than that at a higher one. The peaks are attributed to the electron transition from $2p_{3/2}$ to a vacant 4d state, t_{2g} (d_{xy}, d_{xz} and d_{yz}) and e_g ($d_{x^2-y^2}$ and d_{z^2}). The peak height at the low energy side differs from that at the high energy side. This difference is due to the difference in the transition cross section of the molecular orbital of Mo(4d)-O(2p); theoretically, the intensity is $t_{2g} : e_g = 3 : 2$ for octahedron. The spectrum of Type-I appeared at little lower energy side than that of MoO_3. Type-I make a minor rearrangement in the Mo-O framework of MoO_6 octahedron which is caused by insertion of hydrogen into MoO_3 intra-layer.[4] The hydrogen atoms are stabilized by bonding to the lattice oxygens in the intra-layer.[4] The energy gap between the peak to peak width, Δ, is used as a parameter of the ligand field splitting of the final state 4d orbital because of reflecting the coordinated environment around Mo atom.[5-7] The second derivatives as shown in Fig.1(II) are used to determine the energy gap. Δ of Type-I and MoO_3 was determined to be 3.2 and 3.4eV, respectively. This result is very reasonable because Δ takes 3.1~4.5eV for the octahedral compounds as shown in Table 1. We obtained Δ=2.5eV for MoO_2. This value was good agreement with that of the reported value of 2.4eV.[7] Δ of MoO_2 having Mo^{4+} ions should be smaller than that of the material having Mo^{6+} ions, because of the less effect of perturbation by the ligand field of six O ions. This result indicates clearly that the reduction of Mo ions leads to the condensation of a total 4d state, and makes the energy gap much smaller.

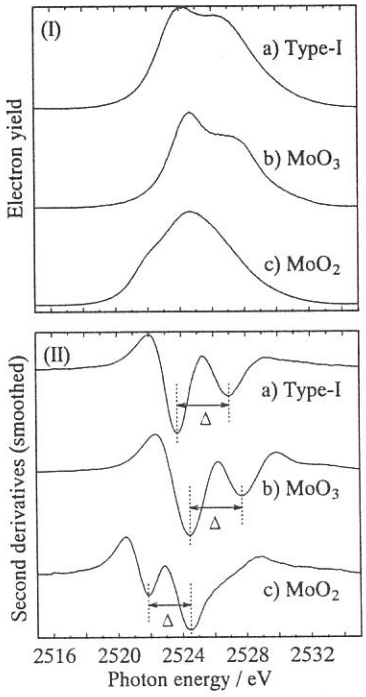

Fig.1 Mo L_3-edge XANES spectra (I) and the second derivatives (II) of reference compounds; a) Type-I, b) MoO_3 and c) MoO_2.

Figure 2 shows the Mo L_3-edge XANES patterns (I) and their second derivatives (II) of Type-I treated at various temperatures *in vacuo*. Δ is summarized in Table 1. The XANES spectra looked like no change at all treated temperature. The second derivative above 723K showed the interesting peak at around 2522eV. Below 673K Δ took 3.1~3.2eV, and above 673K, that gave two value, 3.1~3.2eV and 2.2eV. The former Δ is due to Type-I and/or MoO_3 which have octahedral symmetry, and the later, to MoO_2. We observed MoO_2 by XRD when Type-I was treated at 573K *in vacuo*. It suggests the formation of MoO_2 is easier by about 150K in the bulk than that on the surface. Moreover, we have reported that the formation of MoO_2 is accompanied by the formation of the defect structure. This result strongly suggests the formation of the defect structure in the bulk of Type-I and its diffuse to the surface. We are now studying to reveal the surface composition and their proportion.

Table 1 d-orbital splitting, Δ, of molybdenum compounds.

Sample	Local Structure	Δ / eV
$CoMoO_4$	octahedral	3.3[6]
MoO_3	octahedral	3.4*, 4.0[6], 3.4[7]
Type-I **	octahedral	3.2*, 3.1[7]
Type-II **	octahedral	3.1[7]
$(NH_4)_6Mo_7O_{24}$	octahedral	3.6[6], 2.9[7],
Ba_2CaMoO_6	octahedral	4.5[6]
MoO_2	octahedral	2.5*, 2.4[7]
	treated temperature	
Type-I $H_{0.25}MoO_3$	R.T	3.2
	373K	3.2
	473K	3.1
	523K	3.2
	573K	3.2
	623K	3.2
	673K	3.1
	723K	2.2, 3.2
	773K	2.2, 3.1
	873K	2.2, 3.1

*: present work, **: hydrogen molybdenum bronze

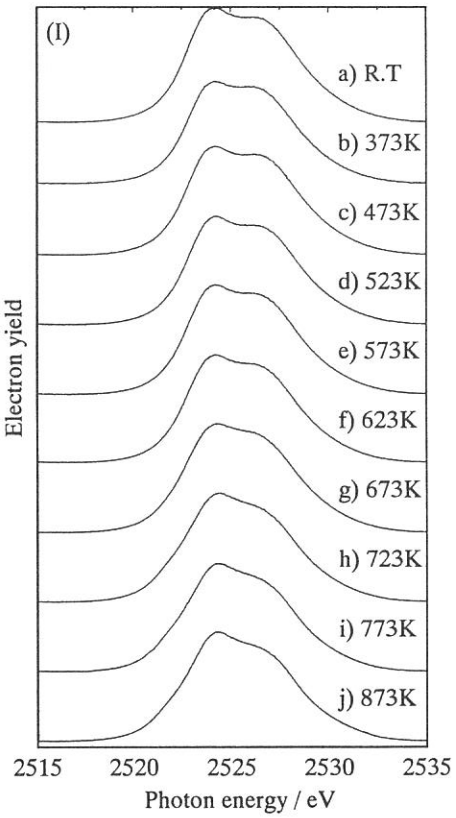

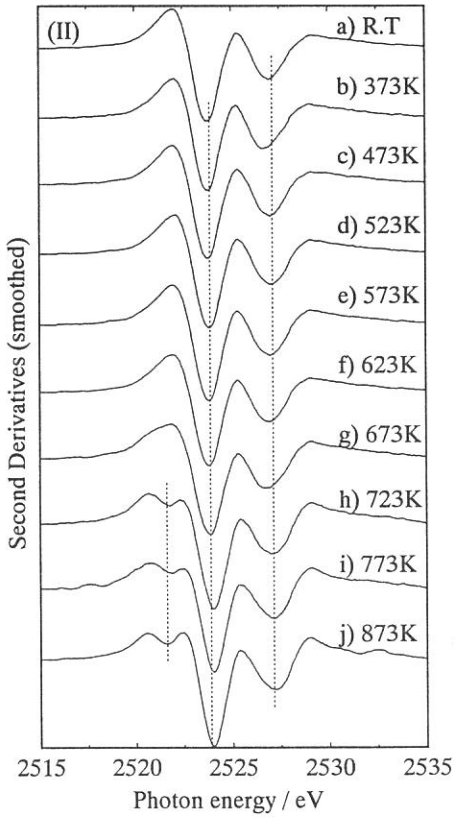

Fig.2 Mo L_3-edge XANES spectra (I) and their second derivatives (II) of Type-I treated at a)room temperature, b)373K, c)473K, d) 523K, e)573K, f)623K, g)673K, h)723K, i)773K, and j)873K in vacuo.

References

1. J. J. Birtill and P. G. Dickens, *Mater Res. Bull.*, **13**, 311 (1978).
2. K. Eda, *J. Mater. Chem.*, **2**, 533 (1992).
3. O. Glemser and G. Lutz, *Z. Anorg. Allg. Chem.*, **264**, 17 (1951); **269**, 93 (1952); **285**, 173 (1956).
4. N. Sotani, K. Eda, and M. Kunitomo, *Trends in Inorganic. Chemistry.*, **1**, 23 (1991).
5. K. Nakamura, K. Eda, N. Sotani, and S. Hasegawa, submitted *J. Chem. Soc. Trans Faraday*.
6. S. R. Bare, G. E. Mitchell, J. J. Maj, G. E. Vrieland and J. L. Gland, *J. Phys. Chem.*, **97**, 6048 (1993).
7. H. Aritani, T. Tanaka, T. Funabiki, S. Yoshida, N. Sotani, K. Eda, and S. Hasegawa, *J. Phys. Chem.*, **100**, 19495 (1996).

(BL7A)

Zr L_3-edge XANES Study of Some ZrO_2 catalysts

Tomomi KOSAKA, Tsutomu OHNARI, Yoshiaki TAKAHASHI and Sadao HASEGAWA

Department of Chemistry, Tokyo Gakugei University, Koganei, Tokyo 184-8501

1 Introduction

Zirconium oxide is a very interesting material because of its thermal stability, its mechanical properties and its acidic, basic surface properties[1]. Sulfated ZrO_2 was known as superacid, for example, which has catalytic function of skeletal isomerization for alkane. Comelli et. al. reported the catalytic activity of sulfated ZrO_2 is not dependent of the precursor salts and of the $Zr(OH)_4$ preparation method[2]. These prompt us to carry out systematic studies on the electron states and catalytic activity of sulfated ZrO_2 catalysts.

In the present study, we described the change of localized electron states and its effect to catalytic activity of sulfated and non-sulfated ZrO_2 catalysts against calcination temperature by Zr L_3-edge XANES analysis.

2 Experiment

Zirconium oxychloride was dissolved in water at R. T., then stirring and slowly added aqueous ammonia (25% NH_3) to obtain $Zr(OH)_4$ until the solution change into pH8. After $Zr(OH)_4$ was washed by a large quantity water, dried at 383K for 24h. Sulfated ZrO_2 was prepared in a solution of 1N H_2SO_4 for 6h with stirring after the mixture were filtered, dried at 383K for 24h. Each $Zr(OH)_4$ calcined at 873K for 3h in air, then non-sulfated ZrO_2 (hereafter it is referred to as ZrO_2) and sulfated one were obtained.

The measurements of Zr L_3-edge XANES spectra were carried out on a facility of BL-7A station of soft X-ray beamline. Each sample was prepared for measurement by grinding with hexane, and mixed with active carbon then spread on a Cu-Be dinode which was attached to a first position of electron multiplier into the beamline chamber. After the chamber had been evacuated, the spectrum was recorded in a total electron yield mode at R. T., using a Ge(111) double crystal monochromator.

3 Results and Discussion

In Fig.1 (A) and (B) shows Zr L_3-edge XANES spectra of ZrO_2 and sulfated ZrO_2 calcined at different temperature. The two peaks (2334 eV (first) and 2336 eV (second)) observed in these spectra that were corresponding to transfer from $2s_{3/2}$ to t_{2g} and e_g of 4d orbital, respectively.

While XRD results of ZrO_2 and sulfated ZrO_2 are exhibited in Fig.2 (A) and (B). The both of catalysts calcined at 473K have amorphous phase. Calcined at 873K, the main structure is metastable tetragonal phase, however a mixture of the tetragonal and monoclinic phase of ZrO_2 was also observed. And calcined at 1073K, practically the monoclinic phase is detected. Zirconium oxide generally changes its crystalline from amorphous to metastable tetragonal, and then monoclinic with increasing calcination temperature[2]. It is explained that SO_4 ion existed in sulfated ZrO_2 was lead to prevent crystal growth. When sulfated ZrO_2 maintained metastble tetragonal phase, activity of skeletal isomerization for n-butane (See as Fig.3) was recognized. In case of monoclinic phase (calcined above 1073K), SO_4 ion was separated from catalyst and sulfated ZrO_2 have no activity of skeletal isomerization.

Thus, these catalysts calcined at 473K has amorphous phase, two peaks was broad and indistinct (in Fig.1). This is supposed that hydroxyl group was obtained in the catalyst cause action, as function of electron donor. When sulfated ZrO_2 catalyst calcined at 873K, the remarkable change of XANES spectra was observed, that is, the intensity of second peak was increased more than that of first peak. It is expected that the electron density between zirconium and oxygen atoms were drawn toward oxygen atom side because SO_4 ion of sulfated ZrO_2 has been electron-accepting. So Zr 4d e_g is nearly empty orbital, electron transfer the higher energy states easily. Calcined above 873K, each spectra are similar shape which intensity of the first peak is higher than that of second peak. It is explained that localization of electron density has became weak due to SO_4 ion desorption

from catalyst, and then reactivity also decreased.

Accordingly, the effect of SO_4 ion addition to electron density of ZrO_2 was depend on the calcined temperature. Sulfated ZrO_2 has a unique electron structure when it was most active for skeletal isomerization. However, further theoretical effort so as to include the electron interaction between catalysts and n-butane is need for understanding of this catalysts activity in detail.

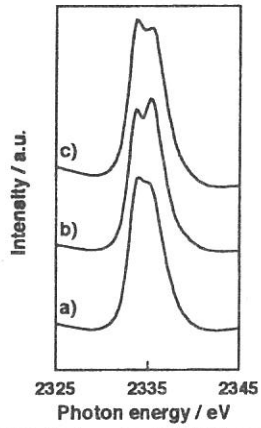

Fig.1 (A) Zr L_3-edge XANES spectra on sulfated ZrO_2 calcined at a) 473K, b) 873K and c) 1073K.

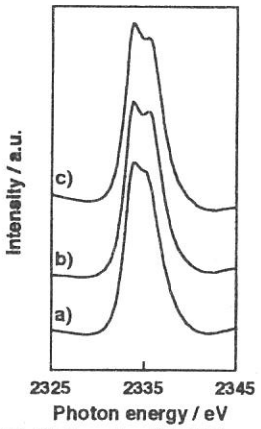

Fig.1 (B) Zr L_3-edge XANES spectra on ZrO_2 calcined at a) 473K, b) 873K and c) 1073K.

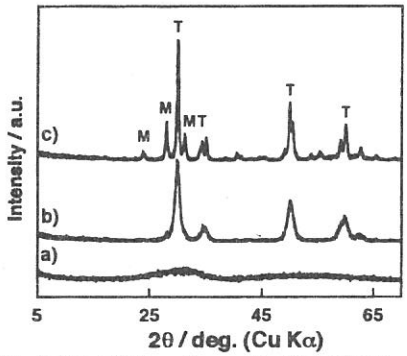

Fig.2 (A) XRD patterns of sulfated ZrO_2 calcined at a) 473K, b) 873K and c)1073K.
T: Tetragonal
M: Monoclinic

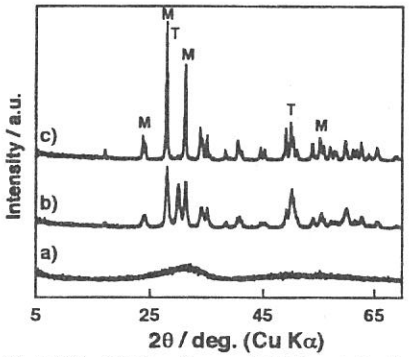

Fig.2 (B) XRD patterns of ZrO_2 calcined at a) 473K, b) 873K and c)1073K.
T: Tetragonal
M: Monoclinic

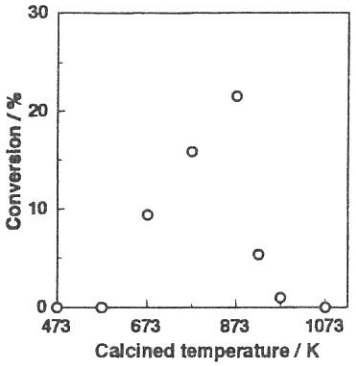

Fig.3 Skeletal isomerization for n-butane on sulfated ZrO_2 against calcined temperature.

1) Y. Nakano, T. Iizuka, H. Hattori, and K. Tanabe., *J. Catal.* **57**, 1 (1979)
2) Raul A. Comelli, Carlos R. Vera, and Jose M. Parera., *J. Catal.* **151** 96 (1995)

(BL7A)

Si K-edge XAFS study of dense vitreous silica

N. Kitamura, H. Mizoguchi, K. Fukumi, H. Kageyama, K. Kadono and M. Makihara

Osaka National Research Institute, AIST, Midorigaoka, Ikeda, Osaka 563-8577

Introduction

Permanent densification of glassy materials is of interest to understand the glass structure and mechanism of the compaction. The structure of densified silica glass has been investigated using infrared absorption, Raman[1] and neutron[2] scattering. However, detail of change in local structure is not clear yet. In this work, we have observed Si K-edge x-ray near-edge structure for pure synthetic and permanently densified silica glasses.

Experimental procedure and results

Synthetic silica glass (Nihon Silica Glass Yamaguchi Co. Ltd.) was used for starting material. Silica glass (3mm in diameter) was densified by heating at 400°C for 2min under 6 GPa with a 6-8 multi-anvil type high pressure apparatus (UHP-2000, Sumitomo Heavy Industry Co. Ltd.). Density of undensified and densified glasses are 2.20 and 2.44 g/cm^3, respectively. X-ray absorption experiments were performed at the double crystal monochromator beam line BL7A. InSb was used as the monochromator crystal. At first, spectra of undensified silica glass were recorded at room temperature by using Total Electron Yield (TEY), Transmission (TR), Drain Current (DC) and Electron Yield (EY) methods. The electron yield spectrum was obtained by an electron multiplier (EM) and an x-ray photo diode (PD) equipped with sample chamber at position of about 45° against beam direction. Non-bias photocurrent is recorded on the PD measurement. Bulk sample put on a manipulator using carbon tape was used on the DC and EY measurements. Powder sample was put on the first photocathode made of Cu-Be of the electron multiplier on the TEY measurement. Powder dispersed film and pure film were used on the TR measurement in the chamber of about 10^{-8} torr. Figure 1 shows the results of the Si K-edge absorption spectra obtained by five methods (EM, PD, TR, DC and EY). The DC curve shows abrupt down in intensity at higher energy side of sharp peak. Since the drop down is suppressed with the increase of scan speed. It will be due to charge up of the sample. The other curves did not depend on scan speed. In the TEY and DC curves, the sharp peak is smaller in intensity than that in the EM or PD curves, although the reason is not clear yet. The EM and PD curves are quite similar with each other. The S/N ratio on the PD measurement is slightly better than in the EM measurement. Since the size of densified glass is small, comparison of absorption spectra for undensified and 11% densified silica glasses was performed by using the TEY measurement. Figure 2 shows the TEY curves for two glasses. They are almost same, but slight difference (small peak) is found near the sharp peak in the XANES spectra. Dominant change in glass structure under densification is decrease of Si-O-Si bond angle[1,2]. An elongation of Si-O bond length is expected from low energy shift of band gap energy which was observed in the vacuum uv reflection spectra at the BL7B[3]. Speculation of the difference in the XANES spectra remains unclear, but the similar behavior is found for some lithium silicate glasses.

References

[1] G. E. Walrafen and M. S. Hokmabadi, Structure and Bonding in Non-Crystalline Solids, ed. By G. E. Walrafen and A. G. Revesz(Plenum, New York, 1986), p.185.

[2] A. Hiramatsu, M. Arai, H. Shibazaki, M. Tsunekawa, T. Otomo, A. C. Hannon, S. M. Bennington, N. Kitamura and A. Ondera, Physica **B219&220**(1996)287.

[3] N. Kitamura, K. Fukumi, K. Kadono, H. Yamashita and K. Suito, Phys. Rev. **B50**(1994)132.

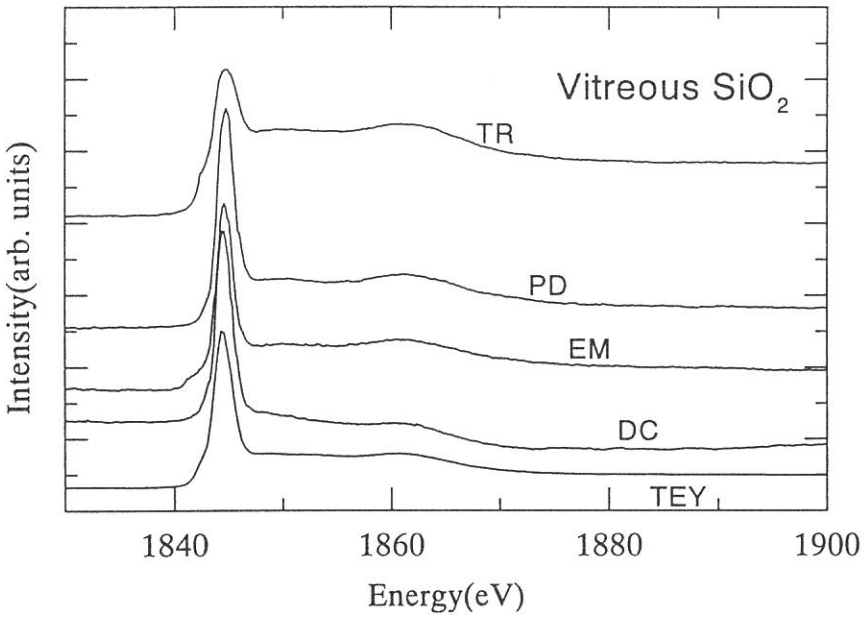

Figure 1 Si K-edge x-ray absorption spectra obtained by total electron yield (TEY), transmission (TR), drain current (DC), electron yield (EM) and x-ray photodiode (PD).

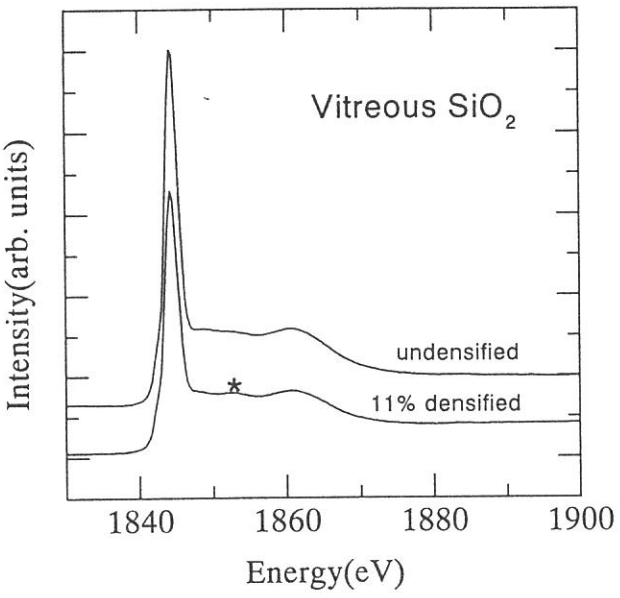

Figure 2 Si K-edge x-ray absorption spectra for undensified and 11% densified silica glasses obtained by total electron yield.

(BL7A)

Si K-edge XANES Study of High Energy Particle Irradiated Silica Glasses

Tomoko Yoshida, Hisao Yoshida[A] and Tetsuo Tanabe

Center for Integrated Research in Science and Engineering, Nagoya University, Furo-cho, Chikusa-ku, Nagoya 464-8603
[A]Department of Applied Chemistry, Graduate School of Engineering, Nagoya University, Furo-cho, Chikusa-ku, Nagoya 464-8603

Introduction

Neutron or high energy ion irradiation effects on silica glass are one of the main concerns for its application for optical windows, insulators and optical fibers in fusion reactors as well as fission reactors. We have studied on the dynamic effects of the irradiation mainly by neutron or ion induced luminescence of silica and revealed that both the electron excitation and the lattice displacement are caused under the irradiation [1,2]. These processes are closely related to the defect formation in silica. However, the structure and the electronic state of the irradiated silica glass are still unclear. In the present study, we investigated the change of local structure and the electronic state of silica glass before and after neutron or He^+ ion irradiation.

Experimental

Synthesized silica glass plates (T-4040) of 15 mm diameter and 2 mm thickness were obtained from Toshiba Ceramics, Japan.

Neutron irradiation experiments were carried out at the nuclear reactor YAYOI. During the experiments YAYOI was operated with a power of 2 kW with an average neutron energy of 1.3 MeV. The fluence of neutron was 6×10^{15} n/cm^2. He^+ ions accelerated up to 20 KeV and mass-analyzed were injected to a silica sample at room temperature through an aperture of 5 mm in diameter. The vacuum of the chamber during the irradiation was maintained below 1×10^{-6} Pa. The fluence of He^+ ions was 2×10^{17} ions/cm^2.

X-ray absorption experiments were carried out on the beam line 7A at UVSOR, Institute for Molecular Science, Okazaki, Japan with a ring energy 750 MeV and stored current 80-200 mA. Spectra were recorded at room temperature in a total electron yield mode, using a two-crystal InSb monochromator. To avoid the charge up by X-ray and to measure a spectrum of only the irradiated part of a sample, unirradiated part of a sample was covered with carbon sheet and Cu sheet having adequate thickness. The sample was put on the first photocathode made of Cu-Be of the electron multiplier.

Results and Discussion

Fig.1 shows Si K-edge XANES spectra of a virgin silica sample (a), its neutron or He^+-irradiated samples (b,c), and a silicon crystal (d). XANES spectrum of a virgin silica glass plate (a) was identical to those of its ground sample and a powder amorphous silica [3]. Therefore, we regarded the charge up effect on the spectrum of a virgin silica sample (plate sample) as negligible. XANES spectrum of a virgin silica sample shows a sharp and prominent peak at around 8 eV (relative energy to Si K-edge). This absorption is possibly due to atomic-like Si 1s to 3p transition. In case of silica, a silicon atom is located at a center of the regular tetrahedron of oxygen atoms. Therefore, Si 3p orbitals should be degenerated resulting in such a sharp absorption.

XANES spectrum of the neutron irradiated silica sample (b) is similar to that of a virgin silica sample (a) , indicating that the local structure around Si atom in silica sample does not change by the neutron irradiation. The neutron fluence, 6×10^{15} n/cm^2 would be too small to bring about a considerable structural change.

On the other hand, XANES spectrum of He^+-irradiated silica sample (c) is different from that of a virgin silica sample (a). The prominent peak at around 8 eV shown in Fig.1 (a) disappears in Fig.1 (c) while a new sharp peak appears at lower energy position. This result may indicate that the reduced Si ion species are formed by He^+ irradiation. According to the TRIM92 calculation, the atomic (oxygen) displacement takes place in the depth region from surface to ca. 300 nm in the present He^+ irradiation experiment. Taking into account this, the presence of the reduced Si ions may be correlated with the formation of Si precipitate due to atomic displacement. Only the irradiated part on surface of silica glass plate was gray and the transmittance of visible light in wavelength region from 300 to 700 nm reduced by He^+ irradiation, supporting the formation of Si precipitate in the vicinity of the surface of a silica glass plate. Since Si K-edge XANES spectra were measured in a total electron yield mode, which mainly monitors X-ray energy dependence of Si KLL Auger electrons yield, the spectrum would reflect such a structural change in the vicinity of the surface. It is clear that the Si precipitate in this He^+-irradiated sample (Fig. 1 c) is not like a Si metal crystalline (Fig. 1 d) . Further approach by EXAFS analysis should be carried out to clarify the local structure of the Si precipitate.

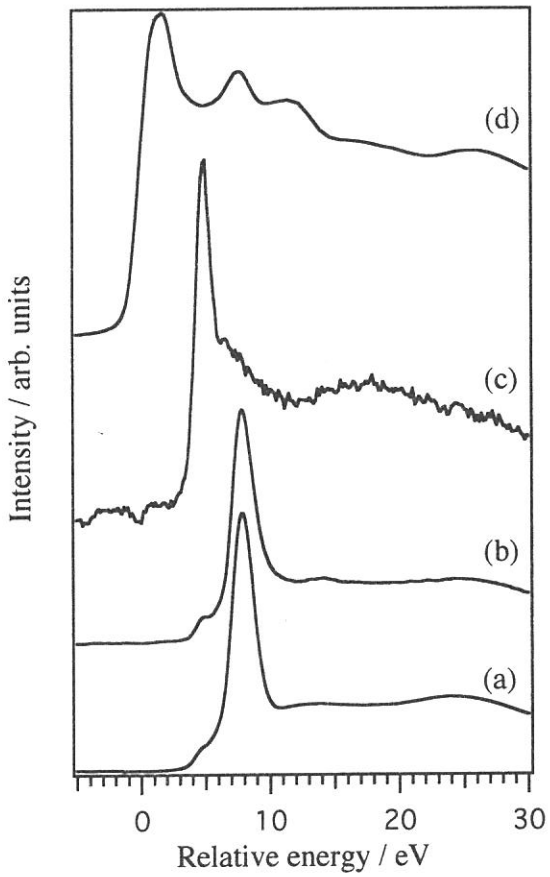

Fig. 1 Si K-edge XANES spectra of a virgin silica sample (a),
its neutron or He^+ -irradiated samples (b,c), and a silicon crystal (d).

References

[1] M. Fujiwara, T. Tanabe, H. Miyamaru and K. Miyazaki, *Nucl. Instr. and Meth. B*, 116 (1996) 536-541.

[2] T. Tanabe, S. Tanaka, K. Yamaguchi. N. Otsuki, T. Iida and M. Yamawaki, *J. Nucl. Mater.*, 212-215 (1994) 1050-1055.

[3] T. Tanaka, S. Yoshida, R. Kanai, T. Shishido, H. Hattori, Y. Takata and K. Kosugi, *J. Phys. IV France*, 7 (1997) 913-914.

(BL7A)

Al K XANES Spectra of Synthetic and Natural Alumina

Takatoshi Murata[A], Giancarlo Della Ventura[B.C], Giannantonio Cibin[C], Augusto Marcelli[C] and Annibale Mottana[B.C]

[A]*Department of Physics, Kyoto University of Education, Kyoto 612-0863, Japan*

[B]*Università di Roma Tre, Dipartimento di Scienze Geologiche, Roma, Italy*

[C]*I.N.F.N.-Laboratori Nazionali di Frascati, Frascati, Italy*

X-ray absorption fine spectra at the Al K-edge were measured experimentally on a chemically pure and physically perfect synthetic α-Al_2O_3 (α-alumina) powder, a natural "ruby/sapphire" (corundum) crystal and a series of artificial "corundums" produced for technical purposes, some of which are physically homogeneous although chemically impure (max. 30,000 atoms per formula unit), and others are impure inhomogeneous phases containing up to 10 vol.% admixed β-alumina. Measurements were done at the soft X-ray beamline BL7A using total yield of the photoelectron. Samples were ground homogeneously to a 3-5 micron size and spread as a fine film on a piece of adhesive tape, which is sticked onto the first photocatode of the Hamamatsu R595 photomultiplier. All measurements were constantly carried out using 0.1 eV steps, so as to assure maximum reproducibility, and warrant meaningful comparison among spectra.

Figure 1 show the XANES spectra fitted to account for the baseline. The Al K edge XANES spectra of α-alumina, "ruby/sapphire" and homogeneous "corundums" differ despite of the identical six-fold co-ordination (short-range arrangement) assumed by O around Al, and vary slightly in relation to the slightly different chemistries of the materials (substitutional defects) as well as on account of the location taken by foreign atoms in the structural lattices (positional defects). The Al K edge XANES spectra of inhomogeneous "corundums" containing the admixed β-alumina phase show additional XANES features reflecting the presence of Al in four-fold co-ordination besides the prevailing six-fold co-ordinated one.

Figure 2 shows the quantitative treatment of the observed changes, which is interpreted in terms of short-range modification of the co-ordination polyhedron and of medium- to long-range modifications in the overall structure; both of them induced by substitutions.

These experiments clearly shows that XAFS spectroscopy it is a reliable technique for both investigate a light element such as Al, and detecting minor co-ordination changes and substitutions (ca. 1~3 wt.% as oxide) of the absorber by dilute other atoms, at least under favourable conditions as those occurring in this system are.

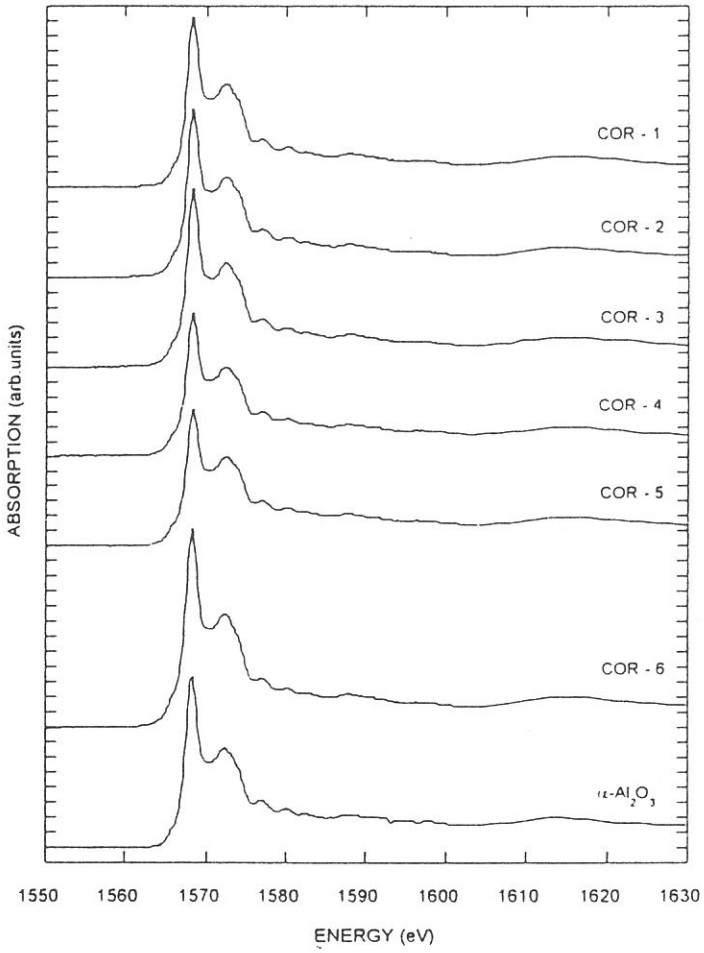

Figure 1

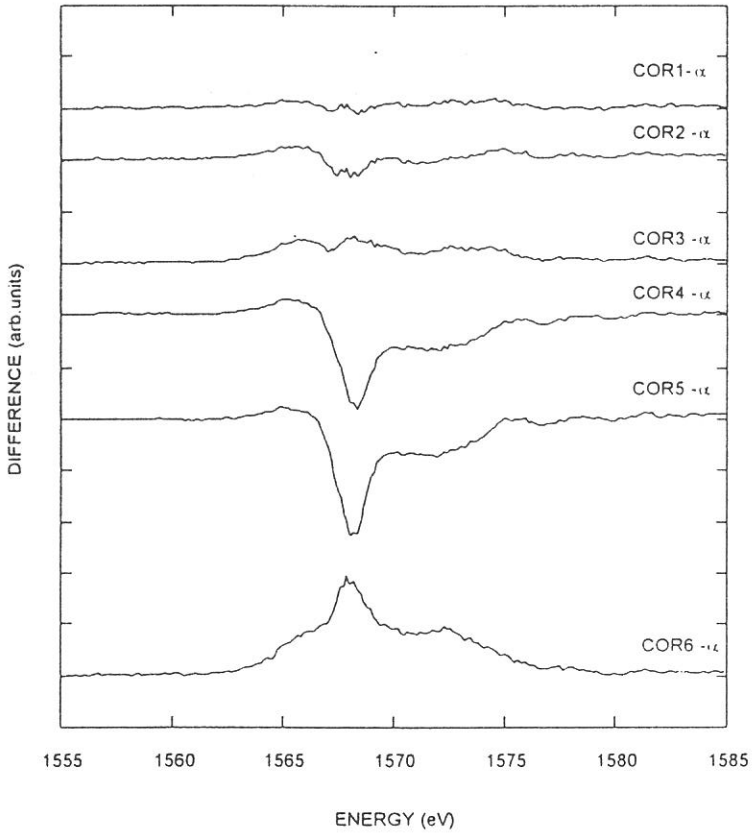

Figure 2

(BL7A)

Polarization-Dependent Alminum K-edge Absorption of AlN and AlGaN

Kazutoshi FUKUI, Ryousuke HIRAI
Faculty of Engineering, Fukui University, Fukui 910-0017, Japan
Fax +81-776-27-8749 fukui@wbase.fuee.fukui-u.ac.jp
Syun-ichi NAOE
Faculty of Engineering, Kanazawa University, Kanazawa 920-11, Japan

The soft X-ray absorption (SXA) around aluminum K-edge have been measured to investigate the electronic structure of the wurzite III-V nitrides (AlN and AlGaN), especially the structure of the unoccupied states. The Al K absorption spectra of III-V nitrides near the Al K-edge in principle represent the partial density of the final states with p symmetry (p-like p-DOS) according to the selection rule. Furthermore, the Al K absorption spectrum gives us the site-specific (aluminum ion site) information, since the core levels are very localized in space. The Al K absorption spectrum also gives us the information about the final states symmetry p_{xy} and p_z, because the incidence soft X-ray light is linearly polarized.

The experiments were carried out at BL7A. Resolutions under the experimental conditions were about 0.8 eV at about 1500 eV. The soft X-ray absorption measurement was performed by using the total photoelectron yield (TY) method. The both AlN and AlGaN thin films which have about 1 μm thickness on SiC were made by the MOCVD method at Riken. All films were cleaned with organic solvents just before the installation into the vacuum chamber, and the measurements were performed at room temperature in the range of 10^{-9} Torr. The sample holder was able to rotate in the vacuum chamber for the angle dependence measurement. The polarization angle α is defined as the angle between the incident light and the normal to the sample surface, i.e., c axis. The α dependence measurements were performed under the p-polarization configuration which means $E \parallel c$ at $\alpha \sim 90$ degree.

Figure 1 shows the Al K absorption spectra of AlN and AlGaN mixed crystals. The energy scale is relative to the threshold energy which correspond to the conduction-band minimum. The threshold energies of AlN, $Al_{0.7}Ga_{0.3}N$, $Al_{0.5}Ga_{0.5}N$ and $Al_{0.3}Ga_{0.7}N$ are 1557.1, 1556.7, 1556.6 and 1555.6 eV respectively. The intensity of each spectrum is normalized at the maximum peak for convenience. They show the similar spectrum shape, but some differences can be seen between AlN and the other AlGaN. This similarity represents that the structure of the p-like p-DOS around the Al ion site almost independent on Ga content, and the differences between AlN and AlGaN show that there are some sensitive Al native electric structures. The energy separation between the lowest energy peak and the main one is gradually decreasing with increasing Ga concentration.

The α dependece absorption measurement was performed each sample which was shown in Fig. 1. Figure 2, for example, shows the Al K absorption of AlN as function of angle α. All spectra are normalized. AlN result in Fig.2 also shows a clear α dependence as well as the other samples. To investigate the symmetry of the unoccupied states, the component analysis of the partial density of the final states with p symmetry (K absorption spectra) have been performed under the assumption as follows; (i) the partial density of the final states with p symmetry consists of p_{xy}, p_z and the α independent components, (ii) the absorption coefficients for $1s \rightarrow p_{xy}$ and $1s \rightarrow p_z$ are proportional to $\cos^2\alpha$ and $\sin^2\alpha$, respectively, where z axis is taken to be parallel to the c axis of the sample. Figure 3 shows the results of the component analysis of the Al K absorption for AlN. The spectrum labeled a represents the α independent component, b the p_z component and c the p_{xy} component, respectively. The component analyses of the Al K absorption for AlGaN were also performed as the same manner. From these results each peak of the p_{xy} and the p_z components is found around the same energy. It suggests that the unoccupied states with p symmetry of III-V nitrides have the similar structure near aluminum site.

The authors would like to thank Dr.S.Tanaka, Dr.Y.Aoyagi (RIKEN) for supply of AlN and AlGaN samples.

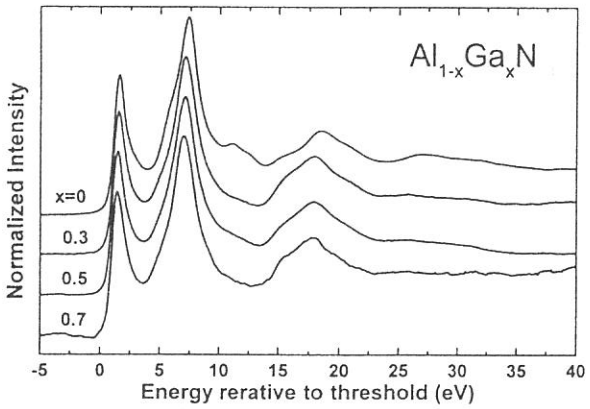

Fig.1 N K absorption spectra of AlN, $Al_{0.7}Ga_{0.3}N$, $Al_{0.5}Ga_{0.5}N$ and $Al_{0.3}Ga_{0.7}N$. The energy scale is relative to the threshold energy.

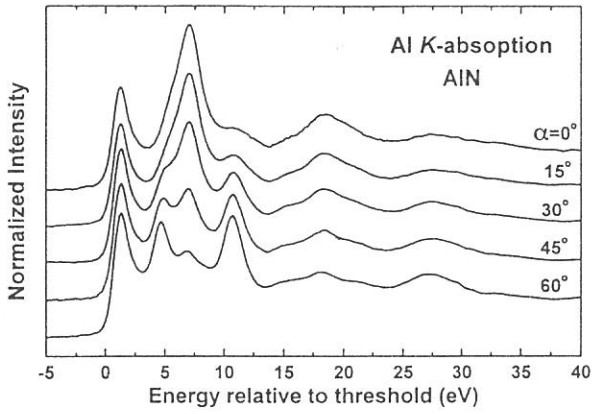

Fig.2 N K absorption spectra of AlN as function of angle which is defined as the angle between the incident light and the normal to the sample surface (c-axis).

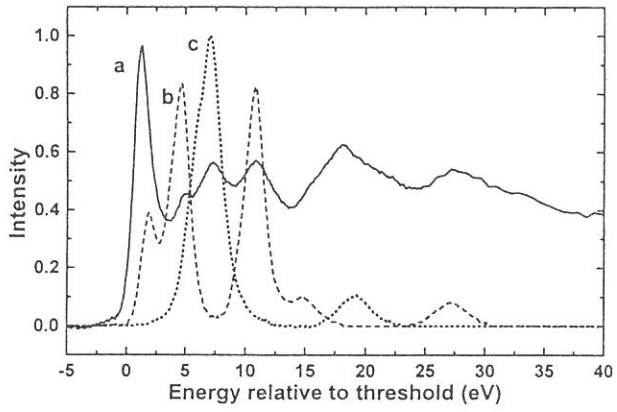

Fig.3 The component analysis results of Fig.2. The spectra labeled a, b and c show the α independent component, p_z and p_{xy} component, respectively.

(BL-7A)

Br L Spectra Measured with YB66 crystal

Tokuo MATSUKAWA, Hiroaki OKUTANI, Kazunori MATSUDA
and Toyohiko KINOSHITA*

Dep. of science, Naruto University of Eduction, Naruto 772-8502, Japan
**UVSOR, Institute for Molecular Science, Okazaki 444-8585, Japan*

1. Introduction

YB_{66} is a new synthesized crystal which has a proper nature to monochromatize soft x-rays from synchrotron radiation.[1] The 2d value of x-ray reflecting (400) plane is 10.76 A , which covers the energy region of 1.2 to 2keV and is suitable for Mg K, Al K and Si K EXAFS experiments.

In this report, we present the recent results of the experiments by using the YB_{66} crystal at the soft x-ray beam line of the UVSOR facility in the Institute for Molecular Science, OKAZAKI. The measurements were carried out on the absorption fine structures at the Br L edges of alkali bromides. As far as we know, there has been no report on the *2p* absorption spectra of bromine ion, whereas a lot of *2p* absorption spectra of chlorine ion had been studied from the very early stages in the history of the synchrotron radiation science. The one of the reasons may be that spectroscopic studies were due to photographic recording in those days and absorption by Br ion in AgBr grains in photographic plates interfere with the spectral features. The other reason is that there has been only few proper crystal with a large 2d value of around 10A for SR studies.

2. Results and discussions

At first, we have tried to use beryl crystal to measure Br L spectra. Figure 1 shows a result on RbBr. The dotted curve I shows a reference signal spectrum and the solid curve I/I0 shows a corrected absorption spectrum with a reference spectrum. At the Br L edge, the both spectra show fluctuating structures which reflect the sharp absorption structures due to the constituent Al atom in beryl crystal. The Al K absorption edge lies accidentally at the Br L_3 edge. The effects of the anomalous dispersion could hardly remove even with a proper correction method. Thus the beryl crystal could not be applied to the spectroscopic studies at Br L edge..

We have measured the Br- L_3 absorption spectra of the alkali-bromides by use of YB_{66} crystal. Figure 2 shows the Br L spectra obtained with total photoelectron yield method. No obstructing structure is observed. The L_2 edge is separated well above the L_3 edge The photon energy was referred to the metallic Al K absorption edge. The resolution was also estimated to be 0.8 eV with a width of a derivative curve of the Al K edge. The spectrum shows characteristic structures which are common among the samples. They are designated A through D. In order to fix the bottom of the conduction band, we evaluated the binding energy of the Br *2p* level and the top of the valence band. The high resolution XPS spectra had been measured by monochromatized Al K x-ray source, and the binding energies were measured carefully referred to Au *4f* line. The binding energy of Br *2p* level was determined by adding the photon energy of the Br $L_{\alpha 1}$ (*3d* to *2p* transition) characteristic x-ray to the binding energy of Br *3d* line. The band gap of the bromides was determined from the binding energy of the top of the valence band. In Fig.2 , the energy of the bottom of the conduction band is shown by an arrow.

The fine structures designated A is bellow the conduction band threshold, and may be due to the x-ray exiton absorption. It is interesting that the spectral features are like those of chlorine L_3 spectra[2], considering a difference in a life time broadening between the case of the chlorine and the bromine ions. It has been well known that chlorine L spectra show several

sharp peaks at the chlorine absorption edges. The separations of the peaks correspond well to those of the characteristic structures of the bromides. Table 1 exhibits the relative energies of the characteristic structures to the bottom of the conduction band. Thus the fine structures at Br-L_3 edge may be interpreted on a same way as in the case of chlorides.

References

1) J.Wong *et al., Nucl. Insr. and Meth.,* A195, 243 (1990)
2) O.Aita *et al., J. Phys. Soc. Japan,* 30, 1414 (1971)

Table 1. Energy positions of characteristic structures measured relative to the bottom of the conduction band .

Energy relative to the bottom of the conduction band (eV)					
	A	B	C	D	E
NaBr	-0.6	1.4	3.8	10.3	12.1
KBr	-1.5	0.0	2.0	8.4	6
RbBr	-0.6	0.6	3.2	8.9	

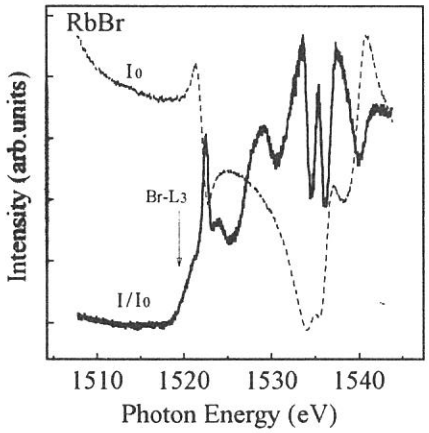

Fig.1. The throughput spectrum with beryl monochromator (I_0) and absorption curve (I/I_0) of RbBr at the Br L_3 edge.

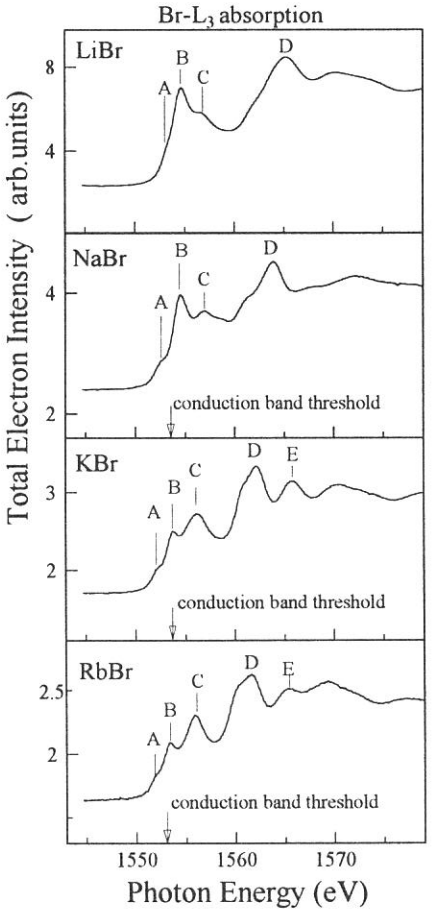

Fig.2. Br L_3 absorption spectra of alkali-bromides. The arrow shows the bottom of the conduction band obtained by XPS .

(BL-7A)

Cu L-edge Absorption Spectra of Copper-aluminate Catalysts

Ken-ichi Shimizu, Hajime Maeshima, Hisao Yoshida and Tadashi Hattori[A]

Department of Applied Chemistry, Graduate School of Engineering, Nagoya University, Chikusa-ku, Nagoya 464-8603

[A]Research Center for Advanced Waste and Emission Management, Nagoya University, Chikusa-ku, Nagoya 464-8603

It is widely accepted that the selective catalytic reduction of NO by hydrocarbons is a potential method to remove NOx practically in excess O_2 [1]. Recently, we have reported that copper-aluminate catalysts having the spinel-type structure show high de-NOx performance, and Cu^{2+} cation interacted with γ-Al_2O_3 matrix is considered to be related to the active species. In this study, we have measured Cu L_3-edge absorption spectra to clarify the local structure of Cu^{2+} cation in Al_2O_3 matrix.

Copper-aluminate samples (Cu-Al_2O_3) with Cu content of 1-30 wt% were prepared by a coprecipitation method. Solutions of copper acetate and aluminum nitrate at the required concentration were coprecipitated using aqueous ammonia. The precipitates were washed, filtered and dried at 395K then calcined in air for 12h at 1073K. Cu-Al_2O_3 with 30 wt% Cu content almost corresponds to $CuAl_2O_4$ (stoichiometric spinel), whose crystal phase was confirmed by XRD.

Cu L-edge X-ray absorption spectra were measured on BL-7A at UVSOR with a ring energy of 750 MeV and a stored current of 70-220 mA in a mode of total electron yields. A double crystal beryl monochromator was used, and the absolute energy scale was calibrated to the Cu2$p_{3/2}$ peak in CuO at 931.3 eV [4]. From each absorption spectrum, subtraction of a sloping background was performed by extrapolating it from the linear region below the threshold. The intensity of the spectra have not been normalized because of missing of an adequate normalizing procedure.

Fig. 1 illustrates Cu L_3-edge absorption spectra of Cu-Al_2O_3 catalysts and $CuAl_2O_4$ (Cu=30 wt%). For 1wt% Cu-Al_2O_3, a peak are seen at 930.8 eV, while for 16wt% Cu-Al_2O_3 and $CuAl_2O_4$, two peaks are seen at 930.1 eV and at 930.8 eV. These peaks exhibited the positions similar to that observed for copper (II) compounds [3,4], and has been considered to be mainly due to $2p \rightarrow 3d$ transitions [4]. By assuming that a single absorption peak results from a single unoccupied d state of Cu^{2+} with an atomic configuration of d^9, the result suggests that the samples contain at least two kinds of Cu^{2+} species with different chemical states and the fraction of such species varies with Cu content.

For a qualitative estimation of the local environment of Cu^{2+} in Cu-Al_2O_3, diffuse reflectance UV-vis spectra were measured. The results showed that Cu^{2+} cations in 16wt% Cu-Al_2O_3 and $CuAl_2O_4$ were both in tetrahedral (λ =7000 cm^{-1}) and octahedral (λ =13000 cm^{-1}) sites, while those in 1wt% Cu-Al_2O_3 were predominantly in octahedral site. Therefore, it is considered that the

absorption peaks at 930.1 eV and at 930.8 eV in Cu L_3-edge spectra should correspond to Cu^{2+} cations in tetrahedral and octahedral sites, respectively.

To estimate the fraction of Cu^{2+} cations in tetrahedral and octahedral sites, we carried out deconvolution of the Cu L_3-edge spectra with two set of curves of a Lorenzians. From the deconvoluted spectrum of $CuAl_2O_4$ (Cu=30 wt%) shown in Fig. 1c, the ratio of the areas of 930.1 eV peak and 930.8 eV peak were determined to be 60/40, which is in good agreement with the ratio of tetrahedral/octahedral obtained by diffraction analysis [5]. Therefore, it is concluded that the ratio of tetrahedral/octahedral can be estimated quantitatively from Cu L_3-edge absorption spectra. By using this method, the ratio of Cu^{2+} cations in tetrahedral and octahedral sites was estimated for a series of Cu-Al_2O_3 and plotted as a function of Cu content (Fig. 2). The result shows that the ratio of tetrahedral/octahedral is a function of composition; it increases as Cu content increases.

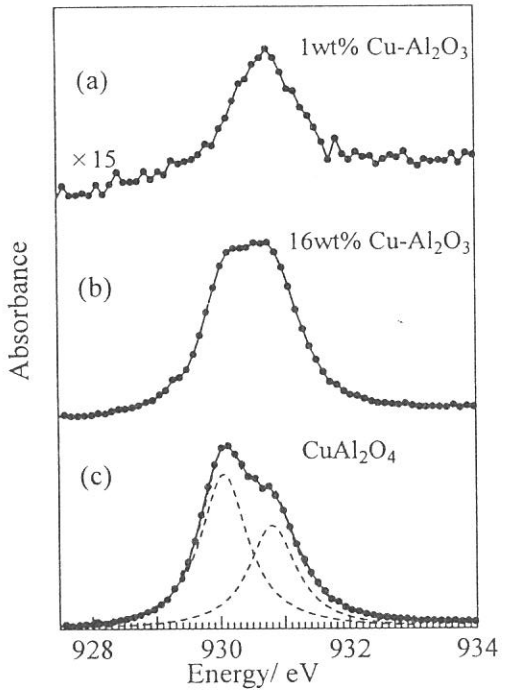

Fig. 1 Cu L_3-edge absorption spectra of (a) 1wt% Cu-Al_2O_3, (b) 16wt% Cu-Al_2O_3 and (c) $CuAl_2O_4$ (Cu=30 wt%) and its deconvoluted spectrum (dotted lines).

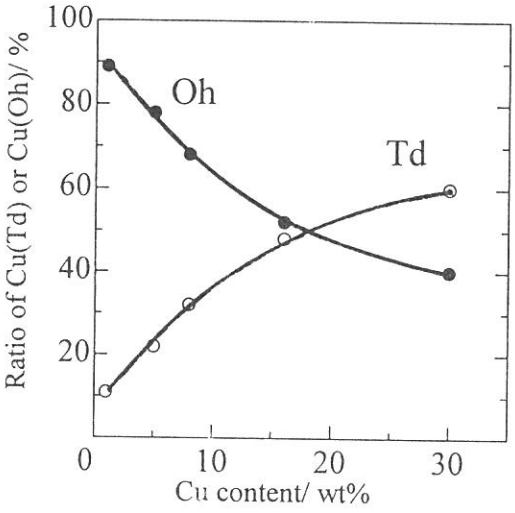

Fig. 2 Ratio of Cu(Td) or Cu(Oh) as a function of Cu content.

[1] M. Iwamoto and H. Yahiro, Catal. Today, 22 (1994) 5.

[2] K. Shimizu, A. Satsuma and T. Hattori, Appl. Catal. B, accepted.

[3] A. S. Koster, Molec. Phys., 26 (1973) 625.

[4] M. Grioni *et al.*, Phys. Rev. B, 39 (1989) 1541.

[5] R. Mark, M. Friedman, J. J. Freeman and F. W. Lytle, J. Catal., 55 (1978) 10.

(BL7A)

Tm4*d* core level resonant photoemission study of TmX (X=S, Se &Te) around Tm3*d* threshold

Krishna G. NATH, Yüksel UFUKTEPE[A*], Shin-ichi KIMURA[A], Toyohiko KINOSHITA[A], Takeshi MATSUMURA[B], Takashi SUZUKI[B], Haruhiko OGASAWARA[C] and Akio KOTANI[C]

Department of Structural Molecular Science, Graduate University for Advanced Studies, Okazaki 444-8585
A) UVSOR facility, Institute for Molecular Science, Okazaki 444-8585
B) Department of Physics, Tohoku University, Sendai 980-77
C) Institute for Solid State Physics, University of Tokyo, Tokyo 106

The applications of resonant photoemssion (RESPES) are important especially for studies of rare earth systems where the multiplet structures are complex due to existence of unfilled and localized 4*f*-shell[1]. In the previous reports[2,3], thulium compounds have been studied by RESPES to know the 4*f* electronic structures for two kinds of ions, Tm^{2+} and Tm^{3+}. It was found in these experiments that a large resonant enhancement occurs in Tm 4*f* emission around Tm4*d* absorption edges[2] and also around Tm3*d* absorption edges[3]. On the other hand, the resonance behavior of deeper core levels such as 4*d* has not been studied extensively so far. The efficiency of other decay channels of core-4*f* resonant transition can be derived using core level RESPES. In addition, the dynamics of collapsing core hole to its ground state can be directly observed through the lifetime-broadened features in the core level photoemission spectra.

In this report, we present the Tm-4*d* RESPES results at the 3*d*-4*f* resonance absorption edges (hν= 1450-1520eV) for mixed-valence Tm-compounds TmS, TmSe and TmTe. Because of different Tm ionic states, these compounds show different physical and electrical properties. The results of this study give us the resonant behaviors of the peaks of 4*d* multiplet and two Tm-valences. The lifetime broadening effect in the 4*d* emission depending on the multiplet structure is discussed herewith. The results of the theoretical calculation are compared with the experimental ones.

The experiments were performed at the beam line, BL7A, with an YB_{66} double crystal monochromator. The VG ESCALAB 220i-XL photoelectron analyzer system with a base pressure of less than $2x10^{-10}$ mbar was connected to the beam line for these experiments. The overall energy resolution of the core level photoemission spectra was less than 1eV both for on- and off-resonant condition. The surfaces of the single crystal samples were cleaned by Ar ion bombardment or by scraping. Oxygen contamination was checked by monitoring the O (1*s*) XPS peak and found to be negligible.

Figures 1(a-d) show the on- and off- resonant 4*d* core level photoemission results for TmS at various photon energies

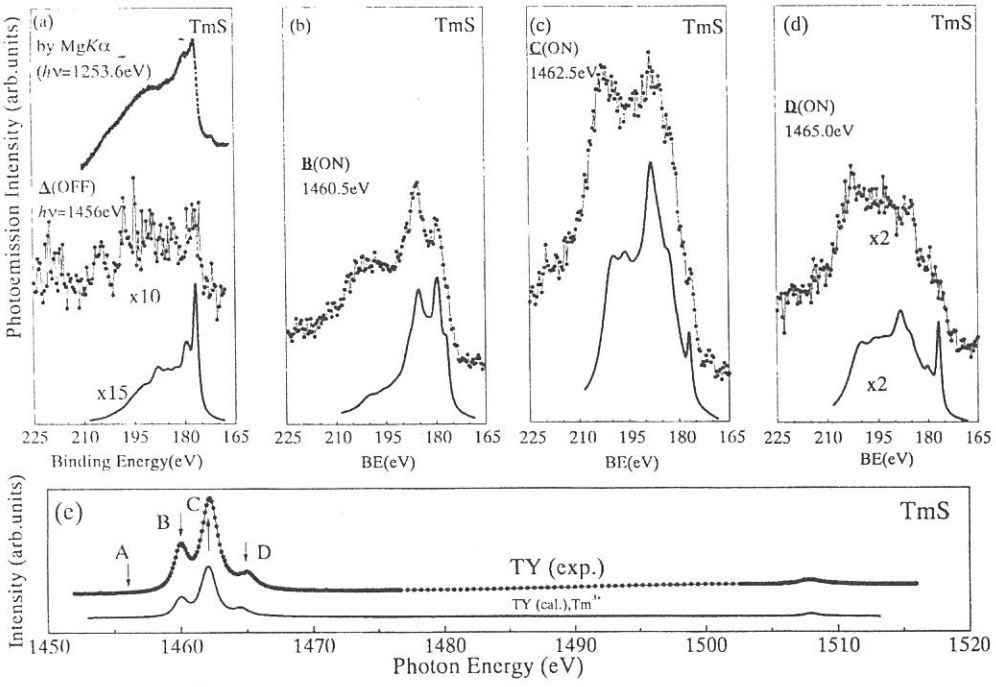

Figure 1. (a-d):Tm 4*d* photoemission spectra of TmS. All solid curves represent the calculated for each resonance condition of the trivalent Tm ion. (a):Off-resonant spectrum along with the XPS spectrum excited by MgKα radiation. (b-d): On-resonant spectra. (e): 3*d*-4*f* total photoelectron yield spectrum of TmS. The marks B, C and D indicate the resonance peak maxima of trivalent features.

along with the XPS spectrum excited by Mg$K\alpha$ radiation. The observed spectra show mostly trivalent nature, but there is small amount of the divalent component. The excitation energies indicated by alphabet (A-D) are selected from the total yield (TY) spectrum shown in Fig.1 (e). Three of these excitation energies (B-D) represent the resonant conditions of trivalent Tm ion, namely correspond to $^3H_6$, $^3G_5$, and $^1H_5$ intermediate states. It is noticed that the 4*d* spectra are strongly enhanced (about 10 times of off-resonant one) under the 3*d*-4*f* resonant condition. The resonance effect of spectra in Figs.1 (b-d) is explained by considering the interference between the direct 4*d* photoemission and the 4*d* excitation to continuum state due to the decay channel, $3d^{10}4d^{10}4f^{12} + h\nu \rightarrow 3d^{9}4d^{10}4f^{13} \rightarrow 3d^{10}4d^{9}4f^{12} + \varepsilon l$. We observed several multiplet peaks in both off- and on-resonant spectra in Figs. 1(b-d). Each 4*d*-multiplet spectrum is extended over the binding energy width of 40eV. The off-resonant spectrum excited by Mg$K\alpha$ radiation in Fig.1 (a) also has the complex multiplet structures.

In Figure 2, we show the resonance effect of the 4*d* spectrum corresponding to Tm^{2+} ion for TmSe, which is considered as a typical mixed valent compound. Figures 2 (b-c) correspond to on- and off- resonant 4*d*-XPS results for TmSe around the 3*d*-excitation region. In order to clarify the divalent component of 4*d* core level, the off-resonant XPS spectra for TmSe, TmS and TmTe, are shown together in Fig.2 (a). The TY spectrum for TmSe in Fig.2 (d) has to be considered as a superposition of Tm^{3+} and Tm^{2+} peaks. The dominant features of the TY spectra are similar to that of TmS in Fig. 1(e), i.e., trivalent peaks at the photon energy of 1460.5, 1462.5, 1465 and 1508eV. In addition, there exits obviously a shoulder at the photon energy of 1459.6eV that belongs to the divalent component as shown in the calculated curve. This is the condition for on-resonant photoemission spectrum of divalent 4*d*-level in Fig.2 (c) that shows also large resonance enhancement comparing with off-resonant one.

The lifetime broadening of the several core-states in the multiplet structure strongly varies with their binding energy that was explained in details by Ogasawara and co-workers[4]. The lifetime of core hole depends on the super-Coster-Kronig transition rate involving 4*f* electrons. The broadening effect according to the selective Auger transition can be easily understood by spin-selection rule and electron correlation effect[5]. The general tendency of 4*d* spectrum is to be more broadened at higher binding energy than the lower one, so that the lower binding energy peaks are sharp with long lifetime as seen for different on- and off-resonant spectra in the Fig.1 and 2. In the lower binding energy sides in the 4d-spectra for TmS and TmSe, the experiments show good agreement with calculation. But there are some disagreements in the higher binding energy sides as seen it the both figures. The origin of this disagreement is not still known.

The core level RESPES study gives us the different spectral features of 4*d* multiplet in the final state vary according to the excitation conditions and different Tm-valences. At the same time, the lifetime broadening phenomenon is also introduced to describe the variation of spectral shape.

We would like to thank the staff members of UVSOR facility staff for their technical support.

*Visiting Scientist on leave from Physics Department, University of Cukurova, 01330 Adana, Turkey

1. A. Kotani, Inner shell photoelectron process in solids, (Handbook on synchrotron Radiation, vol.2, edited by G.V.Marr (North-Holland Physics publishing, Amsterdam, 1987): A.Kotani et al. J. Electron Spectrosc. Relat. Phenom. **60**, 257 (1992).
2. S.-J. Oh *et al.*, Phys. Rev. B **30,** 1937 (1984), Y. Ufuktepe *et al.*, submitted to J. Phys. Soc. Jpn. ;UVSOR Act.Rept. (1996) P.102.
3 T. Kinoshita *et al.*, J. Electron Spectrosc. Relat. Phenom., in print :C.Laubschat *et al.*, Physica. Scripta. **41**, 124 (1990).
4 H. Ogasawara *et al.*, Phys. Rev. B **50,** 12332 (1994).
5. M. Ohno *et al.*, Phys. Rev. A **31**, 2318 (1985): E. G. McGuire, Phys. Rev. A **9**,1840 (1974).

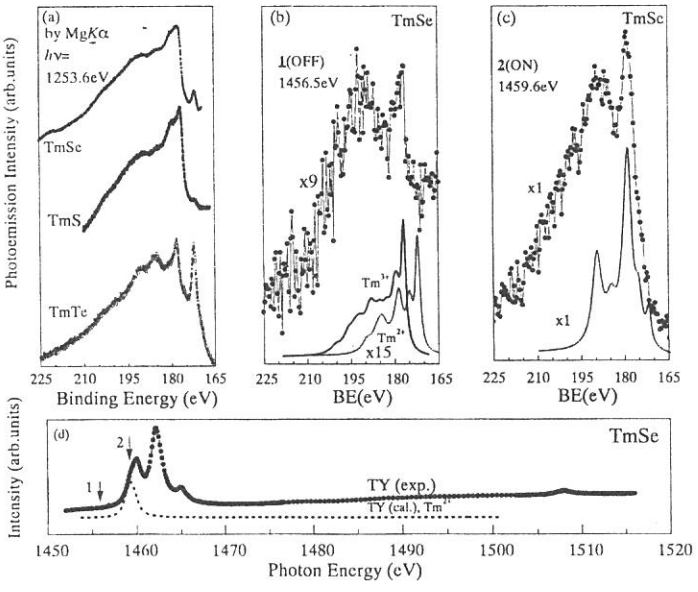

Figure 2. (a): The XPS spectra of TmX (X=S, Se & Te) excited by Mg$K\alpha$ line are used to clarify the divalent and trivalent nature of the 4*d* core level spectra. (b,c): Tm-4*d* core level photoemission spectra near the 3*d*-4*f* excitation conditions for TmSe. (d): 3*d*-4*f* TY spectra of TmSe where the positions 1 and 2 for ON and OFF resonance conditions of divalent component respectively.

(BL7A)

EXAFS Studies in Defective Perovskite Type Oxides Such as $Ba_2In_2O_5$ and $La_{1-x/2}Y_xSc_{1-x/2}O_3$

Yoshiharu UCHIMOTO, Takeshi YAO, Yoshiyuki ITO, and Koichi KAJIHARA

Department of Fundamental Energy Science,
Graduate School of Energy Science, Kyoto University,
Yoshida, Sakyo-ku, Kyoto 606-8317, JAPAN

Recently, a significant amount of work has been devoted to solid oxide fuel cells (SOFCs) utilizing oxide ion conductors as electrolyte. When the operating temperature is reduced to intermediate temperature range (700-800°C), SOFCs could be constructed by less costly materials for interconectors, for example alloys, and technical advantages such as increase reliability and life time will be attained. Since oxide ion conductivity of stabilized zirconia decreases at such temperatures, the development of electrolyte materials having high oxide ion conductivity at the intermediate temperatures is of considerable interest.

Defective perovskite type oxides are excellent candidates for electrolytes of SOFCs operating at intermediate temperature. The perovskite type of oxides such as $Ba_2In_2O_5$ doped with Ca and/or $La_{1-x/2}Y_xSc_{1-x/2}O_3$ are the most promising candidate for electrolytes of intermediate SOFCs. In the perovskite oxides, there are two kinds of cation sites, that is A-site:12 coordination with larger space and B-site:6 coordination with smaller space. Crystal structure, especially local structure of cations must influence the oxide ionic conductivity. In this work, the crystal structure were analyzed by powder X-ray Rietveld method and EXAFS analysis.

Pure and Ca doped $Ba_2In_2O_5$ powder was prepared by usual solid state reaction starting with $BaCO_3$, In_2O_3 and CaO. For the Preparation of $La_{1-x/2}Y_xSc_{1-x/2}O_3$, lanthanum oxide, scandium oxide and yttrium oxide were weighed with molar ratio as La:Y:Sc=1-x/2:x:1-x/2(x=0.00, 0.10, 0.20, 0.30, 0.40) and mixed for 5 h by electric mortar. The mixtures were pressed into disk, heat-treated at 1600℃ for 5 h in air, then left cool in the furnace.

Figure 1 shows fourier transform of Sc K-edge EXAFS function for $La_{0.90}Y_{0.20}Sc_{0.90}O_3$. A peak between 1.0 and 2.5 Å was observed for each sample. This peak was attributed to oxide ions neighboring the absorbing Sc^{3+} ion. Figure 2 shows the inverse Fourier transform of the peak and the result of the parameter fit for each sample. Table 1 shows obtained parameters by the parameter fit. The local interatomic distances of Sc-O which are obtained by the EXAFS analysis are increase with increase of Y dopant content.

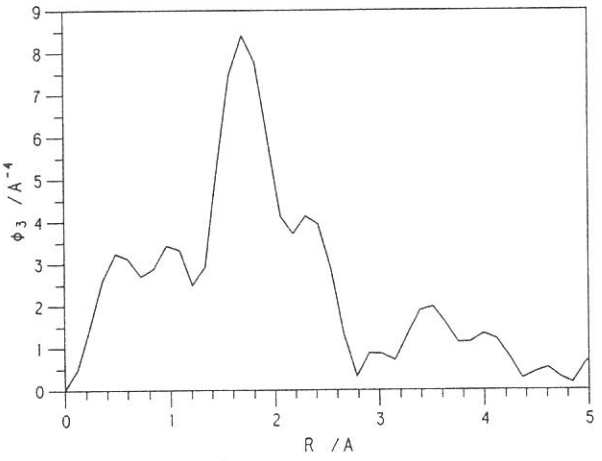

Figure 1 Fourier transform of Sc K-edge EXAFS function for $La_{0.90}Y_{0.20}Sc_{0.90}O_3$

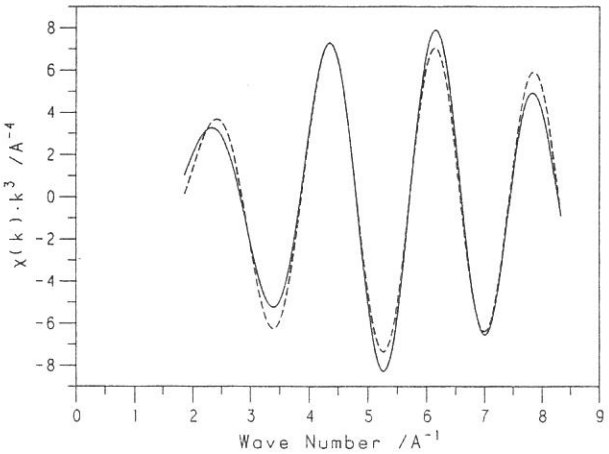

Figure 2 Results of the parameter fitting of the EXAFS function for $La_{0.90}Y_{0.20}Sc_{0.90}O_3$. The solid and broken lines present the experiment and calculation, respectively.

Table 1 Refined parameters of $La_{1-x/2}Y_xSc_{1-x/2}O_3$(x= 0.10, 0.20, 0.30) and reliability factors obtained by the Rietveld analysis.

x	Sc-O / Å	a / Å	b / Å	c / Å
0.0	2.09	5.7973	8.1014	5.6833
0.2	2.10	5.8327	8.1326	5.6867
0.3	2.12	5.8513	8.1545	5.6948

(BL8B1)

Oxidation States in $LiMn_2O_4$ Spinel Oxides from Manganese L-edge Spectroscopy

Yoshiharu UCHIMOTO, Takeshi YAO, Dan ISHIZAKI, and Koichi KAJIHARA

Department of Fundamental Energy Science,
Graduate School of Energy Science, Kyoto University,
Yoshida, Sakyo-ku, Kyoto 606-8317, JAPAN

$LiMn_2O_4$ based spinel type oxides are one of the most promising cathode materials used in lithium ion batteries because their low cost, high theoretical energy density. It is important to clarify valency change and structural change during charge and discharge process in order to understand their electrochemical properties. In the present study, oxidation state of manganese ion in the $LiMn_2O_4$ spinels were determined by using a measurement of Mn L_{23}-edge X-ray absorption near edge structure.

A mixture of Li_2CO_3 and $MnCO_3$ in a mole ratio of 1:4 was heated at 850 ℃ for 48 h in air. The crystal structure of the product was determined by XRD using CuKα radiation to confirm the formation of a well characterized $LiMn_2O_4$. Figure 1 shows a low rate discharge curve of $LiMn_2O_4$. The $LiMn_2O_4$ shows mainly 2 different regions. Between x = 0.2 to 0.5 ($Li_xMn_2O_4$), the discharge voltage was of 4.10 to 4.0 V and then the voltage fell rapidly down to 2.9 V at x = 0.5. XANES analysis were performed to clarify the oxidation state of manganese for various x values in $Li_xMn_2O_4$.

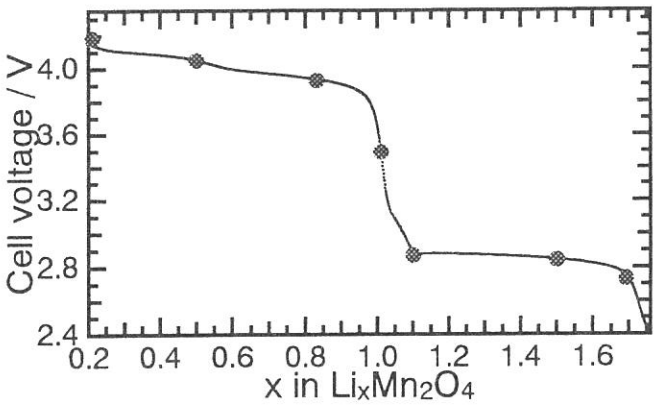

Fig. 1 Variations of electrode potential with capacity upon first discharging of $LiMn_2O_4$.

Fig. 2 shows the Mn L-edge X-ray absorption spectrum of $Li_xMn_2O_4$ (x=0.22, 0.50, 0.87, 0.98, 1.10, 1.50, and 1.70) together with MnO_2 (Mn^{4+}) and Mn_2O_3 (Mn^{3+}). The spectra correspond to $Mn2p^63d^n$ to $Mn2p^53d^{n+1}$ transitions. Figure 2 shows that the Mn L_3 absorption edge of Mn_2O_3 is about 642.0 eV and that of MnO_2 is 643.4 eV. These results indicated that increasing the oxidation state of manganese, the Mn L_3 absorption edge shift to higher energy.

As shown in Fig. 2, the peak of $Li_{0.98}Mn_2O_4$ is a combination of peak of Mn_2O_3 and MnO_2. At high x value such as x = 1.70, contribution of Mn^{3+} increase. On the other hand, at low x values of 0.22, contribution of Mn^{4+} increase. In conclusion, the average manganese valence in $LiMn_2O_4$ is between 3 and 4 and the valence is increase during the electrochemical extraction of lithium.

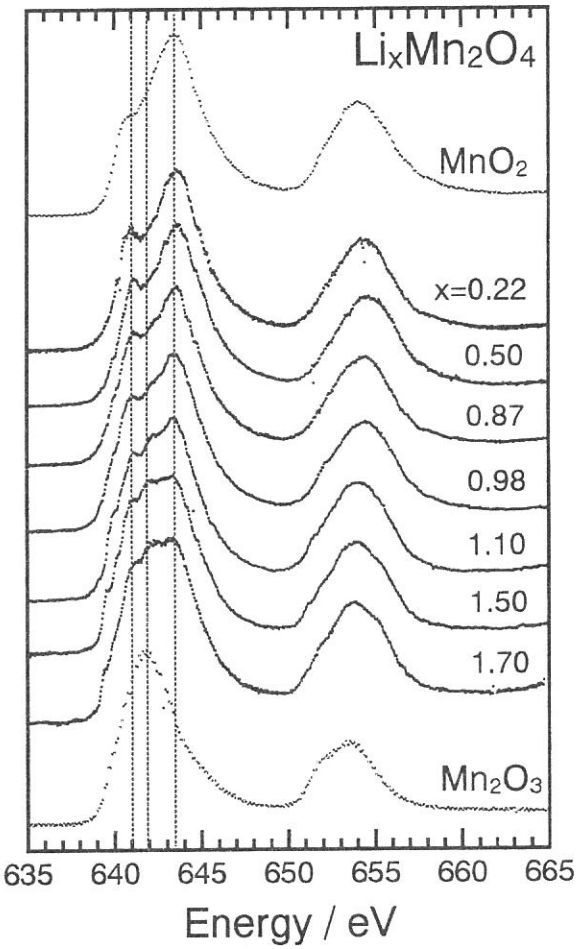

Fig. 2. Mn L-edge XANES of $LiMn_2O_4$ at various x values ($Li_xMn_2O_4$) potentials. x = x=0.22, 0.50, 0.87, 0.98, 1.10, 1.50, and 1.70

(BL8B1)

Mn-*L* absorption spectra in the paramagnetic and antiferromagnetic state in the intermetallic compounds YMn_2 and YMn_{12}

I.S. Dubenko[1], T. Gejo[2], E. Gratz[3], Y. Hosokoshi[2], K. Inoue[2],

S. Kimura[2], T. Kinoshita[2], A.S. Markosyan[2,1],

[1]*Faculy of Physics, Moscow State University, 119899 Moscow, Russia.*

[2]*Institute for Molecular Science, Myodaiji, Okazaki 444-8585, Japan,*

[3]*Institute for Experimental Physics, Technical University Vienna, A-1040 Wien Austria*

The nature of magnetism of the intermetallic compound YMn_2 is a subject of a long term discussion. It orders antiferromagnetically by a first order type phase transition with a wide hysteresis over a range 80 - 105 K. This transition is accompanied by a large volume expansion of ≈6 % and a tetragonal distortion. In the paramagnetic state, the thermal expansion of YMn_2 is essentially enhanced and $\alpha = d(\ln L)/dT$ attains 55×10^{-6} K^{-1}. Different models, geometrical frustration, metamagnetism, critical Mn-Mn distance [1-3], proposed to account for the anomalous properties of YMn_2 have a descriptive character and do not analyse the mechansims of magnetic instability. Recently was found that the paramagnetic thermal expansion coefficient is strongly enhanced in other binary Y-Mn compounds, too [4]. It was suggested that the anomalous properties of the binary Y-Mn compounds are related to the Mn electronic structure instability; one of the possible explanations could be a continuous temperature induced change in the Mn electronic structure (an itinerant analog of the intermadiate valence state), which can provide a strong temperature dependence of the local spin density on Mn sites and, hence, give rise to an enhancement of the thermal expansion. A change in the Mn electronic structure was recently observed by XAS investigation performed at the Mn *K*-edge in the $Y(Mn_{1-x}Ni_x)_2$ system [5].

In this work an attempt is made to observe directly the possible co-existence of different Mn-states in YMn_2 and YMn_{12} by recording the soft X-ray absorption spectra of the $2p$ (Mn) and $4d$ (Y) core levels at different temperatures above and below the Neel temperature (52, 85, 125 and 300 K) by using the BL8B1 beam line.

Table. Basic characteristics of YMn_2 and YMn_{12}.

Compound	YMn_2	YMn_{12}
Crystal structure and paramaters (Å)	Cubic, *Fd3m*, $a = 7.675$	Tetragonal, *I4/mm*, $a = 8.579$, $c = 4.760$
T_N (K)	80 - 105	110
μ_{Mn} at 4 K (μ_B)	2.7	0.66 (Mn(8i)) 0.66 (Mn(8j)) 0.22 (Mn(8f))

In Fig. 1 the Mn *L*-egde absorption spectra of YMn_2 and YMn_{12} are shown at different temperatures. The spectra correspond to Mn $2p^63d^n \rightarrow 2p^53d^{n+1}$ transitions and present two well resolved peaks separated by the spin-orbital interaction of the Mn $2p$ core hole.

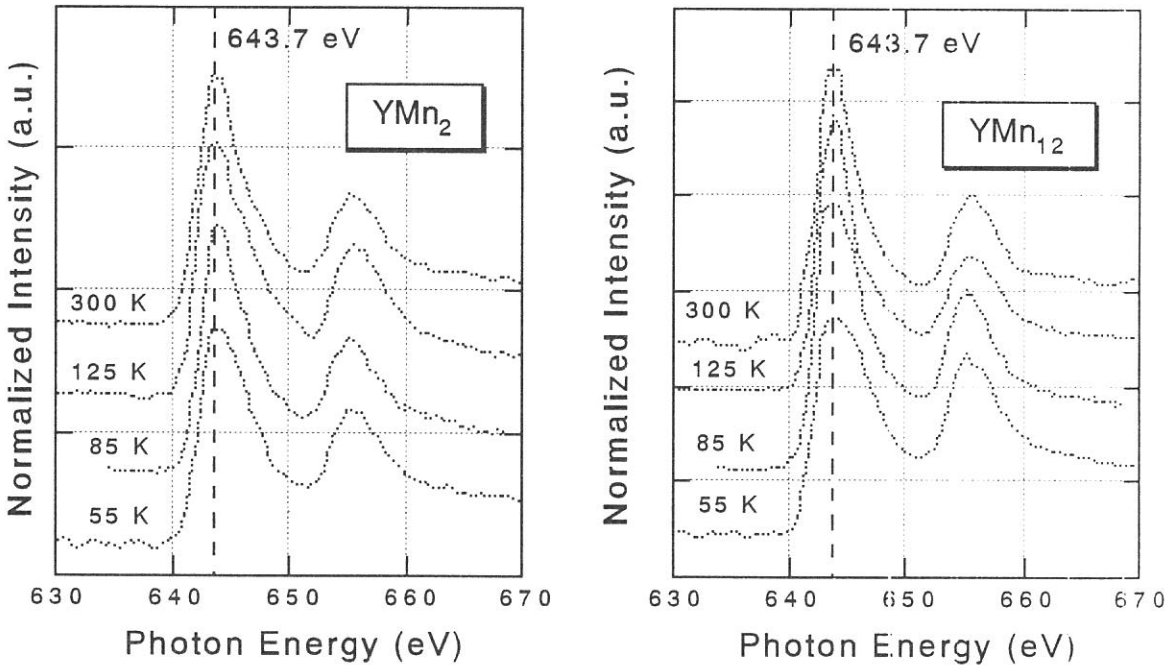

Fig. 1 Mn L-edge absorption spectra of YMn_2 and YMn_{12} at differen temperatures.

The position of the L_3 absorption edge, 643.7 eV, is very near to that observed in MnO_2 (Mn^{4+}) by XANES measurements [6]. From the magnetic data, the Mn state in YMn_2 is rather close to Mn^{3+}, while in YMn_{12} it is close to Mn^{6+}. A close inspection of the linewidth shows a weak temperature variation with a broadening below T_N (Fig. 2). This can be ascribed to a change in the Mn-electronic structure induced by a magnetic order. However, in order to investigate the influence of the 3*d*-electron shell on the Mn core levels, higher resolution is required. Similar behavior was observed when collecting Y K-egde absorption spectra of these intermetallics.

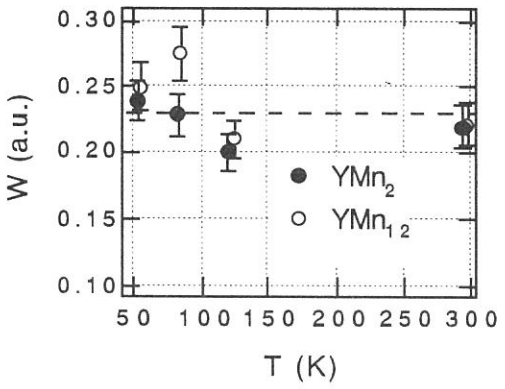

Fig. 2. Linewidth vs. T for YMn_2 and YMn_{12}

References

1. R. Ballou, J. Deportes, R. Lemaire and B. Ouladdiaf, J. Appl. Phys. **63**, 3487 (1988).
2. I.Yu. Gaidukova, I.S. Dubenko, R.Z. Levitin, A.S. Markosyan and A.N. Pirogov, Zh. Eksp. Teor. Fiz. **94**, 234 (1988) [Sov. Phys. JETP **67**, 2522 (1988)].
3. M. Shiga, Physica **B 149**, 249 (1988).
4. I.S. Dubenko, I.Yu. Gaidukova, S.A. Granovsky, E. Gratz, D. Gurjazkas, A.S. Markosyan and H. Mueller, Sol. State Commun. **103**, 495 (1997).
5. J. Chaboy, A. Marcelli, M.R. Ibarra and A. del Moral, Sol. State Commun. **91**, 859 (1994).
6. R.S. Liu, L.Y. Jang, J.M. Chen, Y.C. Tsai, Y.D. Hwang and R.G. Liu, J. Sol. State Chem. **128**, 326 (1997).

(BL8B1)

Polarization-Dependent Nitrogen K-edge Absorption of AlN, GaN, InN and AlGaN

Kazutoshi FUKUI, Ryousuke HIRAI, Akio YAMAMOTO
Faculty of Engineering, Fukui University, Fukui 910-0017, Japan
Fax +81-776-27-8749 fukui@wbase.fuee.fukui-u.ac.jp

The soft X-ray absorption (SXA) around nitrogen K-edge have been measured to investigate the electronic structure of the wurzite III-V nitrides, especially the structure of the unoccupied states. The N K absorption spectra of III-V nitrides near the N K-edge in principle represent the partial density of the final states with p symmetry according to the selection rule. Furthermore, the N K absorption spectrum gives us the site-specific (nitrogen ion site) information, since the core levels are very localized in space. The N K absorption spectrum also gives us the information about the final states symmetry p_{xy} and p_z, because the incidence soft X-ray light is linearly polarized.

The experiments were carried out at BL8B1. Resolutions under the experimental conditions were about 0.5 eV at 400 eV. The soft X-ray absorption measurement was performed by using the total photoelectron yield (TY) method. Thin films were made by the MOCVD method at Nichia Chemical (GaN), Riken (AlN and AlGaN) and Fukui University (InN). GaN thin film is 2.8 μm thickness on α-Al_2O_3 substrate. Both AlN and AlGaN thin films are 1 μm on SiC, and InN thin film is 0.1 μm on GaAs(111). All films were cleaned with organic solvents just before the installation into the vacuum chamber, and the measurements were performed at room temperature in the range of 10^{-8} Torr. The sample holder was able to rotate in the vacuum chamber for the angle dependence measurement. The polarization angle α is defined as the angle between the incident light and the normal to the sample surface, i.e., c axis. The α dependence measurements were performed under the p-polarization configuration which means $E \parallel c$ at $\alpha \sim 90$ degree. We were also performed the α dependence measurements at the N K absorption under the s-polarization configuration ($E \perp c$ at any α), and found that there was no angle dependence.

Figure 1(a) shows the N K absorption spectra of AlN, GaN and InN, and Fig.1(b) shows those of AlGaN mixed crystal. The energy scale is relative to the threshold energy which correspond to the conduction-band minimum. The threshold energies of AlN, GaN and InN are 395.0, 395.0 and 392.2 eV respectively. The labels A to G are corresponding to those for GaN in Ref. 1. The intensity of each spectrum is normalized at the peak B for convenience. The spectra feature of GaN and InN are good agreement with the previous works [1-3]. All spectra seem to be explained by the same labelling. It may be suggested that the electric structures of the unoccupied states around nitrogen ion for III-V nitrides basically consist of the similar components.

The α dependence absorption measurement was performed each sample which was shown in Fig. 1(a) and (b). Figure 2, for example, shows the N K absorption of AlN as function of angle α. All spectra are normalized. AlN result in Fig.2 also shows a clear α dependence as well as the other samples. Both the angle independence under the s polarization configuration and the clear angle dependence under the p polarization configuration are good agreement with the fact that the III-V nitrides are hexagonal and their c axes are perpendicular to the surface. To investigate the symmetry of the unoccupied states, the component analysis of the partial density of the final states with p symmetry (K absorption spectra) have been performed under the assumption as follows; (i) the partial density of the final states with p symmetry consists of p_{xy}, p_z and the α independent components, (ii) the absorption coefficients for $1s \rightarrow p_{xy}$ and $1s \rightarrow p_z$ are proportional to $\cos^2\alpha$ and $\sin^2\alpha$, respectively, where z axis is taken to be parallel to the c axis of the sample. Figure 3 shows the results of the component analysis of the N K absorption for AlN. The spectrum labeled a represents the α independent component, b the p_z component and c the p_{xy} component, respectively. The component analyses of the N K absorption for GaN, InN and AlGaN were also performed as the same manner. From these results each peak of the p_{xy} and the p_z components is found around the same energy. It suggests that

the unoccupied states with p symmetry of III-V nitrides have the similar structure near nitrogen site. Our results also show that the intensity ratio of the α independent component to the α dependent components is increasing with decreasing the cation mass. They will give us the information about the ionisity and the covalency of III-V nitrides.

The authors would like to thank Dr.S.Tanaka, Dr.Y.Aoyagi (RIKEN) for supply of AlN and AlGaN samples and Dr.S.Nakamura (Nichia Chemical) for supply of GaN samples.

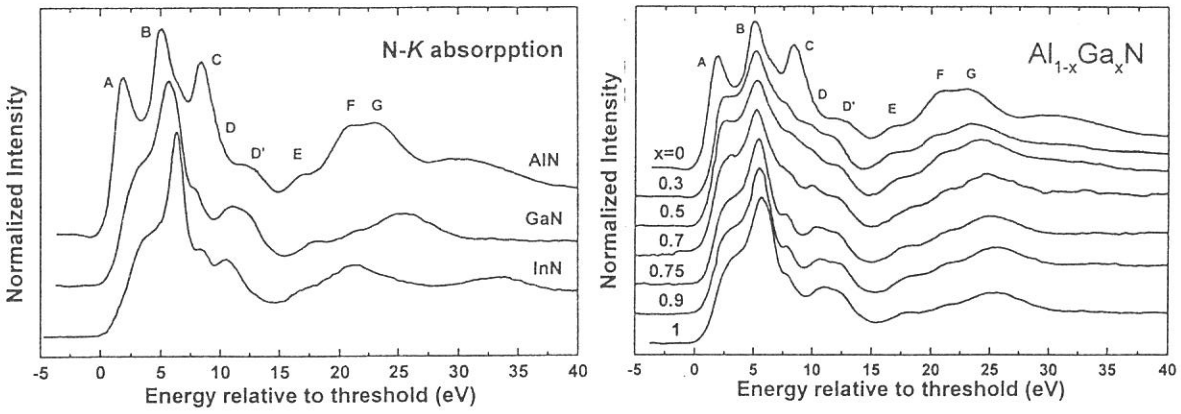

Fig.1 N K absorption spectra of AlN, GaN and InN(a), and those of AlGaN(b). The energy scale is relative to the threshold energy.

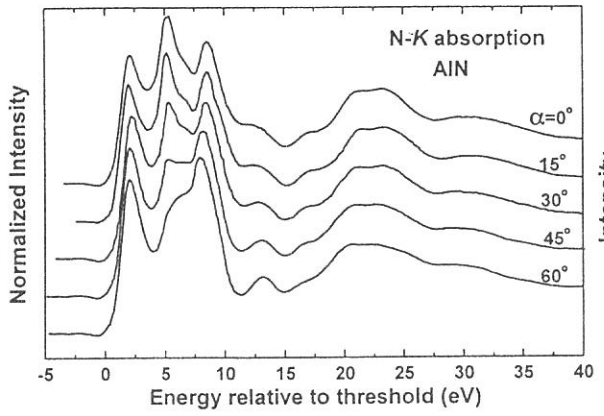

Fig.2 N K absorption spectra of AlN as function of angle which is defined as the angle between the incident light and the normal to the sample surface (c-axis).

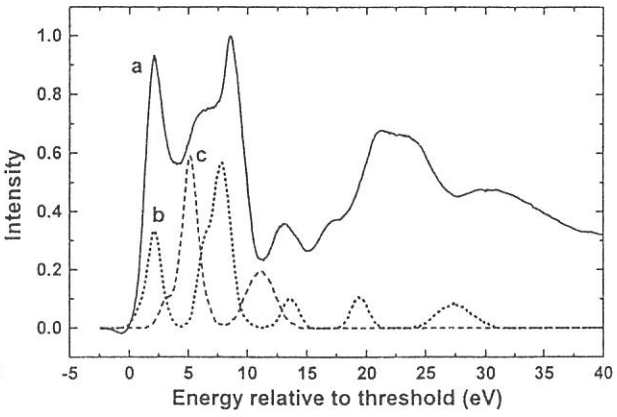

Fig.3 The coponent analysis results of Fig.2. The spectra labeled a, b and c show the α independent component, p_z and p_{xy} component, respectively.

References

[1] W.R.L.Lambrecht et al., Phys. Rev. B **55** (1997) 2612.

[2] C.B.Stagarescu et al., Phys. Rev. B **54** (1996) R17335.

[3] K.Fukui, M.Ichikawa, A.Yamamoto and M.Kamada, Solid State Electronics **41** (1997) 299.

(BL8B2)

Angle-resolved UPS of thin films of chloroalminium phthalocyanine (ClAlPc) on MoS_2 Surfaces

K.K.Okudaira[a], M.Tutui[b], T.Hasebe[b], Y.Azuma[a], A.Aoki[c], Y.Harada[a], and N.Ueno[d]

aDepartment of Material Science, Faculty of Engineering, Chiba University, Chiba 263
bGraduate School of Science and Technology, Chiba University, Chiba 263
cCollege of Arts and Sciences, The University of Tokyo, Tokyo 153
dInstitute for Molecular Science. Okazaki, 444

The angle-resolved ultraviolet photoelectron spectroscopy (ARUPS) using synchrotron radiation is a powerful method to investigate the geometrical structure of the ultrathin films of functional organic molecules as well as the electronic structure.

In the previous work we analyzed the take-off angle (θ) and azimuthal angle (ϕ) dependences of ARUPS of thin films of large organic molecules using the independent-atomic-center and single-scattering approximations combined with molecular orbital calculation (IAC/MO and SS/MO) and succeeded to determine the molecular orientation of copper phthalocyanine[1] and bis(1,2,5-thiadiazolo)-*p*-quinobis(1,3-dithiole) on MoS_2 surfaces.[2]

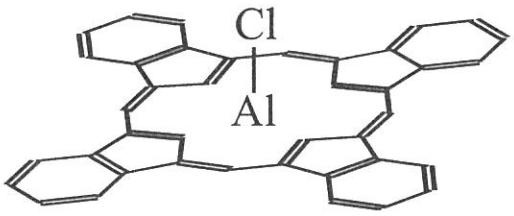

Figure 1 Structure of ClAlPc molecule.

In the present work we found that the θ dependences of the photoelectron intensities from the HOMO band of thin films of chloroalminium phthalocyanine (ClAlPc) on MoS_2 surfaces depend on the temperature. The purpose of this report is to investigate the temperature dependences of molecular orientation by the analysis of the photoelectron angular distribution. The molecular structure of ClAlPc is shown in Fig.1.

ARUPS measurements were carried out at the beam line BL8B2 at Institute for Molecular Science. The θ dependences of photoelectron spectra were measured at normal incidence [incidence angle of photon (α)=0°] and at hν=40eV. ClAlPc molecules were deposited on the MoS_2 substrate cooled at about -100℃. The film thickness was 8 Å.

Figure 2 shows the ARUPS (i) observed at -150℃ for as-deposited film, (ii) observed at room temperature (RT) for the film annealed at RT for 12 h, and (iii) observed at -150℃ for the film annealed at 110℃ for 8 h after 12-h annealing at RT. It is noted that the feature B, which originates from MoS_2, appearing in the ARUPS spectra of the as-deposited film disappears by the annealing at RT. Furthermore, while the energy position of HOMO band A which originates from the single π band shifts to the higher binding energy by about 0.2eV with the annealing at RT, it does not change after the additional annealing at 110℃. These results indicate that the as-deposited film consists of islands, and by annealing at RT the molecules spread over the substrate surface.

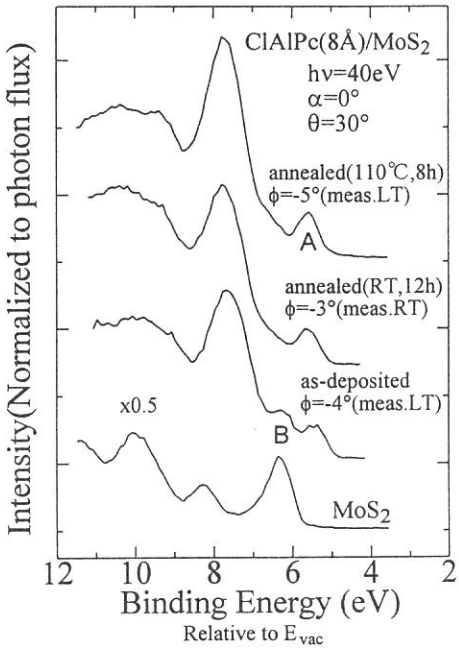

Figure 2 ARUPS spectra of ClAlPc films (8 Å) on the cooled MoS_2 (-100℃) at hν=40eV, α=0° and θ=30°. The ARUPS of as-deposited film, the film annealed at RT for 12 h, and the film annealed at 110℃ for 8 h after 12-h annealing at RT are measured at -150℃, RT, and -150℃, respectively. The substrate spectrum observed at RT is shown for comparison.

Figure 3 shows the θ dependences of photoelectron intensity from the HOMO band for the as-deposited film and for the film annealed at 110℃. For the annealed film, the θ dependence at RT is slightly broader than that at -150℃. It is

considered that the origin of the broadening is due to the vibrational excitations of ClAlPc molecules at RT. On the other hand, the θ dependence observed at -150℃ for the annealed film is sharper than that for the as-deposited film. It means that the molecular orientation changes by the annealing.

To estimate the change of the molecular orientation quantitatively, we calculate the θ dependences of photoelectron intensity from the HOMO band. We used SS/MO method to calculate the photoelectron intensity. The phase shifts and radial matrix elements were calculated using Muffin-tin potential.[3] The theoretical formula of SS/MO approximation were described in Ref.4. In this calculation we averaged the six azimuthal molecular orientations which are expected from analyses of LEED and ϕ dependences of photoelectron intensity.

The calculated and observed θ dependences are compared in Figs.4 (a) and (b). In Fig.4(a), the observed θ dependence for the as-deposited film agrees with calculated one for β=5°, where β is the molecular inclination angle. For the film annealed at 110℃, the observed θ dependence is in good agreement with calculated one for β=0° as shown in Fig.4 (b). These results indicate that on the cooled MoS_2, the molecules incline at about 5° with respect to the substrate surface, and after annealing at 110℃ they lie flat.

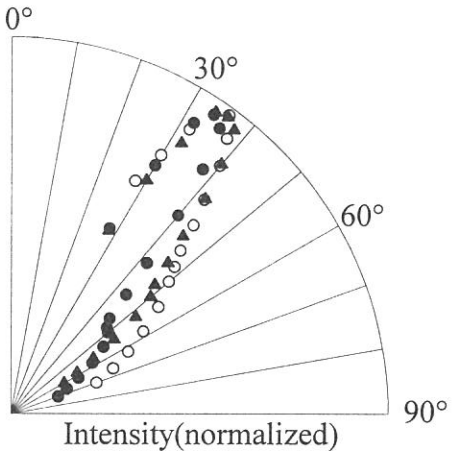

Figure 3 The take-off angle (θ) dependences of the photoelectron intensity of the HOMO band of ClAlPc films (8Å) on the cooled MoS_2 (-100℃) at hν=40eV and α=0°. The result of as-deposited film is shown by ○ (measured at -150℃). The results for the film annealed at 110℃ for 8 h after 12-h annealing at RT are shown by ▲ (measured at RT) and ● (measured at -150℃).

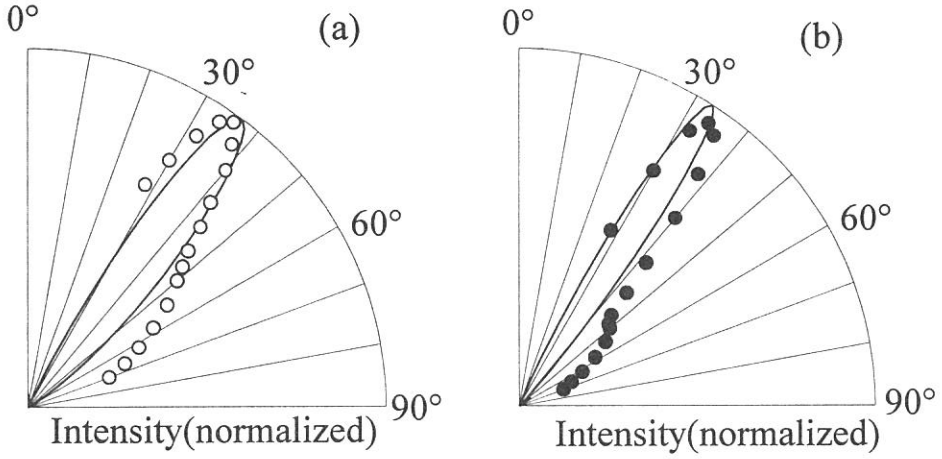

Figure 4 The comparison between calculated (——) and observed take-off angle (θ) dependences. The experimental results at -150℃ are shown by ○ (as-deposited film) and ● (the film annealed at 110℃ for 8 h after 12-h annealing at RT). The calculations were performed with SS/MO approximation at hν=40eV and α=0° for β=5° (panel(a)) and for β=0° (panel (b)).

REFERENCES

[1]K.Kamiya, M.Momose, A.Kitamura, Y.Harada, N.Ueno, S.Hasegawa, T.Miyazaki, H.Inokuchi, S.Narioka, H.Ishii, and K.Seki, J.Electron Spectrosc.Relat.Phenom., **76** 213 (1995).

[2]N.Ueno, A.Kitamura, K.K.Okudaira, T.Miyamae, S.Hasegawa, H.Ishii, H.Inokuchi, T.Fujikawa, T.Miyazaki, and K.Seki, J.Chem.Phys., **107** 2079(1997).

[3]D.Dill and J.L.Dehmer, J.Chem.Phys., **61** 692 (1974).

[4]N.Ueno, J.Electron Spectrosc.Relat.Phenom., **78** 345 (1996).

(BL8B2) Photoelectron spectra of metallofullerenes, GdC_{82} and La_2C_{80}

Shojun Hino[a,b], Kazunori Umishita [a,b] Kentaro Iwasaki [a], Takafumi Miyazaki[c]*, Takayuki Miyamae [b,c], Koichi Kikuchi [d] and Yohji Achiba [c]

[a] *Faculty of Engineering, Chiba University, Inage-ku, Chiba 263-8522 Japan*
[b] *Graduate School of Science and Technology, Chiba University, Inage-ku, Chiba 263-8522 Japan*
[c] *Institute for Molecular Science, Myoudaiji, Okazaki, Japan 444-8585*
[d] *Faculty of Science, Tokyo Metropolitan University, Hachioji, Tokyo 192-0397 Japan*

Metallofullerenes have attracted a lot of attentions such as their structures including the position of the metal atom(s), their electronic structures as well as the amounts of transferred electrons from the metal atom(s) to the cage, their reactivity and so on. Photoelectron spectroscopy is a powerful tool to clarify their electronic structures. In this article, our recent results of the photoelectron spectroscopy on metallofullerenes, GdC_{82} and La_2C_{80} are presented and their electronic structures are discussed.

Figure 1 shows the incident photon energy dependence of the UPS of the solution dried-up GdC_{82} film heated up to 300 °C in ultrahigh vacuum. Note that the specimen is not vacuum deposited film. The spectral onset is 0.3 eV below the Fermi level and six distinct structures labeled A – E and N are observed in this energy region. In the spectra obtained with lower excitation energy, superposition of secondary electrons is heavy in the higher binding energy region; structure C can be vaguely discerned in the $h\nu$ = 15 – 25 eV spectra and a dip between structures C and D is discerned only in the $h\nu$ = 30 eV spectra. A clear intensity oscillation is observed in structures A and B, as in other fullerenes. Their intensity in the $h\nu$ = 20 and 40 eV spectra is nearly equal, but structure B in other spectra is about one and half times more intense than structure A. This intensity dependence of structures A and B on the incident photon energy is essentially the same as those of C_{82} [1] and LaC_{82} [2].

Figure 2 shows the photoelectron spectra of GdC_{82}, C_{82} and LaC_{82} (excited by $h\nu$ = 20 eV photon). The intensity of the high binding energy region of the spectrum of GdC_{82} is stronger than those of the other two spectra, which is due to the overlap of secondary electrons. Structures A – E have one to one correspondence with those of C_{82} and LaC_{82}. Note the presence of structure N that is also observed in LaC_{82} but absent in C_{82}. The appearance of structure N is the result of electron transfer from the metal atom to the fullerene cage. In order to estimate the amount of transferred electrons, a difference spectrum is obtained by subtracting the spectrum of C_{82} from that of GdC_{82}: both spectra are normalized at the peak position of structure B (3.3 eV). The difference spectrum is shown in the inset of Fig. 2. It can be deconvoluted into two parts, α and β; their peak positions are 0.85 and 1.45 eV, respectively. Their intensity ratio is roughly 1 : 2. This finding and the electron configuration of the Gd atom, $(6s)^2(4f)^7(5d)^1$, support that three electrons are transferred from the metal atom to the C_{82} cage. The difference spectrum between LaC_{82} and C_{82} is very close to the present result [2]. This fact and the resemblance of their absorption spectra [3,4] indicate that the electronic structures of LaC_{82} and GdC_{82} are analogous and that three electrons of the metal are transferred to the cage in both metallofullerenes.

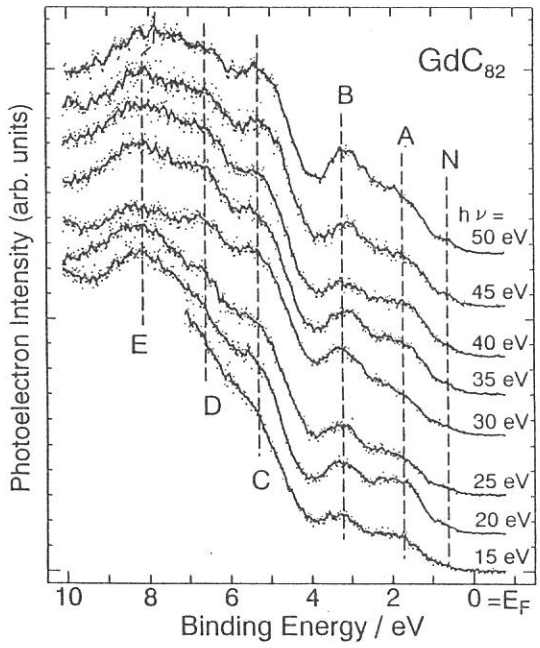

Fig.1 Incident photon energy dependence of the photoelectron spectra of GdC_{82}. Approximate peak positions are indicated by broken lines.

When three electrons are transferred from the Gd metal, the C_{82} cage has odd number electrons to form an open shell molecule. A solid composed of open shell molecules is considered to be metallic, but GdC_{82} is not metallic since the spectral onset does not cross the E_F but is 0.3 eV below the E_F. Both X-ray diffraction study of YC_{82} [5] and a theoretical consideration of metallofullerenes containing one metal atom [6] indicate that the metal atom is located at the off-centered position in the cage. This also seems to hold in GdC_{82}, so that the molecule might have a large dipole moment. In GdC_{82} solid, the molecules might be arranged to cancel its dipole moment to lower the total energy of the solid, and probably pairing of the molecules takes place so that molecular aggregates tend to behave like closed shell molecules. This could be the reason for its semi-conductive nature.

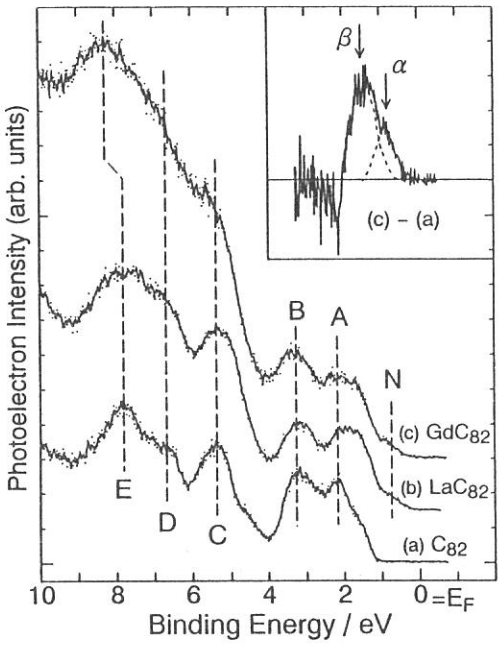

Fig.2 Photoelectron spectra of empty C_{82}, LaC_{82} and GdC_{82} obtained with hν = 20 eV excitation energy. Inset is the difference spectrum obtained by subtracting the C_{82} spectrum from the GdC_{82} spectrum. The intensity of both spectra is normalized at the 3.3 eV peak that seems to be least affected by superposition of secondary electron. The difference spectrum can be deconvoluted into two peak components α and β with an intensity ratio of 1 : 2.

A photoelectron spectrum of the solvent dried-up La_2C_{80} film heated up to 400 °C begins at the Fermi level and show poor structures. The spectrum resembles that of vitreous carbon. A straightforward interpretation of this analogousity brings a conclusion that the electronic structure of La_2C_{80} is somewhat like that of amorphous carbon or La carbide. That is, the metal atoms could be at any place; outside or inside the carbon cage or just in the carbon plane. This is inconsistent with the conclusion obtained from the reactivity of 1,1,2,2,-tetramesityl-1,2-disilirane to La_2C_{80} and the analysis of its nuclear magnetic resonance spectrum [7]; they strongly support its endohedral form. A further investigation is required to settle the conflicting results on La_2C_{80}.

References

[1] S. Hino *et al.*, Phys. Rev. B 48, 8418 (1993).

[2] S. Hino *et al.*, Phys. Rev. Letters 71, 4261 (1993).

[3] K. Kikuchi *et al.*, Chem. Phys. Letters 216, 67 (1993).

[4] T. Suzuki et al., Tetrahedron 52, 4973 (1996).

[5] M. Takada *et al.*, Nature 377, 46 (1995).

[6] S. Nagase *et al.*, Bull. Chem. Soc. Jpn. 69, 2131 (1996), and references there in.

[7] T. Akasaka *et al.*, Angew. Chem. 109, 1716 (1997).

(BL8B2)

UV PHOTOEMISSION OF n-$C_{44}H_{90}$ / Cu(100) : MOLECULAR ORIENTATION OF A LONG-CHAIN OLIGOMER / METAL INTERFACE

H. Ishii[a], D. Yoshimura[a], E. Ito[a], K. Okudaira[b], T. Miyamae[c], S. Hasegawa[c], N. Ueno[b, c], and K. Seki[a]

[a] *Faculty of Science, Nagoya University, Furo-cho, Chikusa-ku, Nagoya 464-8602, Japan*
[b] *Faculty of Engineering, Chiba University, 1-33 Yayoi-cho, Inage-ku, Chiba 263-8522, Japan*
[c] *Institute for Molecular Science, Myodaiji, Okazaki 444-8585, Japan.*

INTRODUCTION

Recently various polymers have attracted wide attention in close relation to electronic devices. The elucidation of geometrical and electronic structure of polymer / metal interfaces is crucial for understanding and improving the performance of such devices. Especially, the study for a simple system with a well-ordered structure is highly desired. However, it is not easy for polymers. The use of the shorter oligomers instead of polymers is one of the solutions because of their definite molecular weight, better crystallinity, and possibility of preparing well ordered thin films by vacuum deposition. In fact, oligomers such as *p*-sexiphenyl (6P) and a-sexithiophene (α-6T) have been applied to devices, and their oriented films have been prepared by vacuum deposition. Very recently, we have found that even for 6P with small number N of repeating units (6), the wavenumber (k) of the valence electron is still a good quantum number but much blurred because of small N [1], indicating that translational nature is still far from that of a polymer with full translational symmetry. Thus the study for a longer oligomer is desired for investigating polymer.

In this study, we investigated the molecular orientation of a long-chain alkane, tetratetracontane (n-$C_{44}H_{90}$, TTC) in thin films on Cu(100) single crystal surface, using low energy electron diffraction (LEED) and angle-resolved UV photoemission (ARUPS). TTC is a model compound of poly(ethylene) which is one of the fundamental polymers. In the case of TTC, the blurring of k is much smaller than that of shorter oligomer such as 6P [2] because of its large number of repeating units of 22. Thus this TTC / Metal system can be regarded as a prototype of polymer/metal interface.

EXPERIMENTAL

The sample of TTC was purchased from Tokyo Chemical Industries Co.Ltd., and purified by recrystallization from the benzene solution. Cu(100) surface was cleaned by several cycles of annealing and Ar^+ ion sputtering. TTC film was prepared by vacuum vapor deposition. The thickness was about 0.4nm in average that corresponds to monolayer thickness in flat-lying orientation. UPS measurement was performed at the beamline 8B2 of the UVSOR synchrotron radiation facility at IMS. Photon energy for UPS was 40 eV. The incidence angle of photon was 70° relative to surface normal.

RESULTS AND DISCUSSION

TTC/Cu(100) surface exhibited LEED pattern as shown in Fig.1, indicating two-dimensional order of the surface. The analysis of this pattern suggested that there are two domains where TTC chain aligns to [110] ([1 $\bar{1}$ 0] in the other domain) direction of the Cu(100) surface. This was confirmed by UPS measurement.

Fig.2 shows UPS spectra of TTC/Cu(100). The abscissa is binding energy relative to the Fermi level of Cu. The polarization vector of photons and the wave vector of emitted electrons were located in the mirror plane which includes surface normal and [110] direction of Cu(100) surface. The spectral features are ascribed as follows: structure A is due to Cu 3d orbital and upper edge of C2p-derivd orbital of TTC. Structures B and C

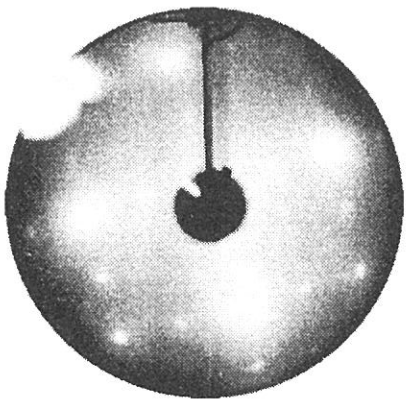

Fig.1 LEED pattern of TTC on Cu(100). Four large spots are [1,0] spots from the Cu substrate.

are due to C2p and C2s-derived orbitals, respectively. Their lineshape exhibited drastic variation by changing the take-off angle θ due to intramolecular band dispersion of TTC. The band structure derived from the spectra observed for a wide range of θ well corresponded to that reported for thick TTC film [2], suggesting that the formation of the interface does not change the translational nature of TTC. This can be explained by weak chemical interaction between TTC and Cu surface.

The simulated spectra for the C2p bands are also shown in Fig.2 as solid lines. They were calculated with independent-atomic-center (IAC) approximation combined with *ab-initio* molecular orbital calculation [3]. The photoemission intensity was calculated for two domains in which TTC axis is parallel to [110] direction with the molecular plane parallel to the surface. As seen in Fig.2, each simulated spectrum is well consistent with the observed one, clearly indicating the flat-on orientation of TTC on Cu(100).

In conclusion, two-dimensionally well-ordered TTC ultrathin film was successfully prepared on Cu(100) as a prototype of polymer / metal interface. The molecular orientation was determined by LEED and ARUPS combined with the theoretical analysis by IAC approximation. This type of experiment for well-defined interface will be useful for obtaining deeper insight for polymer/metal interfaces.

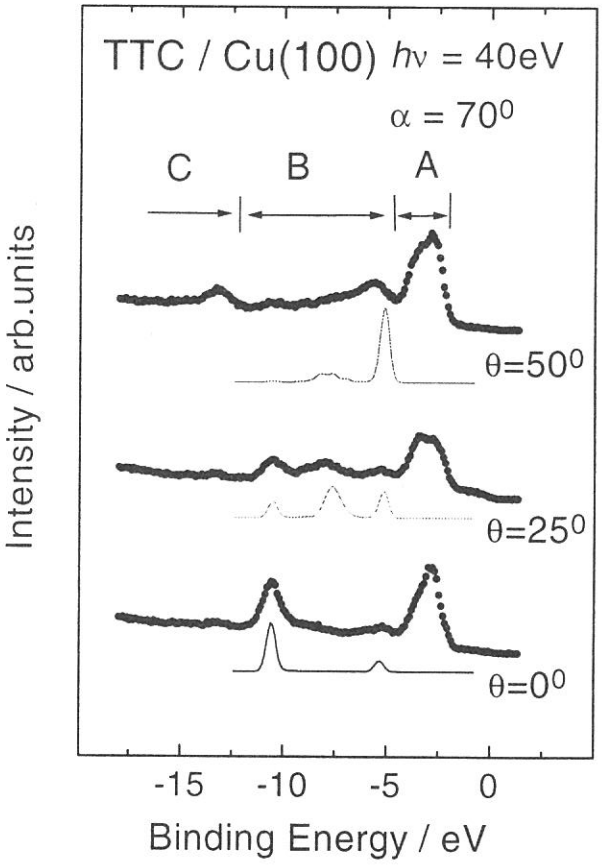

Fig2. Observed ARUPS spectra (dot) and the simulated spectra (solid line) of TTC on Cu(100).

REFERENCES

[1] S. Narioka, H. Ishii, K. Edamatsu, K. Kamiya, S. Hasegawa, T. Ohta, N. Ueno, and K. Seki, *Phys. Rev.*, **B52**, p2362 (1995).
[2] K. Seki, N. Ueno, U.O. Karlsson, R. Engelhardt, and E. Koch, Chem. Phys., **105**, p247 (1986).
[3] S. Hasegawa, S. Tanaka, Y. Yamashita, H. Inokuchi, H. Fujimoto, K. Kamiya, K. Seki and N. Ueno, *Phys. Rev.*, **B48**, p2596 (1993).